CHAIN CONFORMATION AND NANO-PATTERNING OF POLYMER BRUSHES PREPARED BY SURFACE-INITIATED ATOM TRANSFER RADICAL POLYMERIZATION

By

XIANG GAO, B. ENG., M, ENG.

A Thesis

Submitted to the School of Graduate Studies

In Partial Fulfillment of the Requirements

For the Degree of

Doctor of Philosophy

McMaster University

DOCTOR OF PHILOSOPHY (2009) McMaster University

(Chemical Engineering) Hamilton, Ontario

TITLE: Chain conformation and nano-patterning of polymer brushes prepared by surface-initiated atom transfer radical polymerization

AUTHOR: Xiang Gao

B. Eng. (Tianjin University)

M. Eng. (Tianjin University)

SUPERVISOR: Professor Shiping Zhu

NUMBER OF PAGES: xxv, 204

ABSTRACT

Over the past decade, the development of surface-initiated living polymerization methods has brought a breakthrough to surface modification owing to their control ability. Surface-initiated atom transfer radical polymerization (si-ATRP), as the most popular one, has been widely employed to give novel polymer structures and functionalities to various surfaces for the purposes of tailoring surface properties, introducing new functions, or preparing so-called "smart surfaces", which can respond to external stimuli such as solvent type, pH, temperature, electric and magnetic fields etc. In this thesis, the mechanistic study of the si-ATRP was first carried out through modeling to gain good understanding of si-ATRP. Si-ATRP was then employed to prepare different types of polymer brushes to produce "smart surfaces".

The kinetic model was developed using the method of moment. Combined with experimental data, a quantitative analysis was carried out for the si-ATRP mechanism. All information of grafted polymer chains, including active chain concentration, radical concentration, chain length, polydispersity, was illustrated. A new radical termination mechanism, termed as migration-termination, was proposed for si-ATRP.

Si-ATRP was then employed to graft poly(oligo(ethylene glycol) methacrylate) (POEGMA) block poly(methyl methacrylate) (PMMA) brushes on silicon wafer surfaces.

Simple solvent treatment gave nanoscale patterns via the phase segregation of POEGMA and PMMA segments. Various patterns including spherical aggregates, wormlike aggregates, stripe patterns, perforated layers and complete overlayers, were obtained by adjusting the upper block layer thickness. Furthermore, these nanopatterns had a unique stimuli-responsive property, i.e., switching between different morphologies reversibly after being treated with selective solvents.

POEGMA-block-poly(2-(methacryloyloxy)ethyl trimethylammonium chloride) (PMETAC) brushes, having two hydrophilic segments, were synthesized by si-ATRP method. A variety of nanopatterns and their stimuli-responsive ability were observed. The adsorption behaviors of fibrinogen on these patterns were thoroughly studied by ellipsometry, water contact angel measurement, AFM and radio labelling method.

A novel thermo-responsive copolymer, poly(2-(2-methoxyethoxy)ethyl methacrylate -co- oligo(ethylene glycol) methacrylate) (P(MEO_2MA-co-OEGMA)), was also grafted onto silicon wafers. Its thermo-responsive behavior and chain conformation in aqueous solution were studied by neutron reflectometry (NR). Both extended and collapsed brushes exhibited good protein adsorption resistance.

ACKNOWLEDGEMENTS

I would like to express my sincere thanks to all the people who have given me help to finish this work.

I would like to express my deepest gratitude to my supervisor, Professor Shiping Zhu, for his constant guidance and immense support. It is he who brought me to the polymer engineering and science area and sent me to the frontier. His knowledge, enthusiasm, insight, and attention are truly unforgettable.

I would like to thank Professor Michael Thompson and Professor An-Chang Shi. As the members of my supervisory committee, they have provided me numerous valuable advices and help during my study at McMaster.

I would like to thank Professor John Brash and Professor Heather Sheardown. They gave me lots of precious advices regarding this research project and provided great help in writing my papers.

I would like to thank Dr. Mu-Ping Nieh, Dr. Norbert Kučerka and Dr. John Katsaras for their great help with NR experiments at Chalk River.

I am grateful to all my group members, Dr. Wei Feng, Dr. Santiago Faucher, Dr. Hormoz Eslami, Dr. Hualong Pan, Dr. Junwei Zhang, Mary Jin, Helen Gu, Jen Mahon,

Rachel Gong, Sarah Alibeik, Mark Machado, Mohammad Haj Abed, Jason Doggart and Tom Kowpak, for their help and suggestions. I would thank Dr. Andy Duft and Dr. Zhilin Peng for their tremendous help with the facilities.

I thank all the staff members in the department, in particular, Kathy Goodram, Lynn Falkiner, Andrea Vickers, Nanci Cole, Justyna Derkach, Doug Keller, James Lei and Paul Gatt for their assistance.

I thank McMaster University, Department of Chemical Engineering for their support. I also thank the Natural Sciences and Engineering Research Council of Canada (NSERC) for providing financial support to my research and the Canada Foundation of Innovation (CFI) for the lab facilities.

Last, but certainly not the least, I would like to express my sincere thanks to my parents who love and support me for all these years.

TABLE OF CONTENTS

LIST OF FIGURES

LIST OF TABLES

LIST OF SCHEMES

LIST OF ABBREVIATIONS

AFM	atomic force microscopy
aSCF	analytical self-consistent-field
ATRP	atom transfer radical polymerization
bio-MEMS	Biomicroelectromechanical
Bipy	2,2'-bipyridyl
CLRP	controlled/living radical polymerization
EBIB	ethyl α-bromoisobutyrate
EO	ethylene oxide
HOEGMA	hydroxyl-terminated oligo(ethylene glycol) methacrylate
Homo	Homogeneous
HPLC	High-performance liquid chromatography
ICl	iodine monochloride
LCST	lower critical solution temperature
MEO_2MA	2-(2-methoxyethoxy)ethyl methacrylate
Mn	number average molecular weight
MPC	2-methacryloyloxyethyl phosphorylcholine
MWD	molecular weight distribution

NMP	nitroxide mediated polymerization
NR	neutron reflectometry
NRU	National Research Universal
nSCF	numerical self-consistent-field
OEGMA	oligo(ethylene glycol) methacrylate
PD	Polydispersity
PEG	poly(ethylene glycol)
PEO	poly(ethylene oxide)
PMDETA	*N*,*N*,*N'*,*N''*,*N''*- pentamethyldiethylenetriamine
PMETAC	[2-(Methacryloyloxy)ethyl]trimethylammonium chloride
PMMA	poly(methyl methacrylate)
PNIPAM	poly(N-isopropylacrylamide)
PS	Polystyrene
RAFT	reversible addition-fragmentation transfer
S1	sample 1
S2	sample 2
SAM	self-assembled monolayer
s-ATRP	surface-initiated atom transfer radical polymerization
SFRP	stable free-radical polymerization

SLD	scattering length density
TBS	tris buffered saline
TEMPO	2,2,6,6-tetramethyl-1-piperidinoxyl
XPS	x-ray photoelectron spectroscopy

PREFACE

This Ph.D. thesis is organized in a "sandwich" style based on the following published or preparatory articles:

1. Gao, X.; Feng, W.; Zhu, S. P.; Sheardown, H.; Brash, J. L. A facile method of forming nanoscale patterns on poly(ethylene glycol)-based surfaces by self-assembly of randomly grafted block copolymer brushes. *Langmuir* 2008, *24* (15), 8303-8308.

2. Gao, X.; Kučerka, N.; Nieh, M.P.; Katsaras, J.; Zhu, S.; Brash, J. L.; Sheardown, H. Chain conformation of a new class of PEG-based thermo-responsive polymer brushes grafted on silicon as determined by neutron reflectometry. *Langmuir* 2009, *25* (17), 10271-10278.

3. Gao, X.; Feng, W.; Zhu, S. P.; Sheardown, H.; Brash, J. L. Kinetic modeling of surface-initiated atom transfer radical polymerization (Manuscript prepared)

4. Gao, X.; Zhu, S. P.; Sheardown, H.; Brash, J. L. Nanoscale patterning through self-assembly of block copolymer brushes with two hydrophilic blocks. (Manuscript prepared)

Chapter 1
Introduction

1.1 Polymer brushes on surface

1.1.1 Surface modification techniques

Surface modification is a popular technique employed in a wide variety of fields for various applications. When selecting a material for a specific application, the bulk physical and/or chemical properties are very important. In many cases, however, the surface properties of these bulk materials must be modified in order to meet certain criteria. Vascular stents, for instance, are mainly made of metals due to the required structural rigidity. Unfortunately, platelets in the blood can adhere to these metal surfaces quickly, causing serious problems. In order to overcome this biocompatibility issue, these surfaces are modified with biocompatible materials, e.g. poly (ethylene glycol) (PEG).[1] The coating of these biocompatible materials does not affect the metal bulk properties, but does improve the surface properties of the final heart stent products. As a result, rigid metal mesh tubes with biocompatible surface can be obtained.

Among all materials used for surface modification, polymers are the most prevalent.[1-3] As early as in 1850, Michael Faraday demonstrated the use of gelatine to

stabilize gold sols. He showed that gelatins on the surface of these gold particles stabilized them in solution. His samples, displayed in the Royal Institute in London, have remained stable for about 150 years.[4] Until recently, this technique was still widely used to stabilize colloids. More recently there have been numerous natural and synthetic polymers with varying properties available for surface modification. This allows for a wide range of different surface properties to be achieved. Additionally, when compared with metal or ceramic materials, polymers represent an economic choice. This is because the processing of polymers is much simpler and generally occurs at a lower temperature.

Many techniques exist to modify surface properties with polymer materials.[4-6] Surface coating is the most extensively used because of its simplicity. In this method, products are dipped into a polymer solution or melt to obtain a polymer coating. Other methods, e.g. spraying, could also be employed. Coatings have a minimal effect on the bulk properties of the coated materials, and multi-functionality can be obtained by coating more than one layer. Unfortunately, this technique generally yields weak adhesion to bulk materials, which can result in the polymer coating peeling off over time. Furthermore, when the structure has a complex geometry, some coating methods may result in uneven coating, and thus be inapplicable.

For surface modification where the bulk material is also polymeric, another simple method, direct mixing, may be chosen. In this method some surface-active

polymeric materials are added to the bulk material during processing. These surface-active materials are expected to migrate towards the surface of the bulk material, enriching these surfaces with specific properties. A major advantage of this method lies in its simplicity and low-cost. However limitations do exist, with some surface-active polymers remaining inside the bulk and affecting the bulk properties. The choice of surface-active polymers is also limited. Furthermore, the necessity of miscibility between bulk materials and surface-active polymers creates a very narrow operating window. If these two components are very miscible, the surface-active polymer cannot migrate and enrich the surfaces. However, if they are totally immiscible, the surface-active polymers can be simply separated from the bulk materials.

One third method which has shown a great deal of promise is the so called grafting method. Grafting refers to immobilizing a polymer coating on the surface of the bulk material through covalent bonding.[4,6] Some polymeric materials bear reactive groups that can react with surface moieties of the bulk substrate. Although grafting is more complex than physical coating, and thus carries a higher cost, chemical bonding yields a much more stable polymer layer on the surface. As a result, this method is very advantageous when durability and longevity are important, e.g. the surface modification of artificial products for implanting into the body.

1.1.2 Polymer brushes

In the grafting method, various polymer chain conformations can be obtained on the surface.[7-10] When grafting density is low, polymer chains on the surface are separated from each other. As a result, they are in what is known as the mushroom conformation, as shown in Scheme 1-1.

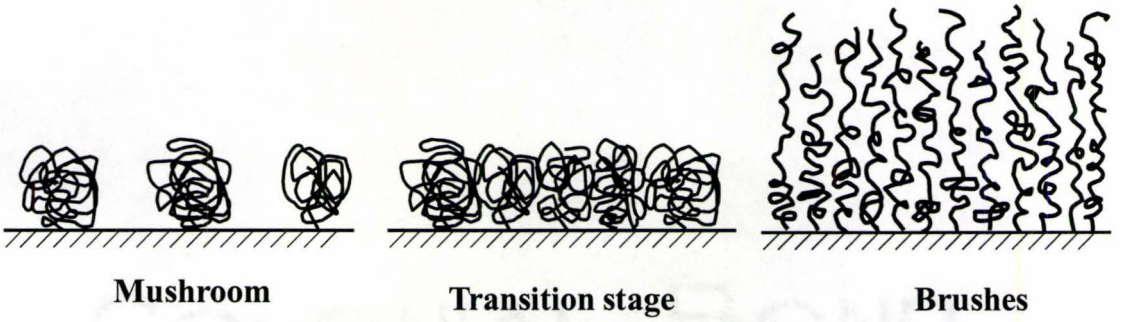

Scheme 1-1 Chain conformations of polymer chains grafted on the surface.

As grafting density increases, grafted polymer chains begin to interact with each other, inducing a change in the conformation from a relaxed mushroom configuration to stretched brushes, as shown in Scheme 1-1.

The transition from mushrooms to brushes is an important stage. It is believed that the transformation occurs when overlapping layers of polymer create a barrier which inhibits the chains from reaching the solid surface. The adjacent polymer chains then start interfering with each other. Determining when this transformation begins is an interesting and important question, as more and more research has shown that chain conformation is

one of the most important factors in determining the performance of modified solid surfaces. Storm *et al.*[11] have pointed out that grafted polymer chains in the transition conformation between "mushroom" and "brush" are best for protein repulsion due to their slightly constricted configuration and high grafting density which ensures that there are no gaps between grafted polymer chains.

Among these three conformations, the brushes conformation has gained the most interest in both theoretical and experimental work.[4,7,12] This is because dense brushes bring about the greatest change to surface properties. With regard to experimental studies, a great variety of polymer brushes have been grafted onto various surfaces to obtain desirable surface properties for applications in the fields of adhesion, biomaterials, protective coatings, tribology, composites, microelectronics, thin-film fields, etc.[4,5,13-17] The effects of polymer type, degree of polymerization, grafting thickness, and initiator density on surface properties are interesting topics which have been extensively investigated.[18-27]

Many theoretical studies have been carried out on grafted polymer chain conformations, resulting in three basic models for polymer brushes: scaling theories, analytical self-consistent-field (aSCF) models, and numerical models (nSCF).[4,10,28] These models are all based on the thermodynamics of polymer brushes in their equilibrium conformation. The grafted monomeric unit density distribution along a surface can be

obtained from these models.

The kinetics of forming polymer brushes on a surface has also been modeled. Most studies involve cases where an interface forms between two immiscible polymers.[29-31] If these two immiscible polymers have reactive chain ends a block copolymer will be formed at the interface. When the concentration of this polymer reaches a certain level, a brush conformation at the interface will result.

Hasegawa *et al.*[32] employed a numerical scheme using dynamical mean field theory to investigate grafting kinetics of end-functionalized polymers onto a solid surface to determine the time evolution of density profile. Shull [33,34] employed a self-consistent field theory and gave a detailed calculation of properties for end-adsorbed polymer chains in the brush equilibrium. Fredrickson[35,36] developed a new theory for diffusion-controlled coupling of two end-functionalized homopolymers at the interface. Monte Carlo methods were also employed for this kind of calculation.[37-41] Studies of polymer brushes on nanoparticles were also carried out. The curved surface of nanoparticles makes them totally different from flat surfaces, as the nanoparticle radius is comparable to grafted polymer layer thickness. This has also been examined by Ball *et al.*[42] with an aSCF-model and Wijmans *et al.*[43] with a nSCF-model.

1.1.3 Grafting polymer brushes onto surfaces

A number of methods have been developed for grafting polymer brushes onto different surfaces or interfaces. These methods can generally be classified into two types: "grafting to" and "grafting from".[6,44] In the "grafting to" method, polymer chains are prepared by conventional polymerization methods in advance. They bear reactive moieties at their chain ends which can react with reactive sites on a surface. Through this method, polymer chains can be covalently attached to a surface. Although this method allows for advance preparation and characterization of the polymer chains, it also has some disadvantages. One of the main disadvantages of this method is that it yields very low graft density. This is due to the fact that during the grafting process the chains need to diffuse from the bulk to the surface in order to react. Unfortunately, chains which have already been grafted can prevent subsequent chains from approaching the surface, resulting in very low grafting density. However, considering the simplicity of the "grafting to" method, it is still very popular for creating polymer brushes on a surface.

Many studies have been carried out on how to improve this grafting density. The chain length of polymer has been shown to be one of the most important factors for the "graft to" method.[45] A detailed study was carried out by Zdyrko *et al.*[46] investigating the influence of chain length on the grafted polymer layer. In their work, carboxylic acid end-functionalized poly(ethylene oxide) (PEO) samples with different molecular weight

of 2 700, 10 000, 22 600, 40 000, and 100 000 Da were grafted onto a surface having poly(glycidyl methacrylate) as an ultrathin film anchoring layer. It was found that the grafting density, surface coverage and grafting thickness all strongly depended on the PEO chain length. A maximum grafting density of 2 chains/nm^2 was achieved with the shortest chain length selected. With the increase of PEO chain length, the grafting density decreased quickly to less than 0.1 chains/nm^2. The grafting thickness also decreased with increased chain length. The surface coverage initially increased when the number of EO units were in the range of 61 to 227 and passed through a maximum of about 12 mg/m^2 at n = 200~300. The surface coverage then decreased dramatically to ~6 mg/m^2 for a larger n. The strong dependence of chain conformation on grafted PEO chain length suggests that the chain length also has a strong effect on the modified surface properties. It is well established that longer chain length leads to lower grafting density because of larger polymer radius. Earlier grafted polymer chains with larger radii are more significant obstacles on the surface. Furthermore, free polymer chains having larger radius are also more difficult to diffuse through the grafted polymer layer. As a result, the saturation state is reached at lower grafting density for longer polymer chain length. However, the effect of chain length on surface coverage and overlapping degree is more complex and is still not very clear. Knowledge about the effect of chain length on diffusion rate during the grafting process is also lacking.

The choice of solvent is another important factor determining chain conformation on the surface as a result of the "graft to" method. A systematic study was carried out by Huang *et al.*[47] on the effect of solvent quality, expressed as χ-parameter, for PEO chains on the silica surface. A series of nonpolar organic solvents having different solvent quality were investigated. The results showed that decreasing solvent quality led to increased grafting density. The reason stated was that decreasing solvent quality decreased the radii of polymer chains. Steric repulsion of grafted polymer layer diminished leading to a lower energy barrier for grafting of later chains. As a result, a higher grafting density was obtained with poor solvent. Based on this observation, the authors suggested the use of poor solvent instead of good solvent to obtain a densely grafted layer. Other factors like solvent temperature and pH have also been investigated. These factors, however, are interrelated and often affect several aspects simultaneously (Flory radius, diffusion property in solution etc.). As a result, their effects are still obscured.

For the "grafting to" process, there are many interesting topics, e.g. polymer reactions on the surface and polymer diffusion through polymer brushes. A picture of the "grafting to" method is given as shown in Scheme 1-2. The grafting process can be divided into three steps:

- Step I: Mass-center diffusion of polymer chains through boundary layer

- Step II: Diffusion of polymer chains through grafted polymer layer on surface
- Step III: Surface reaction between polymer chains and surface active sites

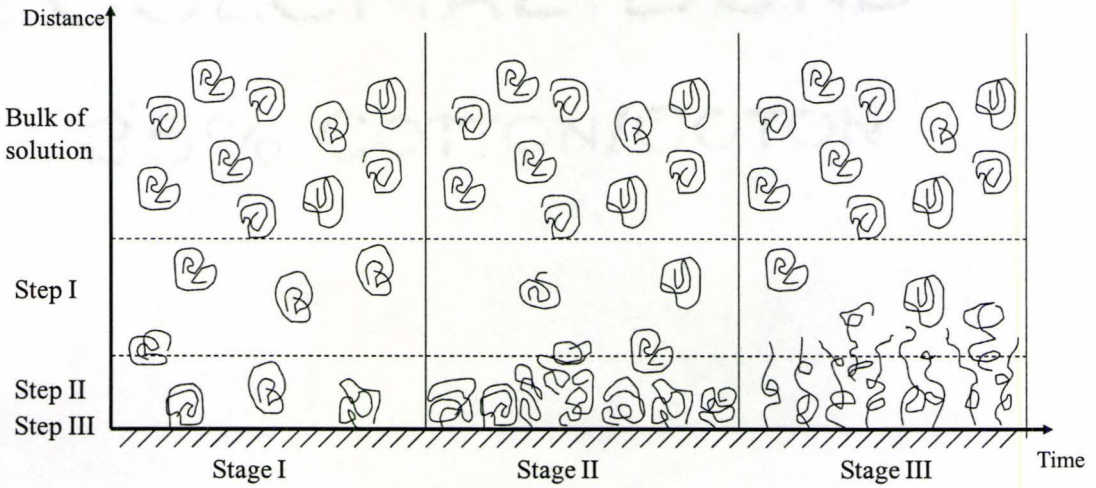

Scheme 1-2 Kinetic scheme of grafting polymer chains onto surface.

The free polymer chains in bulk solution must experience these steps before being attached onto a solid surface through covalent bonding. These three steps are continuous, so a rate-determining step may exist at different stages. Based on the conformation of the grafted polymer chains on surface, the whole grafting process can be divided into three stages:

- Stage I: Mushroom conformation stage
- Stage II: Transition stage between mushroom and brush
- Stage III: Brush conformation stage

In the previous kinetic studies, Stage I and Stage III were readily distinguished

because the grafting rate decreases dramatically in Stage III.[48] Research activities reported in literatures are mainly focused on Stage III. Some research has also been carried out on the transition stage because it determines the change of conformation from mushroom to brush. In Penn's research group, an auto-acceleration was observed in Stage III and a "three stages of kinetics" was proposed.[37]

In Stage I, grafted polymer chains in the mushroom conformation are separated from each other such that former grafted polymer chains on the surface do not influence grafting of later polymer chains. The grafting rate in Stage I is highest throughout the whole process of grafting. The time needed to obtain high grafting density on a solid surface is always long when this "grafting to" method is employed, but it only takes a short time for Stage I to finish.[49,50] As a result, Stage I seems the easiest step to accomplish and it is simply viewed as a mass-center diffusion-control step.[37,51,52] However, in Stage I, there exist two steps for a free polymer chain to be grafted onto surface. These are diffusion of chains to the surface and the surface reaction. Either of these steps could be the rate-determining mechanism in Stage I.

Stage II is an important stage because it determines the time when the chain conformation changes from mushroom to brush. This transformation can be distinguished by a detailed kinetic study of grafting process. Upon the completion of Stage I, the influence of grafted polymer chains can be distinguished by modeling studies. In fact, the

former chains on surface have a barrier effect before they overlap. No detailed kinetic research about Stage I and this transition stage has been reported so far, to our best knowledge.

Stage III determines the brush conformation in the "grafting to" method. The previously grafted chains on the surface form a brush barrier. Free polymer chains must diffuse through the barrier and react with reactive sites on the surface to be grafted. With the increase of grafting density, this grafted layer also becomes denser and denser until a saturation state is reached. The grafting density is the maximum value that can be obtained under this condition. The diffusion ability of free chains through grafted layer is the determining factor for the final grafting density. The diffusion rate is always low and it takes long time to reach the saturation state. Although this diffusion is very important, its understanding is very lacking. This type of diffusion through brush layer differs from typical diffusion in polymer solution. It is termed as inhomogeneous diffusion because of its special character. When a free polymer chain diffuses into grafted polymer brushes from solution, the grafted polymer chains stretch out further to create space for the incoming chain. The incoming chain also stretches due to the crowding of grafted chains on the surface. This process is more complex than a simple diffusion and it is always studied with thermodynamic approaches with an emphasis on the influencing factors which determine the final saturation state.

In the "grafting from" method, however, this diffusion problem does not exist because only small molecules, e.g. monomer and catalyst species, need to diffuse to the surface. As shown in Scheme 1-3, polymer chains grow from initiators bound to surface and a high grafting density can be achieved because of the absence of diffusion limitations. As a result, this method is preferred to prepare polymer brushes from various surfaces with high grafting density. However, the problem with "grafting from" is that it is difficult to control the polymer chain growth from surface. The properties of final grafted polymer chains, e.g. chain length and polydispersity, are very difficult to be measured. In order to overcome these disadvantages, surface-initiated living polymerization method has attracted great interest in this field.

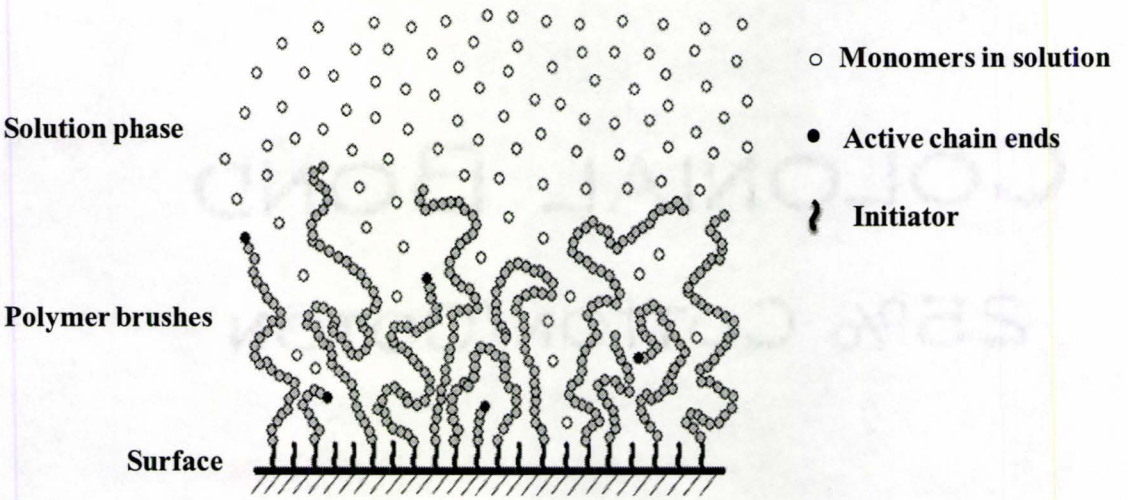

Scheme 1-3 The scheme of surface-initiated polymerization.

1.2 Surface-initiated living radical polymerization

1.2.1 Background of controlled/living radical polymerization

Living polymerization technique is a powerful tool to prepare polymers with controlled molecular weight and low polydispersity. The preparation of controlled architecture, e.g. block copolymers, can only be achieved by a living polymerization method. Living ionic method, which has been applied in industries, is well developed to fulfill these tasks. The limitation of living ionic polymerization lies in its strict requirement of reaction conditions. The ionic reaction centers are so active that they may be terminated easily by solvent and impurities. As a result, the living ionic polymerization is always bearing with high costs. Furthermore, because the ionic reaction centers are sensitive to polar chemicals, the versatility of monomers, radicals and solvents is limited.

Free radical polymerization is the most popular method in the polymer industry for vinyl monomers. Free radical centers are highly active, but less sensitive to impurities. The radical polymerization can be carried out under mild conditions and in polar solvents. They have been applied to a great variety of monomer types, e.g. methyl methacrylate, styrene, ethylene, vinyl chloride, acrylamide, etc. As a result, the development of living radical polymerization method is highly desirable. It enables living polymerization

process under mild conditions.

The key to convert conventional radical polymerization to living process is to control radical termination.[53,54] This can be done through the use of a reversible activation-deactivation reaction. As shown in Scheme 1-4, the dormant species P-X is activated to the reactive radical $P^{\bullet}$. The radicals then react with monomers. Propagation occurs until the radicals are deactivated by a certain kind of deactivator and become dormant again. This reversible activation-deactivation process is very fast. Few monomer molecules can be added to the growing chains during a single cycle. As a result, all chains in the system grow simultaneously with the same probability during the whole reaction, which accounts for the low polydispersity of molecular weight distribution. The radical concentration remains at a very low level to minimize the termination.

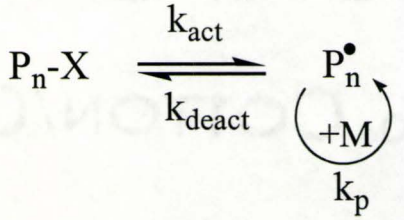

Scheme 1-4 The reversible activation-deactivation process in controlled/living radical polymerization.

There are three capping techniques successfully developed to achieve living radical polymerization: Stable free-radical polymerization (SFRP) using stable nitroxide

radical as radical capping agent,[55] reversible addition-fragmentation chain transfer (RAFT) polymerization using thiocarbonylthio,[56,57] and atom transfer radical polymerization (ATRP) employing halogen atom for the radical capping purpose.[54]

1.2.2 Stable free-radical polymerization (SFRP)

In the stable free-radical polymerization, a nitroxide radical, e.g. 2,2,6,6-tetramethyl-1-piperidinoxyl (TEMPO), is employed to cap the active radicals. Initiators commonly used in conversional free radical polymerization such as peroxides and azo compounds can be employed in SFRP. During the polymerization, the radicals are reversibly capped and released by the nitroxide radicals. The radical concentration in the system is therefore minimized to suppress the radical termination. SFRP is one of the earliest developed living radical polymerization methods. However, it can only be applied to a limited number of monomer types, mainly styrenics.

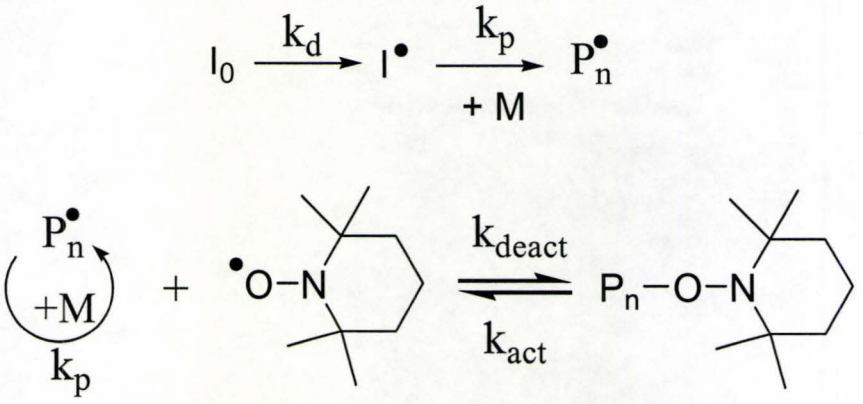

Scheme 1-5 The mechanism of stable free-radical polymerization.

1.2.3 Reversible addition-fragmentation transfer (RAFT)

RAFT polymerization with dithio compounds was discovered by Rizzardo *et al.*[51] A reversible addition-fragmentation chain transfer (Scheme 1-6) process sets up the activation and deactivation mechanism required by living polymerization.

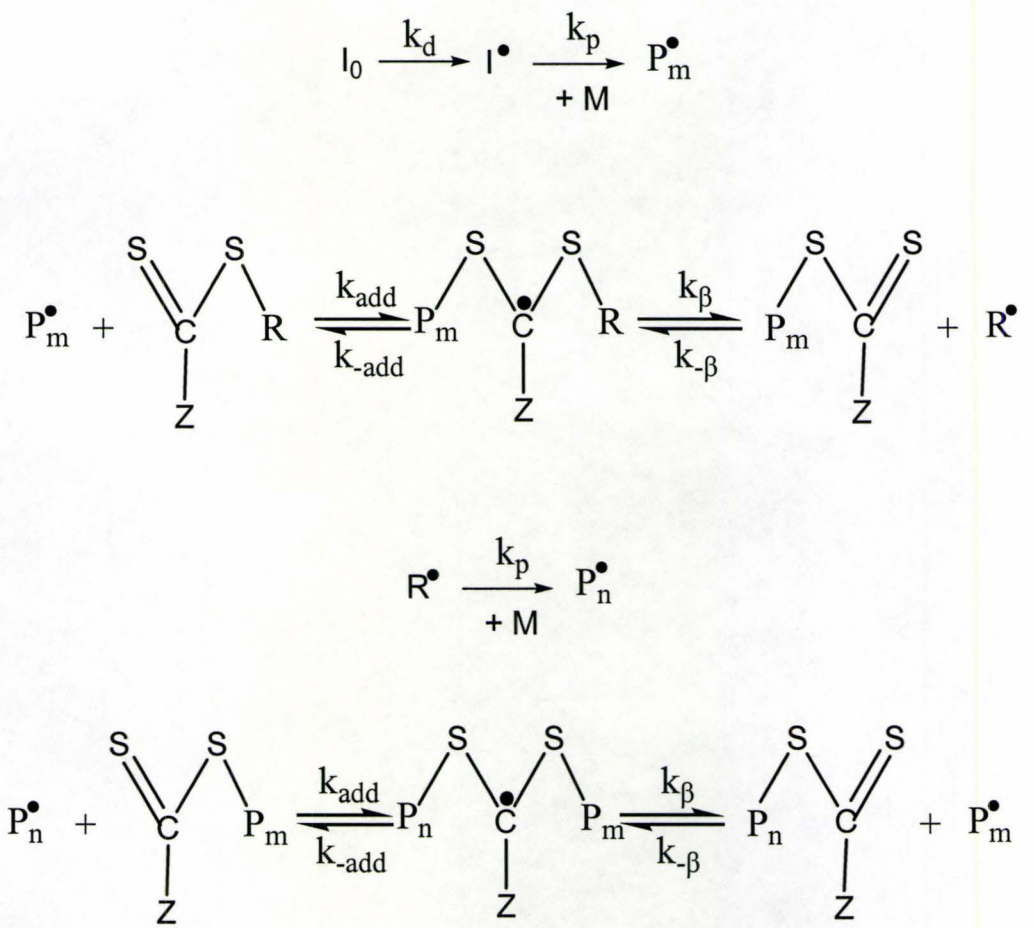

Scheme 1-6 The mechanism of reversible addition-fragmentation chain transfer polymerization.

I_0 is the regular initiator used in conventional free radical polymerizations. The addition of radical $P_m^{\bullet}$ to dormant chain TP_n forms intermediate radicals. The adduct radicals are not stable and fragmentation happens that releases either $P_m^{\bullet}$ or $P_n^{\bullet}$. This reversible addition-fragmentation transfer process is viewed as a degenerative chain transfer process as shown in Scheme 1-7, where k_{tr} is the rate constant of the exchange reaction. A high chain transfer coefficient is the key factor for a successful RAFT polymerization.

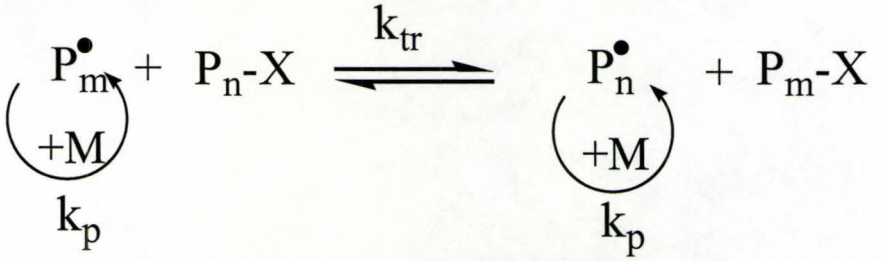

Scheme 1-7 The mechanism of degenerative chain transfer.

Numerous investigations have been done on the RAFT transfer rate and the effect of transfer coefficient on polydispersity. The effect of substituent of various RAFT agents on their transfer coefficient were investigated in great details.[58,59] The use of highly reactive thiocarbonylthio RAFT agents having high chain transfer rate for these systems makes it possible to obtain polymers with narrow molecular weight distribution (MWD). Cumyl dithiobenzoate, cyanoisopropyl dithiobenzoate, methoxycarbonylphenylmethyl dithiobenzoate, and a-cyanobenzyl dithiobenzoate are four examples among the most

popular RAFT agents.[60] The advantages of RAFT lie in its applicability to a wide range of monomer types.

1.2.4 Atom transfer radical polymerization (ATRP)

The atom transfer radical polymerization (ATRP) is one of the most useful discoveries in the field of living polymerization and it is among the most rapidly developing areas of polymer science because of its tolerance to a wide range of functional monomers and less stringent experimental conditions.[54,61,62] The mechanism is shown in Scheme 1-8.

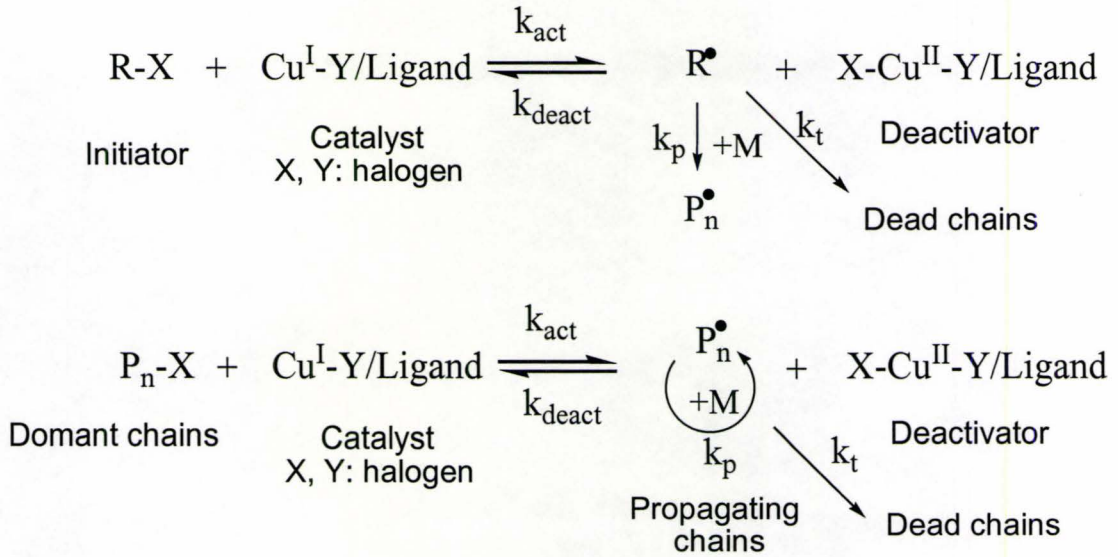

Scheme 1-8 The mechanism of atom transfer radical polymerization.

Alkyl halides are used as the initiator in ATRP. Transition-metal complexs with

ligands, e.g. CuCl, CuBr, are used as catalyst. The catalyst converts dormant species to radicals by taking away the halide group. The dormant species P-X is activated to the reactive radical $P^{\bullet}$. The radicals then react with monomers until the radicals are deactivated by the deactivator species and become dormant again. The deactivation rate is much faster than the activation rate, as a result, this reversible activation-deactivation process is so fast that only few monomer molecules can be added to the chains during a single cycle. All polymerization chains grow at the same time with the same opportunity during the polymerization. This enables the achievement of final polymer products with low polydispersity, normally at the level of 1.1~1.2. The radical concentration in the polymerization system is minimized to decrease termination.

1.2.5 Surface-initiated living polymerization

It was expected that applying the above living polymerization methods to surface-initiated polymerization would allow for excellent control over chain growth from surface. Recently, many studies have employed various living polymerization techniques to grow polymer chains from various surfaces.[12] Among them, RAFT and ATRP have obtained greatest interest, as SFRP are mainly limited to styrenics. However, RAFT and ATRP have tolerance to a wide range of functional monomers and require less stringent experimental conditions.[54,61,62]

When using RAFT for surface-initiated polymerizations, there are three strategies which can be employed. These three strategies exist due to the fact that in surface-initiated RAFT, one can begin with grafting either the initiator, the RAFT agent at the anchoring group (Z) or the RAFT agent at the leaving group (R). When the R group is grafted to surface, the RAFT agent can be attacked by radicals in solution and leaves the surface. A radical on the surface is then generated and a chain starts to grow from the surface. In a very short period of time, it is deactivated by another RAFT agent in solution. During the polymerization, the RAFT moieties are always at polymer chain ends on the surface. However, when the RAFT agent is grafted to the surface by the Z group, it stays on the surface and remains at the bottom. Polymer radicals in solution need to diffuse through the grafted polymer layer to reach the RAFT moieties. For this reason, it can also be viewed as a mixture of "grafting from" and "grafting to" method.

In the surface-initiated RAFT research, grafting the initiator and grafting the RAFT agent at the R group are the two most popular methods of polymerization. Synthesis of an effective RAFT agent is one of the most challenging aspects of this research. A couple of surface modification steps are needed to graft a RAFT agent to surface. Li *et al.*[63] synthesized a RAFT agent which can be directly grafted onto surface by the R group. Grafting a RAFT agent to a surface by the Z group was first accomplished by Perrier *et al.*[64] in 2005 and was then studied by other research

groups.[65-67] However, many steps of surface modification were involved. So far no RAFT agents which can be directly grafted onto surface by Z group without surface modification have been reported.

There are many disadvantages to the use of RAFT for surface modification, however. The most challenging, as was mentioned above, is the difficulty of preparing a RAFT initiator. Also, the slower decomposition rate of the RAFT initiators on the surface will lead to lower grafting density, as the initiators on the surface will be buried quickly by the growing polymer chains. Finally, at the end of grafting by RAFT method a layer of RAFT agents remain at the surface. These RAFT agents may significantly alter the surface properties.

Surface-initiated ATRP, on the other hand, has become the most widely used method for the "graft from" method. In this case, the ATRP initiator is grafted onto the surface. In solution, conventional solution ATRP occurs when free initiators are added to the solution. The solution polymerization is a typical ATRP process including activation, deactivation, propagation, termination and chain transfer. Although the density of initiator on the surface can be high, the total amount is extremely low. It does not influence reactions in the solution. The activation, deactivation, propagation and chain transfer are reactions between polymer chains on the surface and small molecules in the solution (i.e. monomer, catalyst, and deactivator). All polymer chains grow

simultaneously. Although one end of polymer chain is attached to the surface, the free end stretches out into the solution. It is assumed that the other attached end has no effect on it. The small molecules are diffusing around free polymer chain ends as in solution polymerization. As a result, these reactions are the same as those happening in the solution. Many studies have shown that the grafted chain lengths are similar to those formed in the solution,[20,25,68] suggesting that the grafted chains on surface experience similar reactions as the free chains in solution. A great variety of monomer types have been successfully grafted from various surfaces to obtain desirable surface properties. The effects of polymer type, degree of polymerization, grafting thickness, and initiator density on surface properties have been extensively investigated.

1.3 Stimuli-responsive surfaces

1.3.1 Stimuli-responsive surfaces

Stimuli-responsive surfaces, so-called "smart surfaces", refer to surfaces which can change their properties (e.g. hydrophilicity, biological activity, protein adsorption/repulsion, cell adhesion, migration, etc.) in response to small changes in the external environment such as solvent type, pH, temperature, electric and magnetic fields, etc.[69,70]. The stimuli-responsive ability is achieved by the materials grafted onto the surface. These smart materials are mainly self-assembled monolayers (SAMs) or polymer

brushes. SAM is a layer forming spontaneously from surfactants on surface.[71,72] Their properties can be easily controlled. Special functionalities are introduced by choosing different surfactants. Most smart surfaces, however, are prepared by grafting polymer brushes onto surfaces.[73-75]

In biotechnology and medicine fields, there have been great interests in these smart surfaces because of their potential applications to develop novel advanced medical devices.[69] A lot of progress has been seen recently making full use of these smart surfaces in the areas of bioseparation, drug delivery, gene therapy and implants. On the other hand, these surfaces have ability to convert biological events to measurable electronic or opto-electronic signals. They can be thus employed to produce biosensors for bioanalysis, clinical diagnosis and environmental monitoring etc.

1.3.2 Stimuli-responsive block copolymer brushes on surfaces

Grafting polymer brushes with different chemical compositions is one of the strategies to achieve stimuli-responsive properties.[75-78] The difference in properties between two blocks can bring notable variation of surface properties by external stimuli. So far, there are two methods developed to achieve polymer brushes on the surface with more than one composition: mixed polymer brushes or block polymer brushes. The results showed that their stimuli-responsive behaviors are similar.

To obtain mixed polymer brushes on surface by the "grafting from" method, two types of initiators or one type of slowly decomposing initiator must be grafted onto the surface. The polymer chains thus grow from the surface in-situ to form two types of polymer chains. However, the synthesis is difficult, especially when the uniform distribution of two different types of polymers is desired. The properties of these polymers often differ a lot in order to achieve notable surface property variations. As a result, when the first layer of polymer brushes has formed on the surface, it becomes challenging for the later growing of the second type of polymer chains. Furthermore, phase segregation can occur during the preparation process, which decreases the quality of the final surface.

Block copolymer brushes can be precisely controlled in terms of chemical composition on the surface. The first synthesis of block copolymer brushes on a surface by surface-initiated living polymerization was in 1999. Zhao *et al.*[79] prepared polystyrene (PS) -block- poly(methyl methacrylate) (PMMA) brushes on silicate substrates by sequential carbocationic polymerization of styrene and ATRP of MMA. In the following years, other living polymerization methods have also been applied to prepare block copolymer brushes on various surfaces.[14]

The stimuli-responsive capacity of block copolymer brushes on surface was thoroughly investigated by theoretical methods first, rather than experiments. With both

SCF and scaling methods, Zhulina *et al.*[80] predicted the structures of block copolymer brushes on surface at exposure to different solvents. As shown in Scheme 1-9, the conformation of copolymer brushes may differ at different environments. The surface properties change as a result according to the external stimuli. The formation of certain structure is determined by many factors including polymer chain length, grafting density, relative block chain length, composition of the blocks, and the surrounding environment. The possible brush structures, mechanism of phase reconstruction, and influencing factors were all studied in the following years.[73]

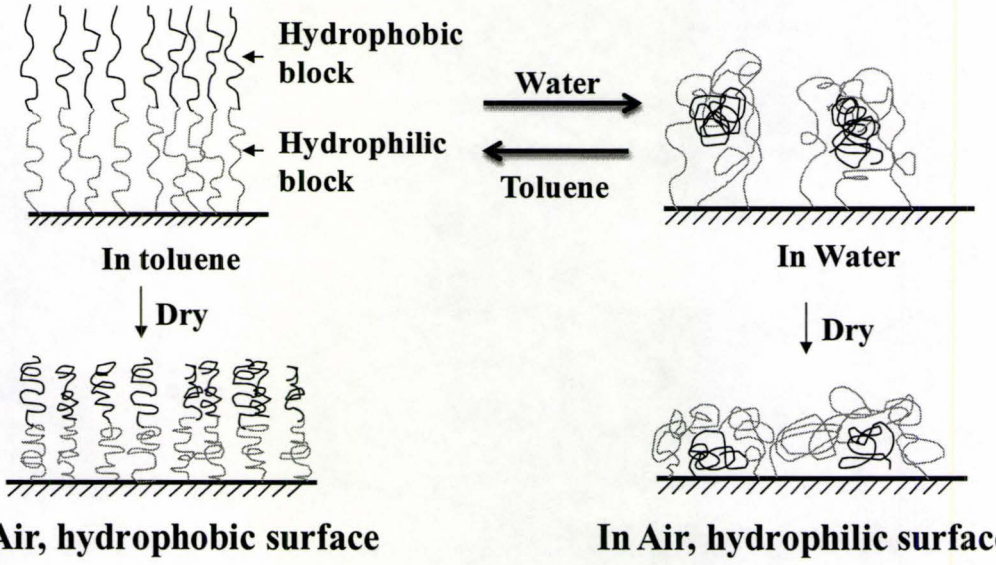

Scheme 1-9 The structures of amphiphilic block copolymer brushes on the surface under different environments.

In 1999 study, Zhao *et al.*[79] experimentally verified the above theoretical prediction of phase reconstruction for block copolymer brushes on surface for the first

time. They synthesized PS-b-PMMA on silicate substrates and demonstrated the phase reconstruction by treating samples in different solvents. In the following years, the stimuli-responsive capacity of the block copolymer brushes grafted on the surface were thoroughly investigated by contact angle method, X-ray photoelectron spectroscopy (XPS), ellipsometry.[79,81-89] Various conformations of polymer brushes on the surface were observed by atomic force microscopy (AFM). Block copolymer brushes with different chemical compositions were synthesized to study the solvent induced reconstruction. Specific research on certain influencing factors predicted by the theoretical methods has also been carried out. For example, Xu *et al.*[87] investigated the effect of relative block lengths on surface response to solvents. They found that there existed three responsive regions according to relative block length: responsive region, partial-responsive region and non-responsive region.

In the following studies, another phenomenon, nanoscale patterns, was observed on the surface grafted with these block copolymer brushes. These nanopatterns were introduced from the phase segregation. The self-assembly of block copolymers is well-known to give different patterns through phase segregation between different blocks. The patterns forming in this way are in the size range of 10 to 100 nm.[77,78,90,91] This phase segregation of grafted block copolymer brushes on the surface was first observed by Zhao *et al.* in 2000.[92] Zhao and Brittain *et al.*[81] grafted PS-b-PMMA brushes onto the flat

surfaces. With AFM method periodic nanopatterns in nanoscale were observed after the treatment of selective solvents.

Lithography has been the most popular technique for the preparation of micro- or nano structures. Various well-designed lithography techniques have been developed to produce nanopatterns for different purposes. However, one major disadvantage of the lithography method is its high cost and time consuming procedure. Electron-beam or certain probe tips, e.g. dip-pens, must be employed when the desired feature size is less than 100 nm.[71,77] On the contrary, self-assembly is a much simpler solution to prepare nanoscale pattern at lower costs. If the self-assembly of block copolymer brushes can also be employed to prepare nanoscale patterns, it could be a powerful method for nanopatterning.

When spin-casting of free block copolymers is employed to prepare nanopatterns on surface, solubility or swelling of polymer films causes some problem.[71] In contrast, graft polymer brushes are chemically grafted onto the surface, therefore stable nanopatterns can be achieved. Furthermore, living polymerization methods can give polymer brushes active chain ends. Further modifications can then introduce special functions to the patterns.[93,94] The unique property of these nanopatterns prepared by the self-assembly of block copolymer brushes is their stimulus-responsive ability. For the applications where only periodic nanopatterns are required, this method could be

advantageous considering its low cost and ability to prepare large area patterns.

After the pioneering work of Zhao *et al.*[92], many studies have been carried out to explore the ability of block copolymer brushes in preparing nanoscale patterns. Genzer and Ruhe *et al.* observed different morphologies including flat, micellar and bicontinuous morphologies when they changed the length of each block.[80,95] In addition, they used the variation of topography to move the nanoscale objects on surfaces[96,97] Choi *et al.* prepared the block copolymer brushes on surface by the surface-initiated ring-opening method.[89] Their results showed that solvent treatments also affect the formation of nanopatterns. In order to achieve more uniform patterns through this method, Bruening and Baker *et al.* prepared amphiphilic triblock copolymer brushes. More uniform domain sizes were obtained in their studies.[83] In 2008, Shi *et al.* proved that the self-assembly of densely grafted block copolymer brushes could give different patterns including spherical aggregate, wormlike and stripe *etc.* when the upper block thickness was varied.[98] All these studies showed that the self-assembly of block copolymer brushes is a novel promising method to give nanoscale patterns.

1.3.3 Thermo-responsive PEG-based polymer brushes on surface

Thermo-responsive surfaces refer to surfaces that can respond to external temperature variation. It is easy to regulate temperate as the stimulus. In addition, a

moderate variation of temperature close to physiological temperature has little effect on biosystems. As a result, thermo-responsive surfaces are one of the most important stimuli-responsive surfaces. Many thermo-responsive surfaces have been developed in the biological and medical fields.[99-102]

Until recently, poly(N-isopropylacrylamide) (PNIPAM) and its copolymers[74,75,103] were the most popular polymer materials used for thermo-responsive purposes. The amide groups in PNIPAM have different hydrogen-bonding interactions with water at different temperatures. When temperature is below its lower critical solution temperature (LCST), 32°C, well-developed hydrogen bonds form between water and the amid groups, causing the PNIPAM polymer brushes to be well-extended in water. However, when temperature is increased to above 32°C, the hydrogen bonds are broken and the polymer chains collapse on the surface. The surface properties change considerably with only small temperature variation. Based on this property, PNIPAM has been used widely for various thermo-responsive surface developments.

Poly(2-(2-methoxyethoxy)ethyl methacrylate -co- oligo(ethylene glycol) methacrylate) (P(MEO_2MA-co-OEGMA)), as shown in Scheme 1-10, is a new class of thermo-responsive materials which has generated a great of attention recently. The oligo(ethylene glycol) component in this type of copolymers has different interactions with water when temperature varies.[104-109] It has a LCST in the same way that PNIPAM

does in water. When temperature is below the LCST, a well-developed hydration layer forms around the oligo(ethylene glycol) groups. The polymer chains are thus very soluble. However, when temperature is increased above LCST, the hydrogen bonds between the polymer chains and water are disrupted. The polymer-polymer interactions are favored over the polymer-water interactions. As a result, the phase transition happens and the polymers precipitate out from water. This phase transition is a reversible process. The LCST can be adjusted from 26 to 92°C by varying the monomer composition.

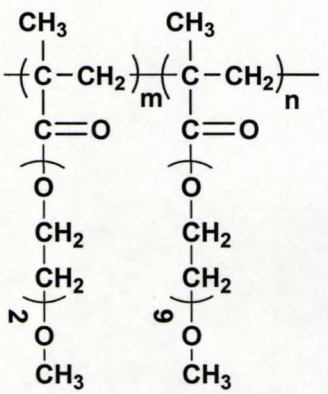

Scheme 1-10 The chemical structure of poly(2-(2-methoxyethoxy)ethyl methacrylate -co- oligo(ethylene glycol) methacrylate).

The main advantage of employing P(MEO_2MA-co-OEGMA) as the thermo-responsive materials is that it is a PEG-based polymer. PEG-based materials have been widely used as biocompatible materials because their ability to resist non-specific protein and cell adsorption. They are also non-toxic and non-immunogenic. The

thermo-responsive surfaces prepared from this type of PEG-based materials may yield new products, which can be used inside the human body.

Until recently, studies on the thermo-responsive surfaces based on P(MEO_2MA-co-OEGMA) were limited. In 2007, Huck *et al.*,[100] for the first time, verified the thermo-responsive behavior of surfaces grafted with P(MEO_2MA-co-OEGMA). They grafted the copolymer onto flat surfaces using a surface-initiated ATRP method. The thermo-responsive collapse transition of polymer brushes on the surface was observed. In 2008, Lutz *et al.*[110] used these thermo-responsive surfaces to control cell-adhesion. The cells had different morphologies when the polymer brushes changed their conformations with the variation of temperature.

The conformation study of P(MEO_2MA-co-OEGMA) brushes on the surface is limited to aqueous AFM work by Huck *et al.*[100]. The AFM can measure the thickness of polymer layer in water directly. The collapse transition of polymer brushes at their LCST was observed. However, the measurement of polymer brush thickness by an aqueous AFM method is approximate, as polymer brushes in a good solvent are well-extended into the solvent. The AFM tip penetrates into the polymer brushes, which further complicates the measurement.

Although the main advantage claimed for these PEG-based materials is their

biocompatibility, the protein repulsion ability of the surfaces modified by this new type of PEG-based brushes has not been studied so far, to our best knowledge. HomoPOEGMA has proven to be good materials for protein resistance, but popular candidates employed for various applications have at least 4.5 repeat EO units.[93,111,112] These new thermo-responsive copolymers, however, have around 90% POEGMA with only two EO repeat units. As a result, the biocompatibility of these materials is still unknown. In addition, no study about the protein resistance of these materials in the collapsed state at temperature above LCST has been reported yet. If the collapsed polymer brushes adsorb large amount of proteins at temperatures above LCST, their applications could be limited.

1.4 References

1. Griffith, L. G. *Acta Mater.* **2000,** *48* (1), 263-277.
2. Brash, J. L. *Biomaterials* **2005,** *26* (35), 7209-7220.
3. Ramakrishna, S.; Mayer, J.; Wintermantel, E.; Leong, K. W. *Compos. Sci. Technol.* **2001,** *61* (9), 1189-1224.
4. Currie, E. P. K.; Norde, W.; Stuart, M. A. C. *Adv. Colloid Interface Sci.* **2003,** *100*, 205-265.
5. Granick, S.; Kumar, S. K.; Amis, E. J.; Antonietti, M.; Balazs, A. C.; Chakraborty, A. K.; Grest, G. S.; Hawker, C.; Janmey, P.; Kramer, E. J.; Nuzzo, R.; Russell, T. P.;

Safinya, C. R. *J. Polym. Sci. Pt. B-Polym. Phys.* **2003,** *41* (22), 2755-2793.

6. Kato, K.; Uchida, E.; Kang, E. T.; Uyama, Y.; Ikada, Y. *Prog. Polym. Sci.* **2003,** *28* (2), 209-259.
7. Martin, J. I.; Wang, Z. G. *J. Phys. Chem.* **1995,** *99* (9), 2833-2844.
8. Naji, A.; Seidel, C.; Netz, R. R. Theoretical approaches to neutral and charged polymer brushes. 2006; pp 149-183.
9. Netz, R. R.; Andelman, D. *Phys. Rep. -Rev. Sec. Phys. Lett.* **2003,** *380* (1-2), 1-95.
10. Netz, R. R.; Schick, M. *Macromolecules* **1998,** *31* (15), 5105-5122.
11. Storm, G.; Belliot, S. O.; Daemen, T.; Lasic, D. D. *Adv. Drug Deliv. Rev.* **1995,** *17* (1), 31-48.
12. Edmondson, S.; Osborne, V. L.; Huck, W. T. S. *Chem. Soc. Rev.* **2004,** *33* (1), 14-22.
13. Bhat, R. R.; Tomlinson, M. R.; Wu, T.; Genzer, J. Surface-grafted polymer gradients: Formation, characterization, and applications. 2006; pp 51-124.
14. Brittain, W. J.; Boyes, S. G.; Granville, A. M.; Baum, M.; Mirous, B. K.; Akgun, B.; Zhao, B.; Blickle, C.; Foster, M. D. Surface rearrangement of diblock copolymer brushes - Stimuli responsive films. 2006; pp 125-147.
15. Matsuda, T. Photoiniferter-driven precision surface graft microarchitectures for biomedical applications. 2006; pp 67-106.

16. Ruhe, J.; Ballauff, M.; Biesalski, M.; Dziezok, P.; Grohn, F.; Johannsmann, D.; Houbenov, N.; Hugenberg, N.; Konradi, R.; Minko, S.; Motornov, M.; Netz, R. R.; Schmidt, M.; Seidel, C.; Stamm, M.; Stephan, T.; Usov, D.; Zhang, H. N. Polyelectrolyte brushes. 2004; pp 79-150.

17. Senaratne, W.; Andruzzi, L.; Ober, C. K. *Biomacromolecules* **2005,** *6* (5), 2427-2448.

18. Devaux, C.; Chapel, J. P.; Beyou, E.; Chaumont, P. *Eur. Phys. J. E* **2002,** *7* (4), 345-352.

19. Ejaz, M.; Ohno, K.; Tsujii, Y.; Fukuda, T. *Macromolecules* **2000,** *33* (8), 2870-2874.

20. Ejaz, M.; Tsujii, Y.; Fukuda, T. *Polymer* **2001,** *42* (16), 6811-6815.

21. Feng, W.; Chen, R. X.; Brash, J. L.; Zhu, S. P. *Macromol. Rapid Commun.* **2005,** *26* (17), 1383-1388.

22. Feng, W.; Brash, J. L.; Zhu, S. P. *Biomaterials* **2006,** *27* (6), 847-855.

23. Jeyaprakash, J. D.; Samuel, S.; Dhamodharan, R.; Ruhe, J. *Macromol. Rapid Commun.* **2002,** *23* (4), 277-281.

24. Jones, D. M.; Brown, A. A.; Huck, W. T. S. *Langmuir* **2002,** *18* (4), 1265-1269.

25. Kizhakkedathu, J. N.; Brooks, D. E. *Macromolecules* **2003,** *36* (3), 591-598.

26. Liu, Y.; Klep, V.; Zdyrko, B.; Luzinov, I. *Langmuir* **2005,** *21* (25), 11806-11813.

27. Zhao, B.; Haasch, R. T.; MacLaren, S. *J. Am. Chem. Soc.* **2004,** *126* (19), 6124-6134.

28. Milchev, A.; Wittmer, J. P.; Landau, D. P. *J. Chem. Phys.* **2000,** *112* (3), 1606-1615.

29. Coote, M. L.; Gordon, D. H.; Hutchings, L. R.; Richards, R. W.; Dalgliesh, R. M. *Polymer* **2003,** *44* (25), 7689-7700.

30. O'Shaughnessy, B.; Vavylonis, D. *J. Phys. -Condes. Matter* **2005,** *17* (2), R63-R99.

31. OShaughnessy, B.; Sawhney, U. *Macromolecules* **1996,** *29* (22), 7230-7239.

32. Hasegawa, R.; Doi, M. *Macromolecules* **1997,** *30* (18), 5490-5493.

33. Shull, K. R. *J. Chem. Phys.* **1991,** *94* (8), 5723-5738.

34. Shull, K. R. *Macromolecules* **1996,** *29* (7), 2659-2666.

35. Fredrickson, G. H. *Phys. Rev. Lett.* **1996,** *76* (18), 3440-3443.

36. Fredrickson, G. H.; Milner, S. T. *Macromolecules* **1996,** *29* (23), 7386-7390.

37. Penn, L. S.; Huang, H.; Sindkhedkar, M. D.; Rankin, S. E.; Chittenden, K.; Quirk, R. P.; Mathers, R. T.; Lee, Y. *Macromolecules* **2002,** *35* (18), 7054-7066.

38. Li, T. L.; Park, K. N. *Comput. Theor. Polymer Sci.* **2001,** *11* (2), 133-142.

39. Lai, P. Y.; Binder, K. *J. Chem. Phys.* **1991,** *95* (12), 9288-9299.

40. Smith, G. D.; Zhang, Y.; Yin, F.; Bedrov, D.; Dadmun, M. D.; Huang, Z. Y.

Langmuir **2006,** *22* (2), 664-675.

41. Kopf, A.; Baschnagel, J.; Wittmer, J.; Binder, K. *Macromolecules* **1996,** *29* (5), 1433-1441.

42. Ball, R. C.; Marko, J. F.; Milner, S. T.; Witten, T. A. *Macromolecules* **1991,** *24* (3), 693-703.

43. Wijmans, C. M.; Zhulina, E. B. *Macromolecules* **1993,** *26* (26), 7214-7224.

44. Zhao, B.; Brittain, W. J. *Prog. Polym. Sci.* **2000,** *25* (5), 677-710.

45. Clarke, C. J.; Jones, R. A. L.; Clough, A. S. *Polymer* **1996,** *37* (17), 3813-3817.

46. Zdyrko, B.; Varshney, S. K.; Luzinov, I. *Langmuir* **2004,** *20* (16), 6727-6735.

47. Huang, H. Q.; Fulchiero, E. C.; Penn, L. S. *J. Polym. Sci. Pol. Chem.* **2004,** *42* (21), 5530-5537.

48. Shybanova, O.; Voronov, S.; Bednarska, O.; Medvedevskikh, Y.; Stamm, M.; Tokarev, V. *Macromol. Symp.* **2001,** *164*, 211-218.

49. Huang, H.; Penn, L. S.; Quirk, R. P.; Cheong, T. H. *Macromolecules* **2004,** *37* (15), 5807-5813.

50. Huang, H. Q.; Rankin, S. E.; Penn, L. S.; Quirk, R. P.; Cheong, T. H. *Langmuir* **2004,** *20* (14), 5770-5775.

51. Kramer, E. J. *Isr. J. Chem.* **1995,** *35* (1), 49-54.

52. Motschmann, H.; Stamm, M.; Toprakcioglu, C. *Macromolecules* **1991,** *24* (12),

3681-3688.

53. Fischer, H. *J. Polym. Sci. Pol. Chem.* **1999,** *37* (13), 1885-1901.

54. Matyjaszewski, K.; Xia, J. H. *Chem. Rev.* **2001,** *101* (9), 2921-2990.

55. Georges, M. K.; Veregin, R. P. N.; Kazmaier, P. M.; Hamer, G. K. *Macromolecules* **1993,** *26* (11), 2987-2988.

56. Moad, G.; Rizzardo, E.; Thang, S. H. *Aust. J. Chem.* **2005,** *58* (6), 379-410.

57. Hawker, C. J.; Bosman, A. W.; Harth, E. *Chem. Rev.* **2001,** *101* (12), 3661-3688.

58. Chiefari, J.; Mayadunne, R. T. A.; Moad, C. L.; Moad, G.; Rizzardo, E.; Postma, A.; Skidmore, M. A.; Thang, S. H. *Macromolecules* **2003,** *36* (7), 2273-2283.

59. Chong, Y. K.; Krstina, J.; Le, T. P. T.; Moad, G.; Postma, A.; Rizzardo, E.; Thang, S. H. *Macromolecules* **2003,** *36* (7), 2256-2272.

60. Perrier, S.; Takolpuckdee, P. *J. Polym. Sci. Pol. Chem.* **2005,** *43* (22), 5347-5393.

61. Matyjaszewski, K.; Miller, P. J.; Shukla, N.; Immaraporn, B.; Gelman, A.; Luokala, B. B.; Siclovan, T. M.; Kickelbick, G.; Vallant, T.; Hoffmann, H.; Pakula, T. *Macromolecules* **1999,** *32* (26), 8716-8724.

62. Pyun, J.; Jia, S.; Kowalewski, T.; Patterson, G. D.; Matyjaszewski, K. *Macromolecules* **2003,** *36* (18), 6952.

63. Li, C. Z.; Benicewicz, B. C. *Macromolecules* **2005,** *38* (14), 5929-5936.

64. Perrier, S.; Takolpuckdee, P.; Mars, C. A. *Macromolecules* **2005,** *38* (16),

6770-6774.

65. Hernandez-Guerrero, M.; Davis, T. P.; Barner-Kowollik, C.; Stenzel, M. H. *Eur. Polym. J.* **2005,** *41* (10), 2264-2277.

66. Peng, Q.; Lai, D. M. Y.; Kang, E. T.; Neoh, K. G. *Macromolecules* **2006,** *39* (16), 5577-5582.

67. Stenzel, M. H.; Zhang, L.; Huck, W. T. S. *Macromol. Rapid Commun.* **2006,** *27* (14), 1121-1126.

68. Yamamoto, K.; Miwa, Y.; Tanaka, H.; Sakaguchi, M.; Shimada, S. *J. Polym. Sci. Pol. Chem.* **2002,** *40* (20), 3350-3359.

69. Galaev, I. Y.; Mattiasson, B. *Trends Biotechnol.* **1999,** *17* (8), 335-340.

70. Mendes, P. M. *Chem. Soc. Rev.* **2008,** *37* (11), 2512-2529.

71. Senaratne, W.; Andruzzi, L.; Ober, C. K. *Biomacromolecules* **2005,** *6* (5), 2427-2448.

72. Cox, J. K.; Eisenberg, A.; Lennox, R. B. *Curr. Opin. Colloid Interface Sci.* **1999,** *4* (1), 52-59.

73. Minko, S. *Polym. Rev.* **2006,** *46* (4), 397-420.

74. Zhou, F.; Huck, W. T. S. *Phys. Chem. Chem. Phys.* **2006,** *8* (33), 3815-3823.

75. Luzinov, I.; Minko, S.; Tsukruk, V. V. *Prog. Polym. Sci.* **2004,** *29* (7), 635-698.

76. Bates, F. S.; Fredrickson, G. H. *Annu. Rev. Phys. Chem.* **1990,** *41*, 525-557.

77. Geissler, M.; Xia, Y. N. *Adv. Mater.* **2004,** *16* (15), 1249-1269.

78. Stoykovich, M. P.; Nealey, P. F. *Mater. Today* **2006,** *9* (9), 20-29.

79. Zhao, B.; Brittain, W. J. *J. Am. Chem. Soc.* **1999,** *121* (14), 3557-3558.

80. Zhulina, E. B.; Singh, C.; Balazs, A. C. *Macromolecules* **1996,** *29* (19), 6338-6348.

81. Zhao, B.; Brittain, W. J.; Zhou, W. S.; Cheng, S. Z. D. *Macromolecules* **2000,** *33* (23), 8821-8827.

82. Kong, X. X.; Kawai, T.; Abe, J.; Iyoda, T. *Macromolecules* **2001,** *34* (6), 1837-1844.

83. Huang, W. X.; Kim, J. B.; Baker, G. L.; Bruening, M. L. *Nanotechnology* **2003,** *14* (10), 1075-1080.

84. Minko, S.; Muller, M.; Motornov, M.; Nitschke, M.; Grundke, K.; Stamm, M. *J. Am. Chem. Soc.* **2003,** *125* (13), 3896-3900.

85. Boyes, S. G.; Akgun, B.; Brittain, W. J.; Foster, M. D. *Macromolecules* **2003,** *36* (25), 9539-9548.

86. Kaholek, M.; Lee, W. K.; LaMattina, B.; Caster, K. C.; Zauscher, S. *Nano Lett.* **2004,** *4* (2), 373-376.

87. Xu, C.; Wu, T.; Drain, C. M.; Batteas, J. D.; Fasolka, M. J.; Beers, K. L. *Macromolecules* **2006,** *39* (9), 3359-3364.

88. Xu, C.; Wu, T.; Batteas, J. D.; Drain, C. M.; Beers, K. L.; Fasolka, M. J. *Appl. Surf. Sci.* **2006,** *252* (7), 2529-2534.

89. Kong, B.; Lee, J. K.; Choi, I. S. *Langmuir* **2007,** *23* (12), 6761-6765.

90. Cheng, J. Y.; Ross, C. A.; Smith, H. I.; Thomas, E. L. *Adv. Mater.* **2006,** *18* (19), 2505-2521.

91. Krausch, G.; Magerle, R. *Adv. Mater.* **2002,** *14* (21), 1579-1583.

92. Zhao, B.; Brittain, W. J.; Zhou, W. S.; Cheng, S. Z. D. *J. Am. Chem. Soc.* **2000,** *122* (10), 2407-2408.

93. Lee, B. S.; Lee, J. K.; Kim, W. J.; Jung, Y. H.; Sim, S. J.; Lee, J.; Choi, I. S. *Biomacromolecules* **2007,** *8* (2), 744-749.

94. Tugulu, S.; Arnold, A.; Sielaff, I.; Johnsson, K.; Klok, H. A. *Biomacromolecules* **2005,** *6* (3), 1602-1607.

95. Tomlinson, M. R.; Genzer, J. *Langmuir* **2005,** *21* (25), 11552-11555.

96. Prokhorova, S. A.; Kopyshev, A.; Ramakrishnan, A.; Zhang, H.; Ruhe, J. *Nanotechnology* **2003,** *14* (10), 1098-1108.

97. Santer, S.; Ruhe, J. *Polymer* **2004,** *45* (25), 8279-8297.

98. Yin, Y. H.; Sun, P. C.; Li, B. H.; Chen, T. H.; Jin, Q. H.; Ding, D. T.; Shi, A. C. *Macromolecules* **2007,** *40* (14), 5161-5170.

99. Van Durme, K.; Rahier, H.; Van Mele, B. *Macromolecules* **2005,** *38* (24),

10155-10163.

100. Jonas, A. M.; Glinel, K.; Oren, R.; Nysten, B.; Huck, W. T. S. *Macromolecules* **2007,** *40* (13), 4403-4405.

101. Tu, H.; Heitzman, C. E.; Braun, P. V. *Langmuir* **2004,** *20* (19), 8313-8320.

102. Collett, J.; Crawford, A.; Hatton, P. V.; Geoghegan, M.; Rimmer, S. *J. R. Soc. Interface* **2007,** *4* (12), 117-126.

103. Liu, Y.; Mu, L.; Liu, B. H.; Kong, J. L. *Chem. -Eur. J.* **2005,** *11* (9), 2622-2631.

104. Han, S.; Hagiwara, M.; Ishizone, T. *Macromolecules* **2003,** *36* (22), 8312-8319.

105. Lutz, J. F.; Akdemir, O.; Hoth, A. *J. Am. Chem. Soc.* **2006,** *128* (40), 13046-13047.

106. Lutz, J. F.; Hoth, A. *Macromolecules* **2006,** *39* (2), 893-896.

107. Lutz, J. F.; Andrieu, J.; Uzgun, S.; Rudolph, C.; Agarwal, S. *Macromolecules* **2007,** *40* (24), 8540-8543.

108. Yamamoto, S.; Pietrasik, J.; Matyjaszewski, K. *Macromolecules* **2007,** *40* (26), 9348-9353.

109. Lutz, J. F. *J. Polym. Sci. Pol. Chem.* **2008,** *46* (11), 3459-3470.

110. Wischerhoff, E.; Uhlig, K.; Lankenau, A.; Borner, H. G.; Laschewsky, A.; Duschl, C.; Lutz, J. F. *Angew. Chem. -Int. Edit.* **2008,** *47* (30), 5666-5668.

111. Dormidontova, E. E. *Macromolecules* **2002,** *35* (3), 987-1001.

112. Ma, H. W.; Li, D. J.; Sheng, X.; Zhao, B.; Chilkoti, A. *Langmuir* **2006,** *22* (8), 3751-3756.

Chapter 2
Research Objectives, Thesis Outline, and Dissemination of Results

2.1 Research objectives

Surface-initiated ATRP is a relatively new technique, which was invented about a decade ago, but it has brought extraordinary development in surface modification areas. A variety of novel polymer structures and functionalities have been introduced to different surfaces with potential applications for various purposes. The objective of this thesis was two-fold. The first objective was to elaborate the detailed surface-initiated ATRP mechanism and develop a kinetic model based on the elaborated mechanism. Combined with experimental results, a quantitative analysis was expected to be achieved from simulation. A thorough understanding of the surface-initiated ATRP mechanism was targeted, which can provide guidance for developing surface-initiated ATRP technique for various applications. The second was to employ the surface-initiated ATRP technique to graft different polymer brushes onto various surfaces with the purpose of achieving "smart surfaces", which can alter their properties (e.g., surface morphology, hydrophilicity, biological activity, protein adsorption/repulsion, cell adhesion, migration, etc.) in response to small changes in the external environment such as solvent type, pH,

temperature, electric and magnetic fields, etc.

2.2 Thesis outline

This thesis consists of seven chapters and it adopts the "sandwich" style following McMaster's guideline for thesis writing. Chapter 1 and Chapter 2 give the introduction and research objectives. Chapter 7 summarizes the contributions of the current work and gives some recommendations for future work. Chapter 3-6 are based on four papers that have been published or are in the final stage of preparation.

Chapter 3 was targeted at the mechanism study of the surface-initiated ATRP to provide guidance for applying this technique. A kinetic model was developed using the method of moment for surface-initiated ATRP. Combined with experimental data, quantitative analysis was carried out. All the information of the grafted polymer chains including active chain concentration, radical concentration, chain length, polydispersity during the surface-initiated ATRP were given. Influencing factors were investigated. Furthermore, a new radical termination mechanism, i.e., migration-termination, was proposed for the surface-initiated living polymerization.

In Chapter 4, the surface-initiated ATRP was employed to graft POEGMA-b-PMMA brushes on silicon wafer surfaces. AFM, ellipsometry and water contact angle methods were employed to study their stimulus-response behaviors. Nanoscale patterns

including spherical aggregates, wormlike aggregates, stripe patterns, perforated layers and complete overlayers were observed after simple solvent treatments. The smallest feature size was less than 10 nm and was tunable on the nanoscale. These patterns could switch between the different morphologies reversibly after the treatment with selective solvents.

In Chapter 5, POEGMA-b-PMETAC brushes were synthesized by the surface-initiated ATRP method to introduce nanopatterns. These brushes consisted of two hydrophilic segments to avoid hydrophobic segments because proteins could change their conformations and lose their activity on a hydrophobic surface. The collapse of polyelectrolyte in salt solution was employed to introduce phase segregation between these two hydrophilic segments. A variety of nanopatterns and their stimuli-responsive ability were observed. The adsorption behavior of fibrinogen on these patterns were studied by ellipsometry, water contact angel measurement, AFM and radio label method.

In Chapter 6, the surface-initiated ATRP was employed to graft thermo-responsive P(MEO_2MA-co-OEGMA) brushes onto the silicon wafer surface. This new class of thermo-responsive polymer surfaces, entirely constructed with poly(ethylene glycol) methacrylate, may lead to products that can hopefully be incorporated into various biomedical devices. Their thermo-responsive behaviors and chain conformations in an aqueous solution were studied by NR method. The effects of

temperature and salt concentration on the polymer conformation were evaluated. The protein adsorption results demonstrated that this PEG-based thermo-responsive surface has good protein adsorption resistance.

2.3 Dissimilation of the research work

Four articles are embodied in the current thesis (Chapter 3-6). Professor Shiping Zhu, my thesis supervisor, provided the initial research ideas and the following guidance. I designed and carried out the experimental and modeling work. Dr. Mu-Ping Nieh and Dr. Norbert Kučerka performed the NR measurements. I prepared the first drafts of these four papers and the responses to the comments from journal reviewers. I worked with Professor Shiping Zhu on the subsequent revisions until they are accepted. The selected journals are top ones in the category of polymer and colloid science.

Chapter 3
Kinetic Modeling of Surface-initiated Atom Transfer Radical Polymerization

This chapter is based on the following article in preparation: Gao, X.; Feng, W.; Zhu, S. P.; Sheardown, H.; Brash, J. L. Kinetic Modeling of Surface-initiated Atom Transfer Radical Polymerization, 2009.

3.1 Abstract

A kinetic model has been developed using the method of moment for surface-initiated atom transfer radical polymerization (s-ATRP) from flat solid surfaces based on a moving boundary physical model. The model takes into account of the effect of polymer brush conformation on the polymerization kinetics and polymer molecular weight development. The model is verified with the experimental data of 2-methacryloyloxyethyl phosphorylcholine from silicon wafer, which were carried out by either adding free initiator (Method I) or excess deactivator (Method II) to the solution. It is shown through the modeling that Method II gives better control over polymer molecular weight and thicker graft layer under similar conditions than Method I. A new mechanism is proposed for the radical termination based on the fact that the rapid activation/deactivation cycle reactions facilitate "migration" of radical centers on the

surface. The rate constant of "migration termination" is thus catalyst concentration dependent with higher catalyst concentration resulting in higher termination. Lowering catalyst concentration suppressed migration termination that could improve the control and livingness of s-ATRP. However, there exists a catalyst concentration for the optimal control performance.

3.2 Introduction

Grafting polymer brushes for modification of surface properties has gained significantly interest in the recent years due to unique performance of polymer brushes in various applications.[1-5] There are two major types of grafting methods, namely, "grafting to" and "grafting from".[2,5] In the "grafting to" method, polymer chains are prepared in advance. The chains bear reactive moieties at their chain ends, which can react with co-reactive sites on surfaces. The polymer chains can thus be covalently attached to the surface forming polymer brushes. The advantage of this method is that polymer chains can be prepared and characterized prior to grafting and thus the chain microstructural properties can be pre-designed and readily controlled. However, the disadvantage of this method is that during the grafting process, polymer chains must diffuse to the surface and react with their co-reactive moieties on the surface. The earlier grafted polymer chains may prevent later chains from approaching to the surface.[6-10] As a result, the grafting density is often low. In many applications, high grafting density is essential to ensure

polymer chains on the surface in a brush conformation.[3,5]

"Grafting from" method can give higher grafting densities due to absence of the diffusion limitations. In "grafting from" method, initiator molecules are immobilized to the surface first, followed by surface-initiated polymerization. Only monomer molecules need to diffuse from solution to the surface for polymer chain growth. Compared to polymer diffusion in "grafting to" method, monomer molecules experience little diffusion limitations. High grafting densities can thus be achieved. "Grafting from" method is preferred to achieve polymer brushes from various surfaces. However, the major challenge associated with this type of method is its difficulty in characterizing grafted polymer chains on the surface. It is also difficult to obtain good control over polymer chain growth on the surface if conventional radical polymerization is employed because of the combination of fast propagation and slow initiation. In conventional free radical polymerization, it takes only seconds for an individual chain to fully grow through the fast propagation, while it takes hours to accumulate chains through the slow initiation. The early born chains interfere growth of the late born chains.

The recent development of controlled/living radical polymerization (CLRP) techniques provides great opportunity for preparation of well-controlled and dense polymer brushes on surfaces.[1,11,12] In surface-initiated CLRP, polymer chains grow simultaneously but slowly from surface. Polymer molecular weights can be conveniently

controlled through variation of polymerization recipe and time. These polymer chains are thus very uniform in microstructural properties. Surface-initiated CLRP methods have been employed for preparation of various kinds of polymer brushes on different surfaces and interfaces.[13-15]

There are three major CLRP mechanisms: atom transfer radical polymerization (ATRP), nitroxide mediated polymerization (NMP) and reversible addition-fragmentation chain transfer radical polymerization (RAFT). Among the three, ATRP is a popular method for surface modification due to its good versatility to a wide range of functional monomers and the requirement of less stringent experimental conditions.[12] Various ATRP initiators suitable for surface immobilization have been synthesized. Ligands and catalysts are available. A great variety of monomer types have been successfully grafted from surfaces to obtain desirable surface properties.[16-21] The effects of polymer type, degree of polymerization, grafting thickness, and initiator density on surface properties have been extensively investigated.[22-27]

Although numerous experimental studies on s-ATRP have been reported, there are still many fundamental questions remained to be answered and lacking of quantitative analyses in particular. In this work, we resolve to a modeling approach. An examination of the literatures reveals that there were several modeling efforts made to describe solution ATRP.[28-32] The effects of some influencing factors on the solution ATRP

kinetics and polymer molecular weight development were investigated through modeling.[28]

In s-ATRP because the amount of grafted initiators on surface is very little, not enough deactivator can be generated during ATRP. As a result, sacrificed initiators (Method I) or extra deactivators (Method II) are needed to be added into solution to give an adequate level of the deactivator concentration. In Method II, the monomer concentration almost remains the same during the grafting process because the initiator on surface consumes very little amount of monomers. Therefore, the growth of polymer layer is supposed to be linear with reaction time. However, it was experimentally observed that the polymer layer growth in grafting deviated linearity in thickness versus time. This deviation was believed to be caused by significant termination of surface radicals because of crowded polymer brushes. The termination decreased the radical concentration on the surface causing the decrease of polymer growth rate.

Several theoretical studies have been carried out in relating polymer brushes layer thickness on the substrate to radical termination.[33,34] Xiao *et al.*[33] assumed the polymer thickness growth rate was proportional to monomer consumption rate in solution. In Method II, the change in monomer concentration was small. Therefore, a simplified analytic expression for the monomer consumption $[M]_0-[M]$ $(=k_p[M]_0[R^{\cdot}]t$, while $[R^{\cdot}]=[R^{\cdot}]_0/(1+k_t[R^{\cdot}]_0t)$ obtained by solving $d[R^{\cdot}]/dt = -kt[R^{\cdot}]^2$ with an initial condition of $[R^{\cdot}]$

$= [R^{\bullet}]_0$) was derived as follows:

$$[M]_0 - [M] = \frac{[M]_0 k_p [R^{\bullet}]_0 t}{1 + [R^{\bullet}]_0 k_t t} \quad (1)$$

where $[M]_0$, $[M]$, $[R^{\bullet}]_0$, k_p, k_t and t are initial monomer concentration, present monomer concentration, initial radical concentration, propagation rate constant, termination rate constant and time, respectively. This equation was fitted to the experimental growth of polymer layer thickness versus time. The simulation results showed that the deviation of the thickness growth from linearity could be caused by significant termination.

Kim *et al.*[34] assumed that the film growth rate at any given time was proportional to the surface radical concentration and calculated that the radical concentration from the following two differential equations:

$$\frac{d[R^{\bullet}]}{dt} = k_{act}[RX][C] - k_{deact}[R^{\bullet}][XC] - k_t[R^{\bullet}]^2 \quad (2)$$

$$\frac{d[RX]}{dt} = k_{act}[RX][C] + k_{deact}[R^{\bullet}][XC] \quad (3)$$

where $[R^{\bullet}]$, $[RX]$, $[C]$, $[XC]$, k_{act}, and k_{deact} are the radical concentration, initiator concentration, catalyst concentration, oxidized catalyst (deactivator) concentration, activation rate constant, and deactivation rate constant, respectively. They also demonstrated that, if the radical termination was significant, the film growth rate would

decrease significantly, deviating from the linearity versus time, as observed in the experimental work.

Correlating the polymer layer thickness on surface to $[M]_0$-[M] (Xiao *et al.*[33]) or to $[R^{\bullet}]$ (Kim *et al.*[34]) gave good quantitative analysis for the s-ATRP grafting process through the solution ATRP models. Both models explained that the radical termination in solution significantly affect the rate of polymer grafting on surface. However, these solution-based models oversimplified the reaction and diffusion events occurring on the surface and could not provide the detailed information about the surface polymerization. Strictly speaking, they are not applicable for the s-ATRP grafting using Method II.

Actually, the s-ATRP is a more complicated process compared with ATRP in solution. Two parallel ATRP systems coexist. One is a 2-D ATRP on the surface and the other is 3-D ATRP in the solution. Both consume the same monomer in the solution, but have different initiators and generate different polymer chains. A comprehensive modeling work can give a full picture of the whole system, which is essential to understand the s-ATRP mechanism and to investigate the influencing factors.

The objective of this chapter is to provide a detailed physical picture for the s-ATRP mechanism through a kinetic modeling approach. Combined with the experimental data, the model offers a thorough analysis for the s-ATRP process.

3.3 Theory

In this work, the s-ATRP mechanism is described, as shown in Scheme 3-1, by a solution ATRP and a surface ATRP from flat solid substrate, separately. In the solution phase, ATRP occurs when a free initiator is added. The solution polymerization includes activation, deactivation, propagation, termination and chain transfer. Although the density of initiator on the surface is high, the total amount is extremely low. It does not influence the reactions in the solution. The solution polymerization mechanism is shown in Table 3-1.

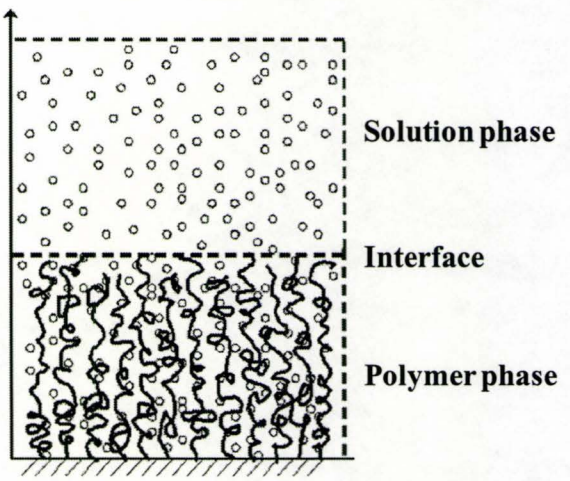

Scheme 3-1 Schematic presentation of the s-ATRP from flat surface.

On the surface, all polymer chains grow simultaneously. The high grafting density leads to a brush conformation with the chains stretching out into the solution. The chain ends reside at the vicinity of the interface between the polymer and solution phases. With

the polymer chains growing on the surface, the polymer layer thickness increases and the interface moves away from the substrate (i.e., a moving boundary problem). The s-ATRP model proposed in this work is thus termed as the moving-boundary brush model.

Table 3-1 Proposed reaction scheme for the s-ATRP from a flat solid substrate.

	Solution phase	Surface
Initiation	$RX_B + C_B \xrightarrow{k_{act}} R^\bullet_B + XC_B$	$RX_S + C_B \xrightarrow{k^s_{act}} R^\bullet_S + XC_B$
Activation	$RM_iX_B + C_B \xrightarrow{k_{act}} RM^\bullet_{iB} + XC_B$	$RM_iX_S + C_B \xrightarrow{k^s_{act}} RM^\bullet_{iS} + XC_B$
Deactivation	$RM^\bullet_{iB} + XC_B \xrightarrow{k_{deact}} RM_iX_B + C_B$	$RM^\bullet_{iS} + XC_B \xrightarrow{k^s_{deact}} RM_iX_S + C_B$
Propagation	$RM^\bullet_{iB} + M_B \xrightarrow{k_p} RM^\bullet_{i+1B}$	$RM^\bullet_{iS} + M_B \xrightarrow{k^s_p} RM^\bullet_{i+1S}$
Termination	$RM^\bullet_{iB} + RM^\bullet_{jB} \xrightarrow{k_{td}} RM_{iB} + RM_{jB}$ $RM^\bullet_{iB} + RM^\bullet_{jB} \xrightarrow{k_{tc}} RM_{i+j}R_B$ $RM^\bullet_{iB} \xrightarrow{k_{tr}} RM_{iB}$	$RM^\bullet_{iS} + RM^\bullet_{jS} \xrightarrow{k^s_{td}} RM_{iS} + RM_{jS}$ $RM^\bullet_{iS} + RM^\bullet_{jS} \xrightarrow{k^s_{tc}} RM_{i+j}R_S$ $RM^\bullet_{iS} \xrightarrow{k^s_{tr}} RM_{iS}$

where $RM^\bullet_i$, RM_iX, RM_i, $RM_{i+j}R$ stand for living chains, dormant chains, dead chains by disproportion, and dead chains combination; i and j are the number of monomeric units in the polymer chains; the subscripts B and S denote "bulk" and "surface" for the corresponding species; k's are the reaction rate constants with the subscript *act* meaning activation, *deact* deactivation, p propagation, *td* termination by disproportion, *tc*

termination by combination, and *tr* chain transfer, respectively. The prime denotes the reactions on the surface.

On the surface, the reactions of activation, deactivation, propagation and chain transfer involve polymer chains on the surface and small molecules in the solution (i.e. monomer, catalyst, and deactivator). As shown in Scheme 3-1, although one end of the chain on the surface is constrained to the surface, the free end stretches out into the solution. It is assumed that the constrained end has no effect on the reactions. The small molecules readily diffuse around the free polymer chain ends as in the solution polymerization. As a result, these reactions can be treated in the same way as those occurring in the solution. Previous work has proven that the chain length of grafted polymer on surface is similar to that of free polymer formed in the solution. The termination between surface and bulk radicals were neglected in this work.

In this work, all the grafted species including grafted chains, initiators, and radicals are based on their surface concentrations (the number of species per unit surface area). By modeling the surface reactions directly, no assumptions are needed to relate the surface species to their solution counterparts. The model is thus more realistic, better representing the actual reaction events on the surface.

Based on the proposed reactions listed in Table 3-1, the mass balance equations

for all the species in the s-ATRP are obtained as shown in Table 3-2. The rate of polymer layer thickness growth follows:

$$\frac{dH}{dt} = \frac{mk'_p[M]_B \sum_{i=0}^{\infty}[RM_i^{\bullet}]_S}{\rho} \tag{4}$$

where m is the monomer molecular weight and ρ is the bulk density of polymer.

In this work, the method of moment is employed to obtain the average chain length and polydispersity. MathCAD 2001 is used for calculation. The detailed calculation method is given as the supporting material.

Table 3-2 Mass balance equations for various species in the solution and on the surface.

Solution polymerization:

$$\frac{d[RM_i^{\bullet}]_B}{dt} = k_p[RM_{i-1}^{\bullet}]_B[M]_B - k_p[RM_i^{\bullet}]_B[M]_B + k_{act}[RM_iX]_B[C]_B - k_{deact}[RM_i^{\bullet}]_B[XC]_B - k_t[RM_i^{\bullet}]_B\sum_{i=0}^{\infty}[RM_i^{\bullet}]_B - k_{tr}[RM_i^{\bullet}]_B$$

$$\frac{d[RM_iX]_B}{dt} = k_{deact}[RM_i^{\bullet}]_B[XC]_B - k_{act}[RM_iX]_B[C]_B$$

$$\frac{d[RM_i]_B}{dt} = k_{td}[RM_i^{\bullet}]_B\sum_{i=0}^{\infty}[RM_i^{\bullet}]_B + k_{tr}[RM_i^{\bullet}]_B$$

$$\frac{d[RM_iR]_B}{dt} = \frac{k_{tc}}{2}\sum_{j=0}^{i}[RM_i^{\bullet}]_B[RM_{i-j}^{\bullet}]_B$$

$$\frac{d[M]_B}{dt} = -k_p\sum_{i=0}^{\infty}[RM^{\bullet}]_B[M]_B$$

Surface polymerization:

$$\frac{d[RM_i^\bullet]_S}{dt} = k'_p[RM_{i-1}^\bullet]_S[M]_B - k'_p[RM_i^\bullet]_S[M]_B + k'_{act}[RM_iX]_S[C]_B - k'_{deact}[RM_i^\bullet]_S[XC]_B - k'_t[RM_i^\bullet]_S\sum_{i=0}^{\infty}[RM_i^\bullet]_S - k'_{tr}[RM_i^\bullet]_S$$

$$\frac{d[RM_iX]_S}{dt} = k'_{deact}[RM_i^\bullet]_S[XC]_B - k'_{act}[RM_iX]_S[C]_B$$

$$\frac{d[RM_i]_S}{dt} = k'_{td}[RM_i^\bullet]_S\sum_{i=0}^{\infty}[RM_i^\bullet]_S + k'_{tr}[RM_i^\bullet]_S$$

$$\frac{d[RM_iR]_S}{dt} = \frac{k'_{tc}}{2}\sum_{j=0}^{i}[RM_i^\bullet]_S[RM_{i-j}^\bullet]_S$$

3.4 Results and discussion

3.4.1 Simulation of the s-ATRP of MPC

The moving-boundary brush model developed above was employed to investigate the s-ATRP of 2-methacryloyloxyethyl phosphorylcholine (MPC) from silicon wafer. MPC is a biomimetic monomer which has attracted great attention as a functional monomer for improving biocompatibility.[35,36] An extensive experimental studies on the grafting poly(MPC) from silicon wafer to reduce protein adsorption have been carried out.[37-39] Influencing factors including grafting methods, catalyst concentration, deactivator concentration, etc. received a thorough investigation. The experimental data are repeatable with the error less than 5%.[37,39] Abundant experimental data enable us to achieve a clear picture of the s-ATRP mechanism through the modeling approach.

MPC is a relatively new biomimetic monomer and no ATRP rate constants have been found in the previous research under the selected experimental conditions. In this work, the rate constants of its solution ATRP were obtained by fitting the model to the experimental data. As shown in Figure 3-1 when k_p =1.6×10^3 L/mol·s, k_{act} =1 L/mol·s, k_{deact} =1×10^6 L/mol·s, k_t =4×10^7 L/mol·s, the simulation gave the best fit to the experimental data. For the surface polymerization rate, it was assumed that the reactions between the grafted chains on the surface and small molecules in the solution were the same as the solution polymerization. Therefore. k'_p=k_p, k'_{act}=k_{act} and k'_{deact}=k_{deact}. The radical termination occurring between the grafted chains on the surface differs from that in the solution. The surface radical termination rate constant, k'_t, was obtained using an approach discussed later.

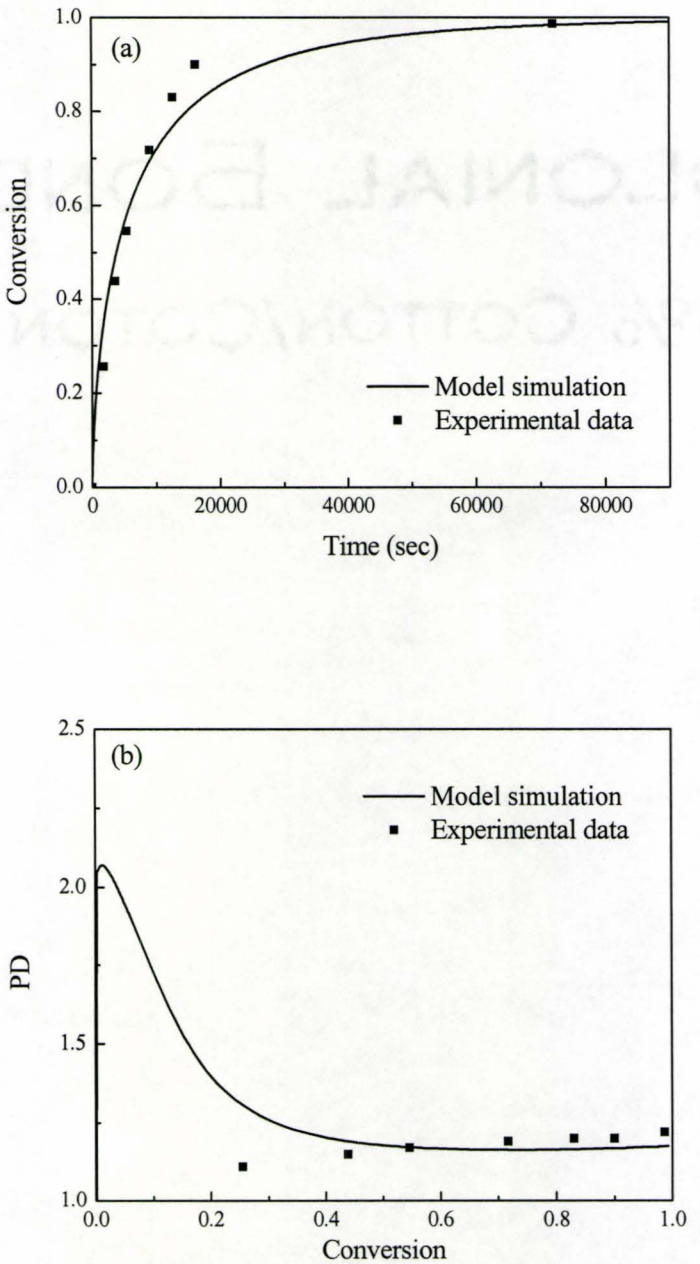

Figure 3-1 The solution ATRP of MPC: (a) conversion versus reaction time and (b) polydispersity versus conversion. Recipe: [MPC]/[CuBr]/[OEGBr]/[bpy]=50:1:1:2,

[MPC]=0.85 mol/L, solvent: methanol.

In the s-ATRP, the amount of deactivator generated from the surface reactions is extremely low. In order to obtain a sufficient level of deactivators in the solution, two approaches are often used: one is to add free initiator in the solution (Method I) and the other is to add deactivator directly (Method II). When free initiator is added into the solution, free polymer chains also form in the solution. This provides an approach to estimate grafting density.[37]

It should be noted that if no deactivator is added to the reaction system the ATRP activation-deactivation equilibrium cannot be set up at the beginning. The absence of deactivator will give longer life time to radicals leading to longer polymer chains. As shown in Figure 3-2(c) the polymer chain length was larger at the very beginning of reaction. With the reaction more and more deactivators will accumulate in the system because of the termination of radicals. Then the new polymer chains will have shorter chain length causing the average chain length to decrease. When the ATRP activation-deactivation equilibrium was reached, the average chain length grew linearly with conversion as indicated from ATRP mechanism. During this short time at very beginning the polydispersity of polymer chains was also higher, as shown in Figure 3-2(d) and Figure 3-1(b), because the reaction was not in the controlled manner.

3.4.1.1 Method I

In our previous research, Method I was employed to grow poly(MPC) from silicon wafer.[37] The experimental recipe and results are shown in Figure 3-2. In order to simulate this surface polymerization process, two more factors are needed: efficient surface initiator concentration and surface termination rate constant. The initiator concentration grafted on the surface can be as high as 5 moieties/nm^2, but only a small fraction of them can be activated and grow into full polymer chains.[25,38,40] The efficient surface initiator concentration (i.e. how many initiators have been activated or equivalently, grafting density) is an important parameter for the surface polymerization. In our experimental work using Method I, the grafting density was estimated to be around 0.25~0.3 chains/nm^2. As a result, 0.3 chains/nm^2 was used in the simulation as the efficient surface initiator concentration.

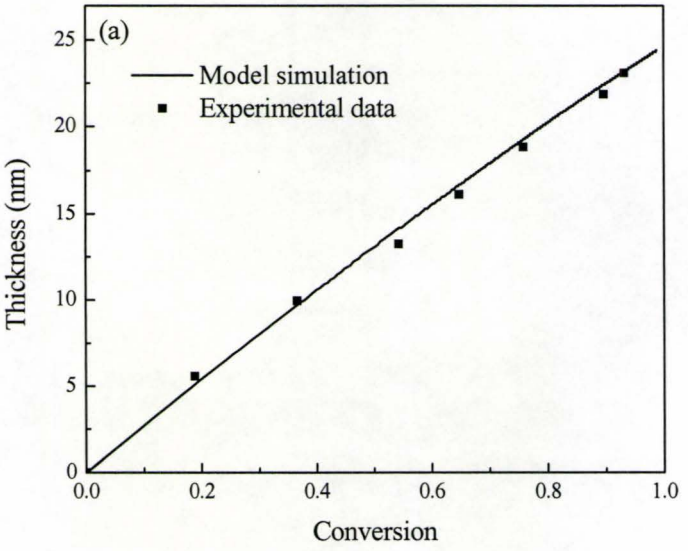
(a)
Model simulation
Experimental data
Thickness (nm)
Conversion
0
5
10
15
20
25
0.0
0.2
0.4
0.6
0.8
1.0

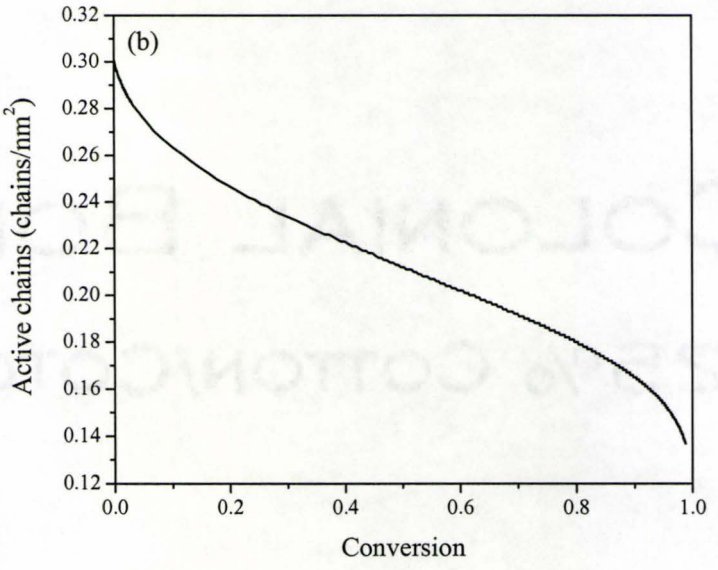
(b)
Active chains (chains/nm^2)
Conversion
0.12
0.14
0.16
0.18
0.20
0.22
0.24
0.26
0.28
0.30
0.32
0.0
0.2
0.4
0.6
0.8
1.0

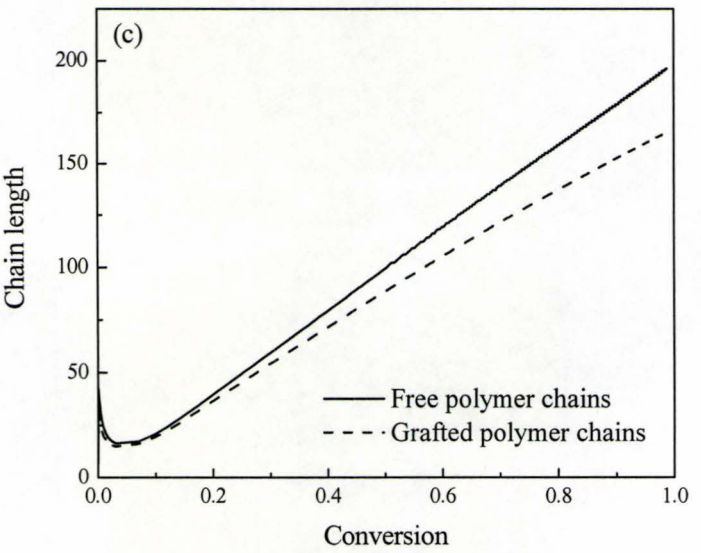
(c)
Chain length
Conversion
Free polymer chains
Grafted polymer chains
0
50
100
150
200
0.0
0.2
0.4
0.6
0.8
1.0

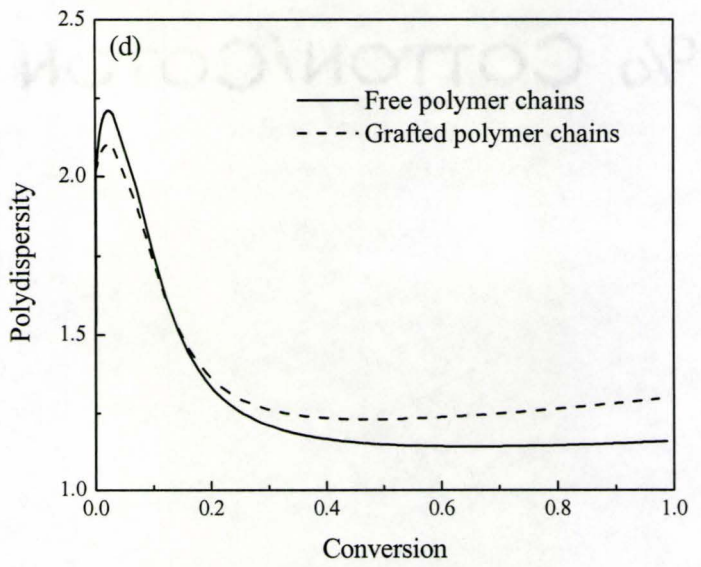
(d)
Polydispersity
Conversion
Free polymer chains
Grafted polymer chains
1.0
1.5
2.0
2.5
0.0
0.2
0.4
0.6
0.8
1.0

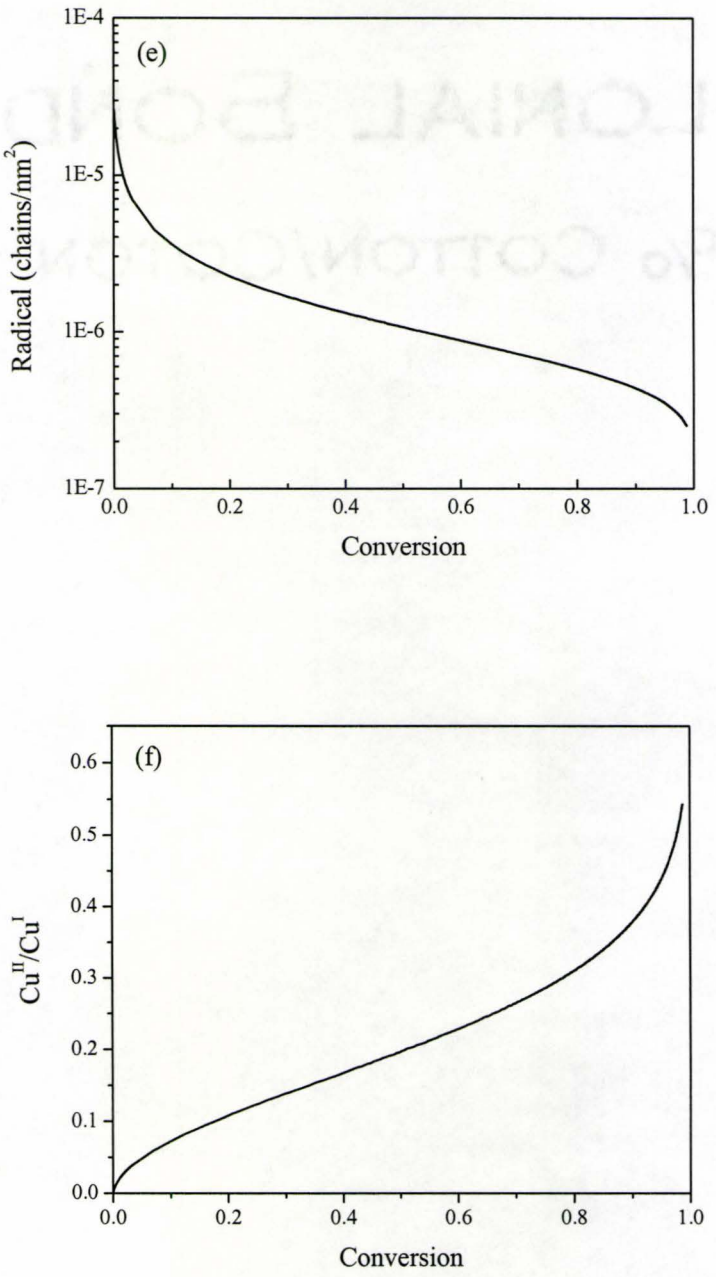

Figure 3-2 Grafting poly(MPC) from silicon wafer with free initiator in the solution (Method I): (a) grafting thickness versus monomer conversion, (b) surface active polymer

chain concentration, (c) chain length, (d) polydispersity, (e) surface radical concentration, and (f) the ratio of $[Cu^{II}]$:$[Cu^{I}]$ in solution. Recipe: [MPC]/[CuBr]/[OEGBr]/[bpy]=200:1:1:2, [MPC]=1.33 mol/L, solvent: methanol.

The surface radical termination rate is an important parameter for the surface polymerization, but no information could be directly obtained from experimental work. In this work, by fitting the model to the experimental data as shown in Figure 3-2(a), the surface termination rate constant, k'_t, was estimated to be 1.2×10^{14} $dm^2/mol\cdot s$. Thus all the parameters needed for the model are obtained through the good fitting to the experimental data.

Figure 3-2(b) gives the variation of the active chain (the sum of dormant and radical chains) concentration on the surface with conversion. The initial concentration is 0.3 chains/nm^2. It can be seen in the figure that the surface termination is very significant. The active chains become dead very quickly. At the end of the reaction, almost half of the chains lost activity through termination. In our previous work to test the remaining activity of polymer chains on the silicon wafer after one grafting process, the surface grafted with poly(MPC) was cleaned and put into MPC solution again to graft more MPC onto the surface for the second time.[37] The thickness obtained during the second grafting process was only about half of the value observed on a fresh initiator-functionalized silicon wafer under the same condition. This can be explained readily by the simulation

shown in Figure 3-2(b): the radical termination on the surface is significant and causes the loss of the grafted polymer chain activity.

Figure 3-2(c) and (d) give the chain length and polydispersity of the grafted polymer. The chain length and polydispersity of the grafted chains are similar to those of the polymer chains in the solution. The shorter chain length and higher polydispersity on the surface show that the termination on the surface is more significant than in the solution in this experiment system. However, the surface polymerization is still a well-controlled living ATRP with low polydispersity.

Figure 3-2(e) gives the information about the surface radical concentration. The concentration is about 3×10^{-6} chains/nm^2. Figure 3-2(f) gives the $[Cu^{II}]$:$[Cu^{I}]$ ratio during the whole reaction. All the information is very important for analyzing the surface polymerization mechanism.

3.4.1.2 Method II

In our previous work, Method II (adding deactivator instead of free initiator into solution) was also employed to grow poly(MPC) from silicon wafer (Figure 3-3).[37] The same recipe as in Method I was chosen including the same catalyst (Cu^{I}) concentration. The only difference was that deactivator instead of free initiator was added. The reaction rate constants did not change. The reaction rate constants obtained from the Method I

simulation with the new recipe were used in the model to predict the experimental data obtained from the Method II experiments. However, as discussed above, when Method II is applied, the grafting density cannot be estimated from the experimental data, which is a disadvantage of using Method II. The grafting density estimated from Method I was used in the models as the first approximate. The prediction results were shown in Figure 3-3.

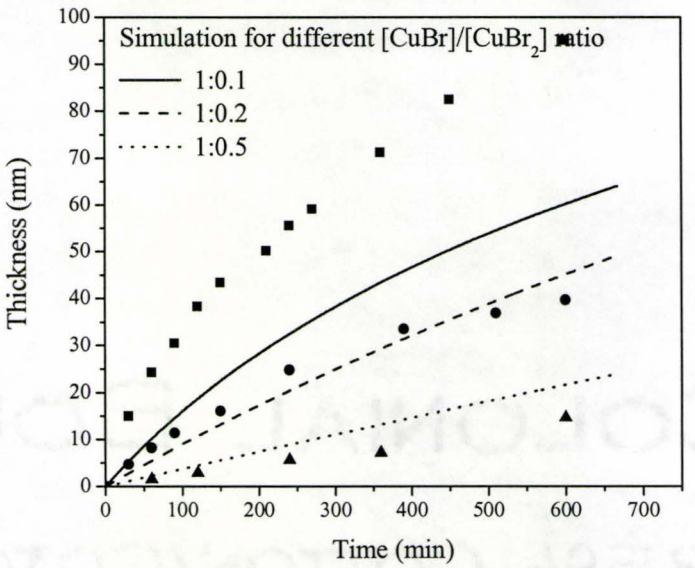

Figure 3-3 Grafting poly(MPC) from silicon wafer with added excess deactivator (Method II) for different [CuBr]/[$CuBr_2$] ratios at [MPC]=1.33 mol/L: (■) [MPC]/[CuBr]/[$CuBr_2$]/[bpy]=200:1:0.1:2.2 (●) [MPC]/[CuBr]/[$CuBr_2$]/[bpy]=200:1:0.2:2.4 (▲) [MPC]/[CuBr]/[$CuBr_2$]/[bpy]=200:1:0.5:3.0. Solvent: methanol.

Different $[Cu^{II}]$:$[Cu^{I}]$ ratios led to different radical concentrations on the surface and different thickness growth rates. The lower the $[Cu^{II}]$:$[Cu^{I}]$ ratio was, the higher the radical concentration on the surface. When the $[Cu^{II}]$:$[Cu^{I}]$ ratio decreased, the thickness growth rate increased. This trend is evident in both experimental data and simulation results.

When the ratio of $[Cu^{II}]$:$[Cu^{I}]$ was at 0.2, the model predicted the experimental data well. This indicated that the same grafting density as in Method I might have been achieved. To verify this, the $[Cu^{II}]$:$[Cu^{I}]$ ratio in Method I was investigated because the only difference between these two methods could be the $[Cu^{II}]$:$[Cu^{I}]$ ratios.

The $[Cu^{II}]$:$[Cu^{I}]$ ratio in Method I is shown in Figure 3-2(f). It can be seen that the $[Cu^{II}]$:$[Cu^{I}]$ ratio was around 0.2. The ratio of 0.2 in Method II is thus close to that in Method I. The grafting density would be about 0.3 chains/nm^2. This explains why the model predicted the experimental data well when the ratio of $[Cu^{II}]$:$[Cu^{I}]$ was 0.2.

3.4.1.3 Comparison between Method I and Method II

Other difference may still exist between Method I and II. Simulation allows us for a full comparison between these two methods. Figure 3-4(a) shows that under the similar reaction conditions Method II gives a much higher grafting thickness and better controlled process. In Method II, an adequate level of deactivator is added into the recipe

so that the polymerization is under good control during the whole ATRP.

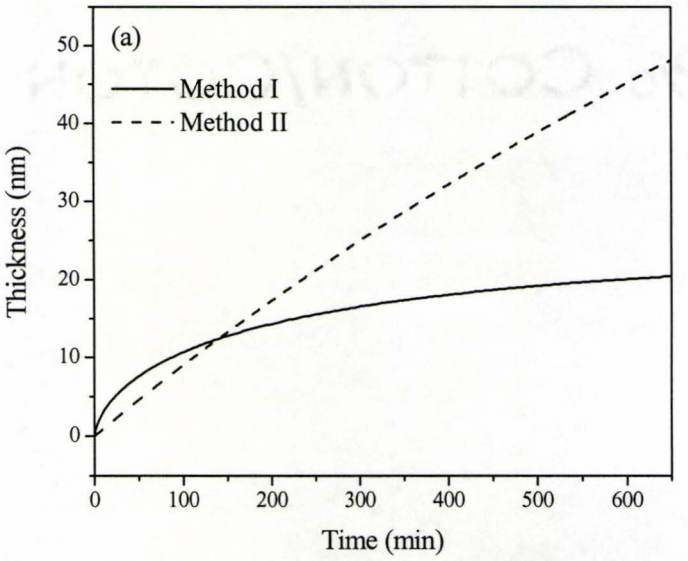

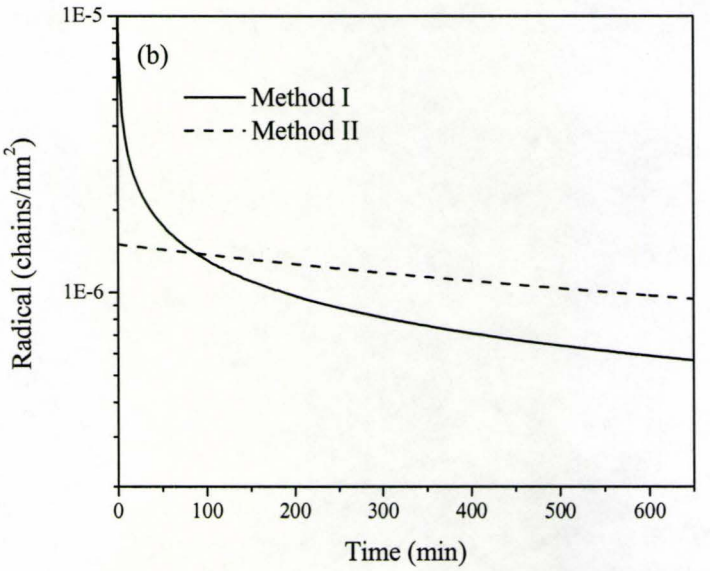

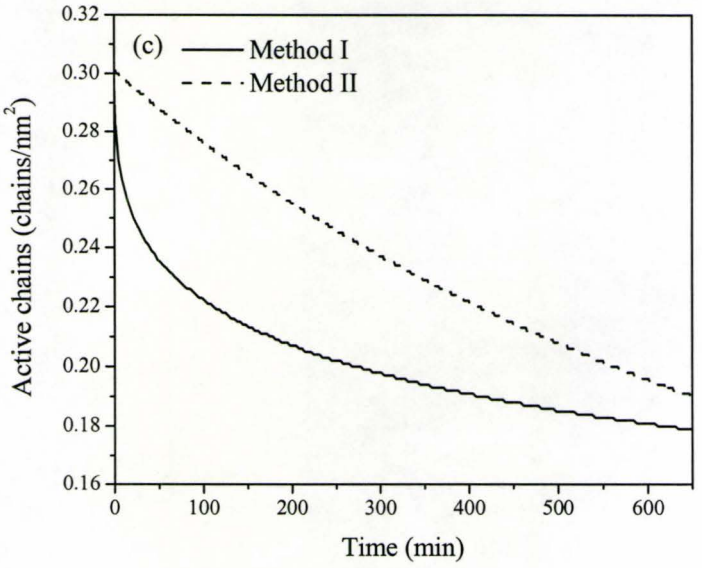

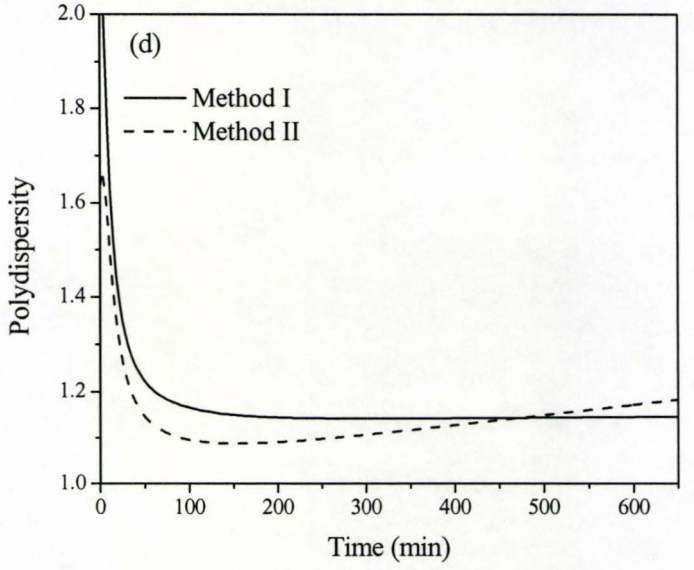

Figure 3-4 Comparison between Method I (add free initiator) and Method II (add excess deactivator) under similar conditions. Method I:

[MPC]/[CuBr]/[OEGBr]/[bpy]=200:1:1:2, [MPC]=1.33 mol/L, solvent: methanol; Method II: [MPC]/[CuBr]/[$CuBr_2$]/[bpy]=200:1:0.2:2.4, [MPC]=1.33 mol/L, solvent: methanol. (a) Grafting thickness, (b) surface radical chain concentration, (c) surface active chain concentration and (d) polydispersity of grafted polymer chains.

It can be seen in Figure 3-4(b) that the radical concentration in Method II varies little during the polymerization. As a result, the thickness growth rate remains almost constant. In Method I, however, no deactivator is added into the recipe, so the deactivator needs to accumulate according to Fisher's persistent radical effect at the early stage of the reaction.[41] At the very beginning of ATRP, the deactivator concentration is low and thus the radical concentration is high, as shown in Figure 3-4(b). This explains why the thickness growth rate in Method I is faster than that in Method II at the beginning. With the reaction proceeding, the termination decreases the radical concentration and a higher deactivator concentration is accumulated in the solution, leading to a well-controlled ATRP. The steady state of radical concentration is then reached with a value close to that in Method II. However, at this time, the thickness growth rate decreases due to the consumption of monomers in the solution. As a result, a much lower thickness is obtained at the end of reaction.

Figure 3-4(c) gives the active chain concentration variation during the reactions. A constant $[Cu^{II}]$:$[Cu^{I}]$ ratio in Method II gives a constant surface radical termination rate,

while in Method I the termination rate varies due to the variation of deactivator concentration. However, both methods give a controlled polymerization and a low polydispersity, as shown in Figure 3-4(d). From these results, it can be concluded that Method II can give a much better controlled s-ATRP than Method I because of the high deactivator concentration at the very beginning and the nearly constant monomer concentration throughout the whole process. Furthermore, Method II is more practical because it does not consume monomer in solution.

3.4.1.4 Grafting density in Method II

When the $[Cu^{II}]$:$[Cu^{I}]$ ratio was at 0.1, the thickness growth rate was higher than at the ratio of 0.2. This indicates a higher radical concentration on the surface because all the other conditions were identical. The grafted initiator density is high on the surface and only a small fraction of the initiators can grow to polymer chains. When the $[Cu^{II}]$:$[Cu^{I}]$ ratio was lower, more initiators were activated and had chance to fully grow to polymer chains. This means a higher grafting density. The model fits the experimental data with varying grafting densities. The best fits are obtained, as shown in Figure 3-5(a), with the grafting density of 0.72 chains/nm^2 and 0.18 chains/nm^2 for the $[Cu^{II}]$:$[Cu^{I}]$ ratio of 0.1 and 0.5, respectively.

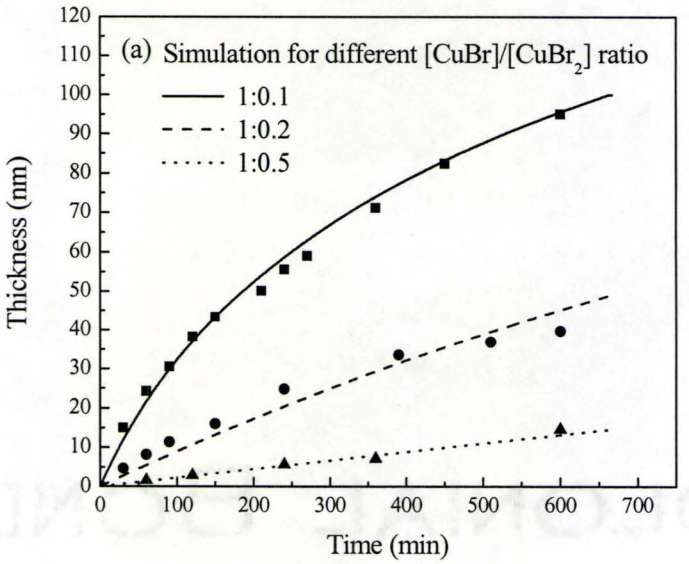
(a) Simulation for different [CuBr]/[CuBr2] ratio
1:0.1
1:0.2
1:0.5
Thickness (nm)
Time (min)
0
10
20
30
40
50
60
70
80
90
100
110
120
0
100
200
300
400
500
600
700

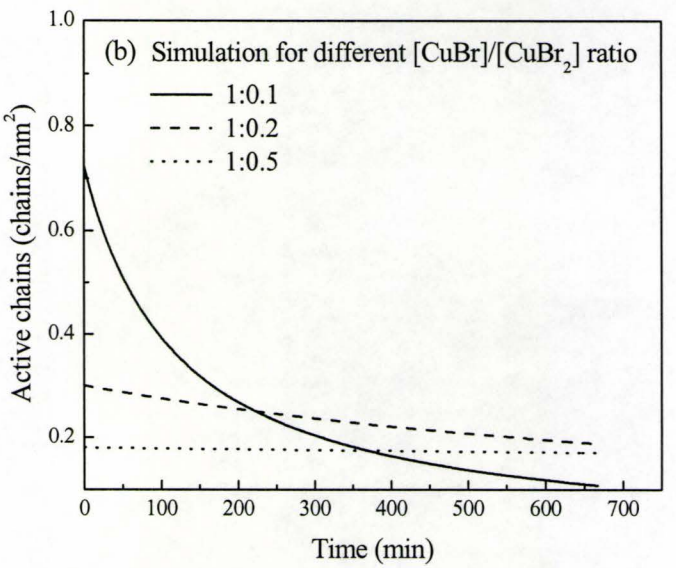
(b) Simulation for different [CuBr]/[CuBr2] ratio
1:0.1
1:0.2
1:0.5
Active chains (chains/nm2)
Time (min)
0.2
0.4
0.6
0.8
1.0
0
100
200
300
400
500
600
700

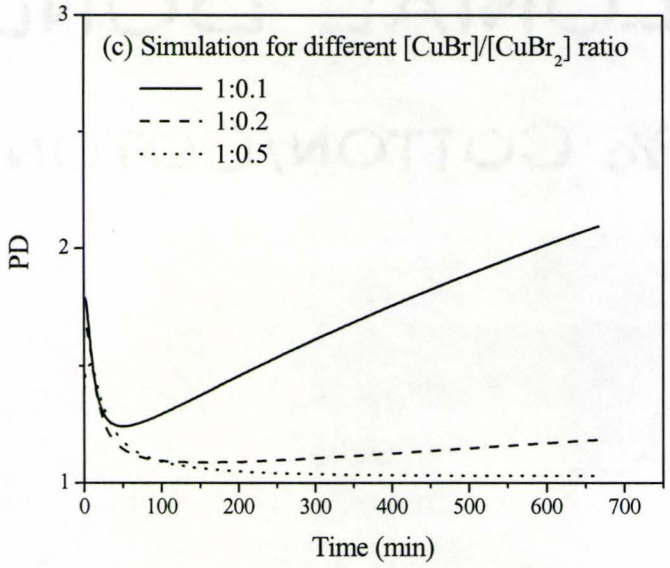

Figure 3-5 Simulating poly(MPC) growth from silicon wafer with added excess deactivator (Method II) for different [CuBr]/[$CuBr_2$] ratios at [MPC]=1.33 mol/L: (a) grafting thickness versus reaction time, (b) surface active chain concentration versus reaction time and (c) polydispersity of grafted polymer chains versus reaction time.

(■) [MPC]/[CuBr]/[$CuBr_2$]/[bpy]=200:1:0.1:2.2

(●) [MPC]/[CuBr]/[$CuBr_2$]/[bpy]=200:1:0.2:2.4

(▲) [MPC]/[CuBr]/[$CuBr_2$]/[bpy]=200:1:0.5:3.0.

Solvent: methanol. Grafting densities obtained from simulation for [CuBr]/[$CuBr_2$] ratio of 1:0.1, 1:0.2 and 1:0.5 are 0.72 chains/nm^2, 0.3 chains/nm^2, and 0.18 chains/nm^2, respectively.

Higher grafting density also means more significant termination on the surface.

Figure 3-5(b) gives the active polymer chain concentration on the surface during the reaction. When the $[Cu^{II}]$:$[Cu^{I}]$ ratio was at 0.1, a high grafting density was achieved at the beginning, but the higher radical concentration on the surface also caused more significant termination. When the $[Cu^{II}]$:$[Cu^{I}]$ ratio was at 0.5, a well-controlled thickness growth was achieved, but a lower grafting density of 0.18 chains/nm^2 was obtained. Figure 3-5(c) gives the polydispersity of grafted chains on the surface. Lower $[Cu^{II}]$:$[Cu^{I}]$ ratio yields higher grafting thickness but also higher polydispersity. On the contrary, a polydispersity as low as 1.04 was obtained when a ratio of 0.5 was selected.

3.4.2 Surface radical termination mechanism in the s-ATRP

3.4.2.1 Quantitative analysis of surface radical termination mechanism

The major difference between s-ATRP and solution ATRP lies in the radical termination mechanism. The general understanding is that the high grafting density leads to crowding of polymer chains on the surface and induces more significant termination. Significant radical termination on the surface is also observed in many experimental studies. However, the detailed study about the surface termination mechanism has never been carried out due to the lack of surface information. In this work, the simulation makes it possible to provide some detailed surface polymerization information.

In Scheme 3-2, a quantitative picture about the s-ATRP is given. The grafting

thickness up to 100 nm, which is often the max value obtained in most investigations reported in literatures. The grafting density estimated from Method I is about 0.3 chains/nm^2, typical of high grafting density brushes. The average distance between grafted polymer chains on the surface is thus estimated as 1.83 nm as shown in Scheme 3-2.

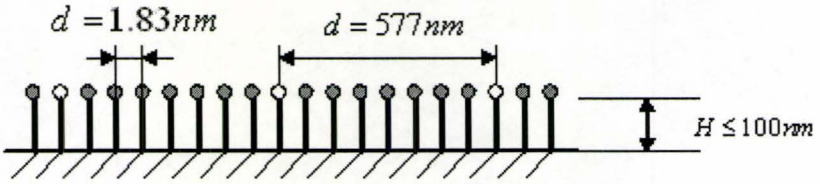

Scheme 3-2 Quantitative picture of the s-ATRP. Filled dots: dormant chain ends; open dots: radical chain ends.

The radical concentration is several orders of magnitude lower than that of dormant chains. Figure 3-2(e) gives the radical concentration on the surface. It is around 3×10^{-6} chains/nm^2 and an average distance between radicals is 577 nm in this case.

On the surface, the grafted polymer chains are crowded forming brush conformation, but such crowding is not the reason leading to significant termination on the surface as believed before. From Scheme 3-2, it can be seen that on the surface the grafted polymer chains have one end attached to the surface, thus they cannot diffuse freely as in the solution. The crowding between grafted polymer chains further limits their movement on the surface. Although the polymer chains are very crowded, the

average distance between radicals is still very large. From Scheme 3-2, it seems that the termination cannot happen because it is difficult to imagine that some radial chains can be long enough to reach other radical chain ends to terminate, considering their average distance is 577 nm. However, the radical termination does happen on the surface. The reason is that the radicals distribute randomly on the surface. As shown in Scheme 3-3, on the surface, most chain ends are dormant species. Only a very small fraction of chain ends are radicals. Most of them are too far away to meet each other but some of them just happen to be close enough (as in circles) to terminate. The surface radical termination occurs in this way.

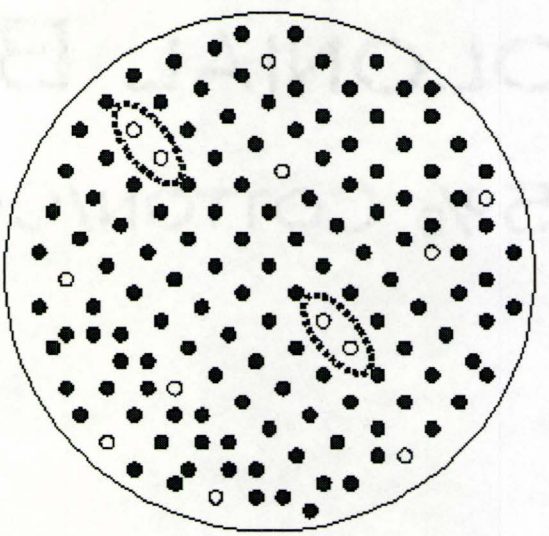

Scheme 3-3 Radical termination on the surface. Filled dots: dormant chain ends; open dots: radical chain ends.

We believe that, in the s-ATRP, the activation-deactivation process could

facilitate radical termination. The activation-deactivation process makes the chain ends change their state between radical and dormant species. As a result, the radical positions keep changing on the surface (i.e. dormant chain ends in different positions are activated at different times). It is the same as those radicals migrate on the surface. When two of them are at vicinity (i.e. migrated to meet each other), the termination occurs.

To the best of our knowledge, this is a new mechanism ever proposed for s-ATRP grafting. The crowding of polymer chains on the surface prevents radicals from termination, instead of promoting more significant termination as previously believed. This can be termed as a 2-dimentional gel-effect. On the contrary, the activation-deactivation process, which is the key factor making ATRP a living process, actually accelerates the termination on the surface. The radical termination rate is very fast, the rate determining step appears to be the migration rate of radicals to meet each other, because the average distance between two radicals is too far. If the activation-deactivation rate is very fast, more radicals change their positions (i.e. migrate faster), and thus more radicals terminate.

3.4.2.2 Experimental study

The activation rate, $k'_{act}[RQ_0X]_S[C]_B$, gives the number of radicals that are activated per unit time. This is also the number of radicals which change their positions

per unit time, influencing the surface termination rate. It is clear that higher catalyst concentration results in higher termination rate. There were many experimental studies on the effect of catalyst concentration on the s-ATRP, which can be used to test this proposed surface termination mechanism.

Figure 3-2 shows the s-ATRP experimental data, in which Method I was employed. The catalyst concentration was 0.0067 mol/L, and the surface termination rate constant was estimated to be 1.2×10^{14} dm^2/mol·s from the above simulation. A catalyst concentration of 0.027 mol/L, which is four times higher, was also used.[37] The experimental results are shown in Figure 3-6. The estimated grafting density of about 0.3 chains/nm^2 was estimated from the experimental work. This also shows that the catalyst concentration did not affect the grafting density. The surface termination rate constant of 4.8×10^{14} dm^2/mol·s (at the catalyst concentration of 0.027 mol/L) was obtained by fitting the model to the experimental data, as shown in Figure 3-6. It is exactly four times higher than 1.2×10^{14} dm^2/mol·s (at 0.0067 mol/L). The termination rate constant is clearly proportional to the catalyst concentration:

$$k'_t \propto r'_{migration} \propto k'_{act}[RQ_0X]_S[C]_B \tag{5}$$

where $r'_{migration}$ is the migration rate of radicals on the surface caused by the activation/deactivation cycles.

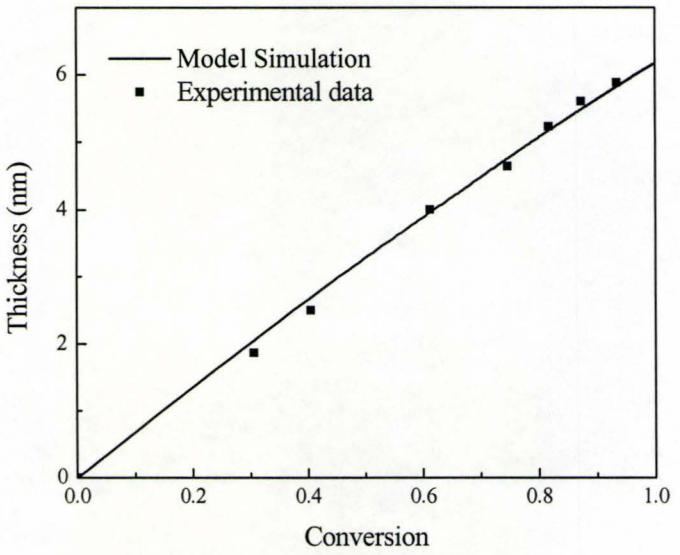

Figure 3-6 Grafting thickness of poly(MPC) from silicon wafer versus monomer conversion with free initiator in the solution (Method I) at higher catalyst concentration:. Recipe: [MPC]/[CuBr]/[OEGBr]/[bpy]=50:1:1:2, [MPC]=1.33 mol/L, solvent: methanol.

When Method II is applied in the s-ATRP, the effect of catalyst concentration can be readily investigated. Figure 3-7(a) gives the s-ATRP experimental results with two levels of catalyst concentrations of 0.0067 mol/L and 0.027 mol/L. It can be seen that at the higher catalyst concentration (0.027 mol/L), the surface termination was much more significant. In a short time, most radicals on the surface terminated and the thickness growth rate reached almost zero.

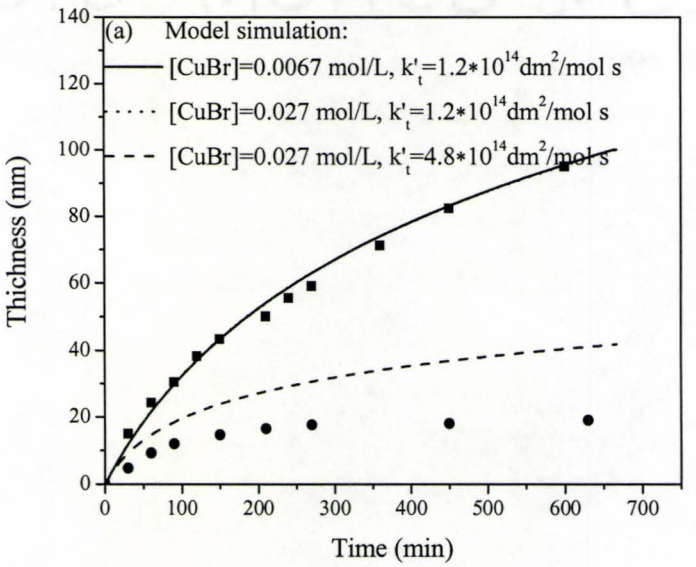
(a) Model simulation:
[CuBr]=0.0067 mol/L, k'$_t$=1.2*10^{14}dm^2/mol s
[CuBr]=0.027 mol/L, k'$_t$=1.2*10^{14}dm^2/mol s
[CuBr]=0.027 mol/L, k'$_t$=4.8*10^{14}dm^2/mol s
Thichness (nm)
Time (min)
0
20
40
60
80
100
120
140
0
100
200
300
400
500
600
700

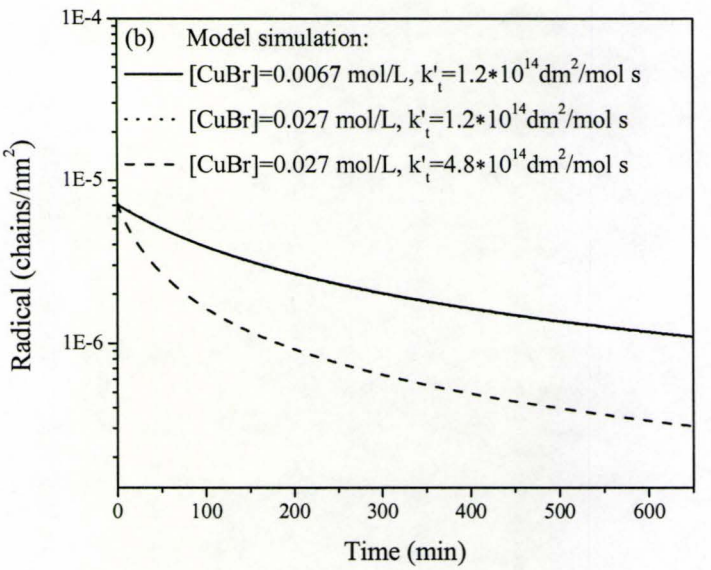
(b) Model simulation:
[CuBr]=0.0067 mol/L, k'$_t$=1.2*10^{14}dm^2/mol s
[CuBr]=0.027 mol/L, k'$_t$=1.2*10^{14}dm^2/mol s
[CuBr]=0.027 mol/L, k'$_t$=4.8*10^{14}dm^2/mol s
Radical (chains/nm^2)
Time (min)
1E-4
1E-5
1E-6
0
100
200
300
400
500
600

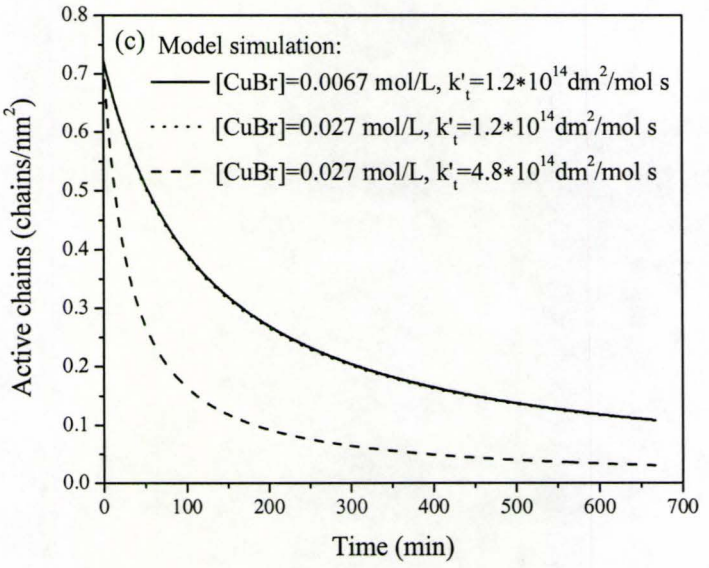

Figure 3-7 Grafting poly(MPC) from silicon wafer with added excess deactivator (Method II) for different catalyst concentration at [MPC]=1.33 mol/L, [CuBr]/[$CuBr_2$]/[bpy]=1:0.1:2.2, solvent: methanol. (■) [CuBr]=0.0067 mol/L, (●) [CuBr]=0.027 mol/L. (a) Grafting thickness versus time, (b) surface radical concentration versus time and (c) surface active chain concentration versus time. Two curves with the same termination constant, 1.2×10^{14} dm^2/mol·s. overlapped in the above figures.

Similar phenomena were also observed by Kim *et al.*[34] In their work, all the radicals on the surface terminated in a very short time at the high catalyst concentration of 0.04 mol/L. The previous explanation for the more significant surface termination at higher catalyst concentration was that the higher catalyst concentration would lead to a

higher stead-state radical concentration on the surface, causing more significant surface radical termimnation.[37] However, this is not a plausible explanation, especially for the significant termination on the surface.

In an ATRP process, the activation-deactivation process reaches the equilibrium of:

$$k_{act}[RQ_0X][Cu^I] = k_{deact}[RQ_0^{\bullet}][XCu^{II}] \quad (6)$$

The radical concentration is:

$$[RQ_0^{\bullet}] = \frac{k_{act}[[RQ_0X][Cu^I]}{k_{deact}[XCu^{II}]} \quad (7)$$

As a result, if the same ratio of $[Cu^{II}]$:$[Cu^{I}]$ is used in the recipe, the radical concentration should be similar and there should not be so significant difference in the termination on the surface. This can readily be proven by simulation.

The simulation for the catalyst concentration 0.0067 mol/L has been done above. The grafting density was about 0.72 chains/nm^2. The experimental data showed that the catalyst concentration did not influence the grafting density and thus this grafting density could be applied in the simulation for the higher catalyst concentration. As shown in Figure 3-7(a), the simulation gave the same results for the same $[Cu^{II}]$:$[Cu^{I}]$ ratio, although the catalyst (Cu^{I}) concentrations were different. The two curves with the same

surface radical termination rate overlapped, despite of the different catalyst concentrations. The reason is obvious: the same $[Cu^{II}]$:$[Cu^{I}]$ ratio and the same surface radical termination rate constant gave the same radical concentration on the surface as shown in Figure 3-7(b) (the two radical concentration curves also overlapped). As a result, the polymer thickness growth rate should be similar. Then there must be other reasons that caused this remarkable termination on the surface.

The radical termination rate is as follows:

$$R_t = k_t[RQ_0^{\bullet}]^2 \tag{8}$$

If the radical concentration is the same, a higher termination rate can only be caused by a higher termination rate constant. It becomes clear that a higher catalyst concentration led to a higher surface termination rate constant, as expected from the proposed surface termination mechanism.

The surface termination rate constant for the catalyst concentration of 0.027 mol/L is 4.8×10^{14} $dm^2/mol\cdot s$, as estimated in the above simulation. It was employed to predict the results for Method II, as shown in Figure 3-7(a). Significant termination on the surface was observed in this case. It confirmed that the significant surface termination observed at the higher catalyst concentration was caused by a higher termination rate constant. Figure 3-7(c) gives the active chain concentration on the surface. With the

surface radical termination rate constant of 4.8×10^{14} $dm^2/mol\cdot s$, the active chain concentration (i.e. grafting density) on the surface decreased rapidly.

The deviation between the experimental and simulation results, as shown in Figure 3-7(a), could be caused by the low grafting density. With a low grafting density (lower than 0.1 chains/nm^2) as shown in Figure 3-7(c), the brush conformation might not form on the surface. The chain ends were not stretched into the solution as in the brush conformation, having full contact with various species in the solution. As a result, the predicted values from the current brush model became higher than the experimental data.

This radical termination mechanism, termed as "migration-termination" in this work, which explained why higher catalyst concentration led to higher termination rate, should be generally applicable in all surface-initiated living polymerization where the polymer chains grow from surface simultaneously. In these cases, all polymer chains are restricted to the surface, while the free diffusion of small activation molecules or capping agents, which differ in different types of living polymerization, enable radicals on the surface "migrate" to facilitate termination. The surface radical termination rate is affected by the concentrations of these small molecules. In solution living polymerization, at high conversions where polymer chains experience diffusion limitations, this kind of "migration-termination" mechanism may also occur.

3.4.2.3 Effect of catalyst concentration

From the above analysis, it seems that a low level of the catalyst concentration should improve the living ATRP on the surface. However, it is not true because the activation-deactivation is another key factor for the livingness of ATRP. In a typical ATRP, the activation and deactivation reactions are very fast so that theoretically less than one monomer can be added to a growing chain in one activation-deactivation circle. This makes all the polymer chains have the same opportunity to grow simultaneously, and a low polydispersity can be achieved. As a result, if the catalyst concentration is too low, the rates of activation and deactivation are too slow and the polymerization loses control.

Figure 3-8 gives the simulation results with varying catalyst concentration. The lower catalyst concentration leads to a higher polydispersity. When the catalyst concentration is 0.000067 mol/L, the polymerization becomes a conventional radical polymerization instead of ATRP, which can be told from its polydispersity curve as shown in Figure 3-8(b). In this case, the polymerization on the surface loses control and the well-modified surface may not be obtained. It is clear that in the s-ATRP, an optimal catalyst concentration exists. If the catalyst concentration is too high, the termination becomes severe. If the catalyst concentration is too low, the activation and deactivation rates are not high enough to assure a living polymerization.

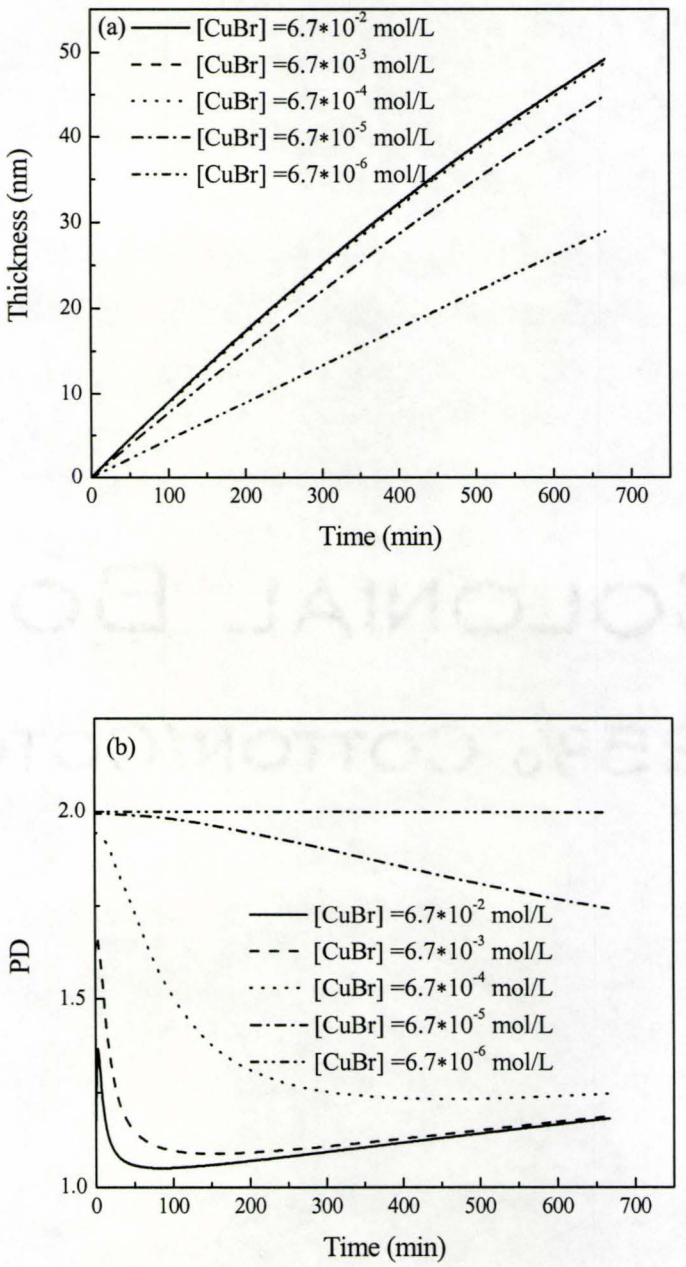

Figure 3-8 Simulation of grafting poly(MPC) from silicon wafer with added excess deactivator (Method II) at lower catalyst concentration. [MPC]=1.33 mol/L,

[CuBr]/[$CuBr_2$]=1:0.2. (a) Grafting thickness versus reaction time and (b) polydispersity versus reaction time.

3.4.2.4 ATRP on surface versus ATRP in solution

We have proposed the new surface migration-termination mechanism for the s-ATRP. The crowding of polymer chains on the surface is not the reason for the significant radical termination as previously believed. On the contrary, this crowding actually imposes a 2-D gel-effect that limits termination. It is a misunderstanding that the ATRP on surface is not as controlled as that in solution. Whether the polymerization on the surface is more or less controlled than in the solution depends on the termination rate on the surface.

In the simulation of Method I, the surface radical termination rate constant was 1.2×10^{14} dm^2/mol·s. It was more significant than that in the solution. As a result, the grafted chain length on the surface was shorter than that in the solution and the polydispersity was higher. If the catalyst concentration was decreased, the surface termination rate decreased. A better controlled and more living ATRP could then be expected on the surface than in the solution.

Assuming the surface radical termination rate constants are 0.6×10^{14} and 0.1×10^{14} dm^2/mol·s, we simulated the results as shown in Figure 3-9. When the surface termination

rate was 0.6×10^{14} $dm^2/mol\cdot s$, the polymer chains on the surface experienced similar termination as those in the solution. As a result, the polymer chain length and polydispersity of the grafted polymer on the surface were the same as those in the solution. When the surface radical termination rate constant was set to 0.1×10^{14} $dm^2/mol\cdot s$, higher chain length and lower polydispersity were found for the grafted chains on the surface, i.e. a better controlled or more living process. The surface polymerization could be a more living process on the surface because of the 2-D gel-effect. The determining factor is the surface termination rate.

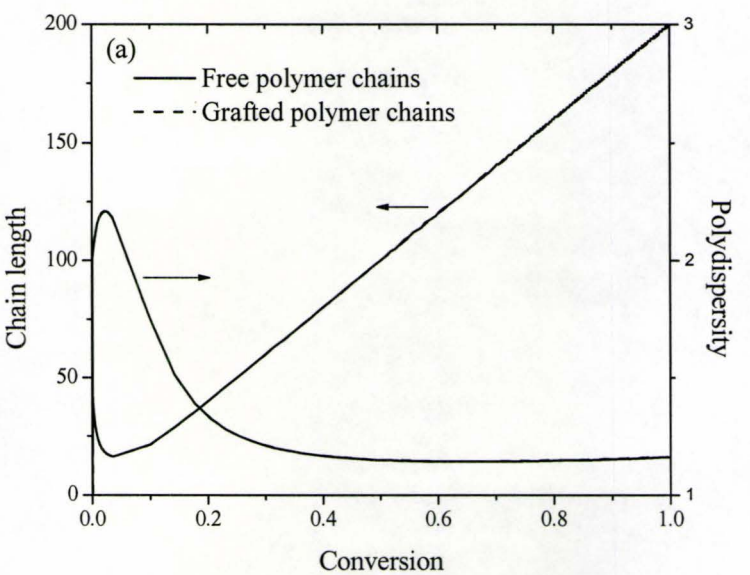

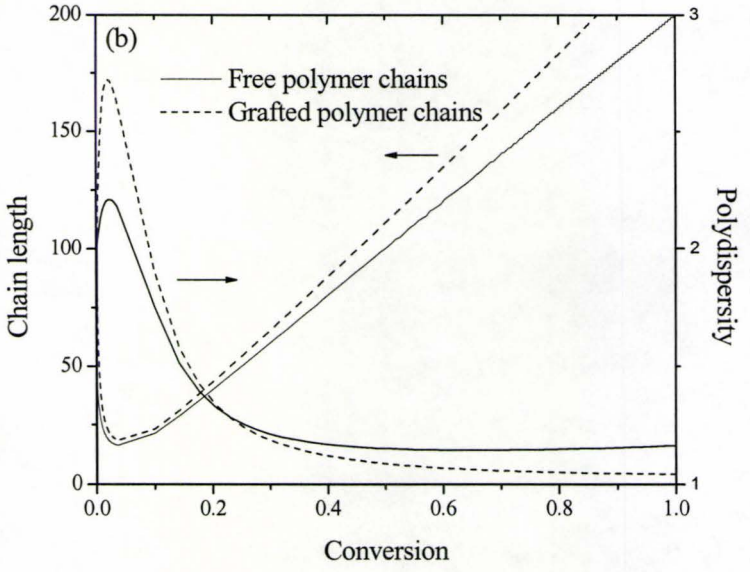

Figure 3-9 Comparison between free polymer chains in the solution and on the surface for different surface termination rates. (a) $k'_t=0.6\times10^{14}$ $dm^2/mol\cdot s$ and (b) $k'_t=0.1\times10^{14}$ $dm^2/mol\cdot s$. [MPC]/[CuBr]/[OEGBr] =200:1:1, [MPC]=1.33 mol/L.

The surface termination rate constant cannot be readily measured. However, the comparison between the chain length and polydispersity of grafted polymer chains on the surface and free polymer chains in the solution can give some indication. There were a few literatures that reported the comparison data. Table 3-3 gives a summary.

Among these studies, about a half found that the surface polymerization gave higher polymer molecular weight and lower polydispersity. Devaux *et al.*[42] found that the chain length of the cleaved chains was 25% higher than that of the free chains. The

polydispersity of the cleaved chains was only 1.05. Most studies concluded that the chain length and polydispersity of the grafted polymers were similar to those in the solution. Little attention was paid to the higher chain length and lower polydispersity on the surface. Based on the present work, it is now understood that the surface living polymerization could be better controlled and more living due to the effect of the proposed migration termination.

Table 3-3 Comparison between grafted and free polymer chains in the surface-initiated living polymerization

Method	Surface	Monomer	Conclusion		Ref.
			Molecular weight	Polydispersity	
NMP	Silica gel particles	Styrene	$Mn_{cleaved} > Mn_{free}$	$PD_{cleaved} < PD_{free}$	Husseman et al.[43]
RAFT	Silica particles	Styrene	$Mn_{cleaved} > Mn_{free}$	$PD_{cleaved} > PD_{free}$	Tsujii et al.[44]
ATRP	Glass filter	MMA	$Mn_{cleaved} < Mn_{free}$	$PD_{cleaved} > PD_{free}$	Ejaz et al.[45]
NMP	Silicon wafer	Styrene	$Mn_{cleaved} > Mn_{free}$	$PD_{cleaved} < PD_{free}$	Devaux et al.[42]
ATRP	High-density polyethylene film	MMA	$Mn_{cleaved} > Mn_{free}$	$PD_{cleaved} \approx D_{free}$	Yamamoto et al.[46]
ATRP	Polystyrene shell latex	*N*,*N*-dimethylacrylamide	$Mn_{cleaved} \approx Mn_{free}$	$PD_{cleaved} < PD_{free}$	Kizhakkedathu et al.[47]

3.5 Conclusion

Based on a moving-boundary brush model, we developed a kinetic model for the

s-ATRP. Combined with the experimental data,[37,39] a comprehensive analysis was carried out to elucidate the s-ATRP mechanism. All information of the grafted polymer chains including active chain concentration, radical concentration, chain length, polydispersity, was calculated using the model. The simulation results showed that the radical termination on the surface was significant and about half of activated chains terminated at the end of reaction in our experimental system. When Method II (add deactivator into solution) was employed, the grafting density, which could not be obtained experimentally, could also be estimated by the simulation. It was found that the deactivator concentration influenced the grafting density. The lower deactivator concentration was, the higher grafting density was achieved. But it also caused a more significant radical termination on the surface. Method I and Method II were compared showing that Method II gave a much better control over molecular weight development of the grafted chains and thicker grafting layer under similar conditions.

A new surface radical termination mechanism, termed migration-termination has been proposed in this work. The crowded polymer chains on the surface caused a 2-dimentional gel-effect, preventing the radical termination, rather than causing more significant termination as previously believed. On the contrary, the activation-deactivation cycle, which is the key making ATRP a living polymerization, made the radicals "migrating" on the surface and facilitated termination. Based on this

mechanism, the catalyst concentration determined the migration rate and the surface radical termination rate in turn. The higher catalyst concentration, the higher surface radical termination rate constant. The simulation in this work also showed that the catalyst concentration should not be too low; otherwise the ATRP could lose its living character.

3.6 Supporting materials

The method of moment is applied in this work to obtain the average molecular weight and polydispersity. The corresponding moments are defined as:

Polymer chain species in the solution:

$$[RQ_j^{\bullet}]_B = \sum_{i=0}^{\infty} i^j [RM_i^{\bullet}]_B$$

$$[RQ_j X]_B = \sum_{i=0}^{\infty} i^j [RM_i X]_B$$

$$[RQ_j]_B = \sum_{i=0}^{\infty} i^j [RM_i]_B$$

$$[RQ_j R]_B = \sum_{i=0}^{\infty} i^j [RM_i R]_B$$

Polymer chain species on the Surface:

$$[RQ_j^{\bullet}]_S = \sum_{i=0}^{\infty} i^j [RM_i^{\bullet}]_S$$

$$[RQ_j X]_S = \sum_{i=0}^{\infty} i^j [RM_i X]_S$$

$$[RQ_j]_S = \sum_{i=0}^{\infty} i^j [RM_i]_S$$

$$[RQ_j R]_S = \sum_{i=0}^{\infty} i^j [RM_i R]_S$$

From mass balance equations, the moment equations can be obtained as follows:

$$\frac{d[RQ_j^{\bullet}]_B}{dt} = k_p \sum_{k=0}^{j-1} \binom{j}{k} [RQ_k^{\bullet}]_B [M]_B + k_{act} [RQ_j X]_B [C]_B - k_{deact} [RQ_j^{\bullet}]_B [XC]_B$$
$$- k_t [RQ_0^{\bullet}]_B [RQ_j^{\bullet}]_B - k_{tr} [RQ_j^{\bullet}]_B$$

$$\frac{d[RQ_j X]_B}{dt} = k_{deact} [RQ_j^{\bullet}]_B [XC]_B - k_{act} [RQ_j X]_B [C]_B$$

$$\frac{d[RQ_j]_B}{dt} = k_{td} [RQ_0^{\bullet}]_B [RQ_j^{\bullet}]_B + k_{tr} [RQ_j^{\bullet}]_B$$

$$\frac{d[RQ_j R]_B}{dt} = \frac{k_{tc}}{2} \sum_{k=0}^{j} \binom{j}{k} [RQ_k^{\bullet}]_B [RQ_{j-k}^{\bullet}]_B$$

For the total chain species:

$$\frac{d([RQ_0^\bullet]_B+[RQ_0X]_B+[RQ_0]_B+[RQ_0R]_B)}{dt}=-\frac{k_{tc}}{2}[RQ_0^\bullet]_B[RQ_0^\bullet]_B$$

$$\frac{d([RQ_j^\bullet]_B+[RQ_jX]_B+[RQ_j]_B+[RQ_jR]_B)}{dt}=k_p\sum_{k=0}^{j-1}\binom{j}{k}[RQ_k^\bullet]_B[M]_B+\frac{k_{tc}}{2}\sum_{k=1}^{j-1}\binom{j}{k}[RQ_k^\bullet]_B[RM_{j-k}^\bullet]_B$$

For the zero moment:

$$\frac{d[RQ_0^\bullet]_B}{dt}=k_{act}[RQ_0X]_B[C]_B-k_{deact}[RQ_0^\bullet]_B[XC]_B-k_t[RQ_0^\bullet]_B[RQ_0^\bullet]_B-k_{tr}[RQ_0^\bullet]_B$$

$$\frac{d[RQ_0X]_B}{dt}=k_{deact}[RQ_0^\bullet]_B[XC]_B-k_{act}[RQ_0X]_B[C]_B$$

$$\frac{d[RQ_0]_B}{dt}=k_{td}[RQ_0^\bullet]_B[RQ_0^\bullet]_B+k_{tr}[RQ_0^\bullet]_B$$

$$\frac{d[RQ_0R]_B}{dt}=\frac{k_{tc}}{2}[RQ_0^\bullet]_B[RQ_0^\bullet]_B$$

For the moment of first order:

$$\frac{d[RQ_1^\bullet]_B}{dt}=k_p[RQ_0^\bullet]_B[M]_B+k_{act}[RQ_1X]_B[C]_B-k_{deact}[RQ_1^\bullet]_B[XC]_B-k_t[RQ_0^\bullet]_B[RQ_1^\bullet]_B-k_{tr}[RQ_1^\bullet]_B$$

$$\frac{d[RQ_1X]_B}{dt}=k_{deact}[RQ_1^\bullet]_B[XC]_B-k_{act}[RQ_1X]_B[C]_B$$

$$\frac{d[RQ_1]_B}{dt} = k_{td}[RQ_0^\bullet]_B[RQ_1^\bullet]_B + k_{tr}[RQ_1^\bullet]_B$$

$$\frac{d[RQ_1R]_B}{dt} = k_{tc}[RQ_0^\bullet]_B[RQ_1^\bullet]_B$$

The moment of second order:

$$\frac{d([RQ_2^\bullet]_B + [RQ_2X]_B + [RQ_2]_B + [RQ_2R]_B)}{dt} = k_p[RQ_0^\bullet]_B[M]_B + 2k_p[RQ_1^\bullet]_B[M]_B + k_{tc}[RQ_1^\bullet]_B[RQ_1^\bullet]_B$$

The average chain lengths and polydispersity can be calculated from the above defined moments as:

$$\bar{r}_n = \frac{[M]_{0B} - [M]_B}{[RQ]_{0B} - [RX]_B - [R^\bullet]_B - [R] - [RR] - [RQ_0R]_B}$$

$$\bar{r}_w = \frac{[RQ_2^\bullet]_B + [RQ_2X]_B + [RQ_2]_B + [RQ_2R]_B}{[M]_{0B} - [M]_B}$$

$$PD = \frac{\bar{r}_w}{\bar{r}_n}$$

For the species on the surface:

Zero moment:

$$\frac{d[RQ_0^\bullet]_S}{dt} = k'_{act}[RQ_0X]_S[C]_B - k'_{deact}[RQ_0^\bullet]_S[XC]_B - k'_t[RQ_0^\bullet]_S[RQ_0^\bullet]_S - k'_{tr}[RQ_0^\bullet]_S$$

$$\frac{d[RQ_0X]_S}{dt} = k'_{deact}[RQ_0^\bullet]_S[XC]_B - k'_{act}[RQ_0X]_S[C]_B$$

$$\frac{d[RQ_0]_S}{dt} = k'_{td}[RQ_0^\bullet]_S[RQ_0^\bullet]_S + k'_{tr}[RQ_0^\bullet]_S$$

$$\frac{d[RQ_0R]_S}{dt} = \frac{k'_{tc}}{2}[RQ_0^\bullet]_S[RQ_0^\bullet]_S$$

For the moment of first order:

$$\frac{d[RQ_1^\bullet]_S}{dt} = k'_p[RQ_0^\bullet]_S[M]_B + k'_{act}[RQ_1X]_S[C]_B - k'_{deact}[RQ_1^\bullet]_S[XC]_B - k'_t[RQ_0^\bullet]_S[RQ_1^\bullet]_S - k'_{tr}[RQ_1^\bullet]_S$$

$$\frac{d[RQ_1X]_S}{dt} = k'_{deact}[RQ_1^\bullet]_S[XC]_B - k'_{act}[RQ_1X]_S[C]_B$$

$$\frac{d[RQ_1]_S}{dt} = k'_{td}[RQ_0^\bullet]_S[RQ_1^\bullet]_S + k'_{tr}[RQ_1^\bullet]_S$$

$$\frac{d[RQ_1R]_S}{dt} = k'_{tc}[RQ_0^\bullet]_S[RQ_1^\bullet]_S$$

The moment of second order:

$$\frac{d([RQ_2^\bullet]_S + [RQ_2X]_S + [RQ_2]_S + [RQ_2R]_S)}{dt} = k'_p[RQ_0^\bullet]_S[M]_B + 2k'_p[RQ_1^\bullet]_S[M]_B + k'_{tc}[RQ_1^\bullet]_S[RQ_1^\bullet]_S$$

Similar to the bulk, we have

$$\bar{r}_n^s = \frac{[RQ_1^\bullet]_S + [RQ_1X]_S + [RQ_1]_S + [RQ_1R]_S}{[RQ]_{0S} - [RX]_S - [R^\bullet]_S - [R]_S - [RR]_S - [RQ_0R]_S)}$$

$$\bar{r}_w^s = \frac{[RQ_2^\bullet]_S + [RQ_2X]_S + [RQ_2]_S + [RQ_2R]_S}{[RQ_1^\bullet]_S + [RQ_1X]_S + [RQ_1]_S + [RQ_1R]_S}$$

$$PD^s = \frac{\bar{r}_w^s}{\bar{r}_n^s}$$

The following conservation equations are also applied:

$$[RQ_0^\bullet]_B + [RQ_0X]_B + [RQ_0]_B + 2[RQ_0R]_B = [RX]_0$$

i.e., the total number of initiator moiety R remains constant.

$$[RQ_0X]_B + [XC]_B = [RX]_0$$

i.e., the total number of atom X remains constant.

$$[C]_B + [XC]_B = [C]_0$$

i.e., the total number of catalyst C remains constant.

$$[RQ_1^\bullet]_B + [RQ_1X]_B + [RQ_1]_B + [RQ_1R]_B = [M]_{0B} - [M]_B$$

i.e., the number of monomeric units remains constant.

The above set of equations can be solved by MathCAD 2001 to obtain the concentrations, chain lengths and polydispersity of various chain species in the solution and on the surface.

3.7 References

1. Edmondson, S.; Osborne, V. L.; Huck, W. T. S. *Chem. Soc. Rev.* **2004,** *33* (1), 14-22.
2. Kato, K.; Uchida, E.; Kang, E. T.; Uyama, Y.; Ikada, Y. *Prog. Polym. Sci.* **2003,** *28* (2), 209-259.
3. Netz, R. R.; Schick, M. *Macromolecules* **1998,** *31* (15), 5105-5122.
4. Currie, E. P. K.; Norde, W.; Stuart, M. A. C. *Adv. Colloid Interface Sci.* **2003,** *100*, 205-265.
5. Zhao, B.; Brittain, W. J. *Prog. Polym. Sci.* **2000,** *25* (5), 677-710.
6. Araki, J.; Kuga, S.; Magoshi, J. *J. Appl. Polym. Sci.* **2002,** *85* (6), 1349-1352.
7. Bridger, K.; Vincent, B. *Eur. Polym. J.* **1980,** *16* (10), 1017-1021.
8. Corbierre, M. K.; Cameron, N. S.; Lennox, R. B. *Langmuir* **2004,** *20* (7), 2867-2873.
9. Dorgan, J. R.; Stamm, M.; Toprakcioglu, C.; Jerome, R.; Fetters, L. J. *Macromolecules* **1993,** *26* (20), 5321-5330.

10. Emoto, K.; Harris, J. M.; VanAlstine, J. M. *Anal. Chem.* **1996,** *68* (21), 3751-3757.

11. Advincula, R. Polymer brushes by anionic and cationic Surface-Initiated Polymerization (SIP). 2006; pp 107-136.

12. Pyun, J.; Kowalewski, T.; Matyjaszewski, K. *Macromol. Rapid Commun.* **2003,** *24* (18), 1043-1059.

13. Matyjaszewski, K.; Xia, J. H. *Chem. Rev.* **2001,** *101* (9), 2921-2990.

14. Matyjaszewski, K.; Miller, P. J.; Shukla, N.; Immaraporn, B.; Gelman, A.; Luokala, B. B.; Siclovan, T. M.; Kickelbick, G.; Vallant, T.; Hoffmann, H.; Pakula, T. *Macromolecules* **1999,** *32* (26), 8716-8724.

15. Pyun, J.; Jia, S.; Kowalewski, T.; Patterson, G. D.; Matyjaszewski, K. *Macromolecules* **2003,** *36* (18), 6952.

16. Gao, X.; Feng, W.; Zhu, S. P.; Sheardown, H.; Brash, J. L. *Langmuir* **2008,** *24* (15), 8303-8308.

17. Gao, X.; Kucerka, N.; Nieh, M. P.; Katsaras, J.; Zhu, S. P.; Brash, J. L.; Sheardown, H. *Langmuir* **2009,** *25* (17), 10271-10278.

18. Kim, J. B.; Bruening, M. L.; Baker, G. L. *J. Am. Chem. Soc.* **2000,** *122* (31), 7616-7617.

19. Boyes, S. G.; Brittain, W. J.; Weng, X.; Cheng, S. Z. D. *Macromolecules* **2002,** *35* (13), 4960-4967.

20. Ma, H. W.; Li, D. J.; Sheng, X.; Zhao, B.; Chilkoti, A. *Langmuir* **2006,** *22* (8), 3751-3756.

21. Treat, N. D.; Ayres, N.; Boyes, S. G.; Brittain, W. J. *Macromolecules* **2006,** *39* (1), 26-29.

22. Ejaz, M.; Yamamoto, S.; Ohno, K.; Tsujii, Y.; Fukuda, T. *Macromolecules* **1998,** *31* (17), 5934-5936.

23. Ejaz, M.; Yamamoto, S.; Tsujii, Y.; Fukuda, T. *Macromolecules* **2002,** *35* (4), 1412-1418.

24. Feng, W.; Chen, R. X.; Brash, J. L.; Zhu, S. P. *Macromol. Rapid Commun.* **2005,** *26* (17), 1383-1388.

25. Jones, D. M.; Brown, A. A.; Huck, W. T. S. *Langmuir* **2002,** *18* (4), 1265-1269.

26. Pietrasik, J.; Bombalski, L.; Cusick, B.; Huang, J. Y.; Pyun, J.; Kowalewski, T.; Matyjaszewski, K. Controlling polymer chain topology and architecture by ATRP from flat surfaces. 2005; pp 28-42.

27. Tsujii, Y.; Ejaz, M.; Yamamoto, S.; Fukuda, T.; Shigeto, K.; Mibu, K.; Shinjo, T. *Polymer* **2002,** *43* (13), 3837-3841.

28. Zhu, S. P. *Macromol. Theory Simul.* **1999,** *8* (1), 29-37.

29. Genzer, J. *Macromolecules* **2006,** *39* (20), 7157-7169.

30. Al-Harthi, M.; Soares, J. B. R.; Simon, L. C. *Macromol. Mater. Eng.* **2006,** *291* (8), 993-1003.

31. Tang, W.; Matyjaszewski, K. *Macromol. Theory Simul.* **2008,** *17* (7-8), 359-375.

32. Al-Harthi, M.; Soares, J. B. P.; Simon, L. C. *Macromol. Theory Simul.* **2006,** *15* (3), 198-214.

33. Xiao, D. Q.; Wirth, M. J. *Macromolecules* **2002,** *35* (8), 2919-2925.

34. Kim, J. B.; Huang, W. X.; Miller, M. D.; Baker, G. L.; Bruening, M. L. *J. Polym. Sci. Pol. Chem.* **2003,** *41* (3), 386-394.

35. Ishihara, K.; Ueda, T.; Nakabayashi, N. *Polym. J.* **1990,** *22* (5), 355-360.

36. Ishihara, K.; Nomura, H.; Mihara, T.; Kurita, K.; Iwasaki, Y.; Nakabayashi, N. *J. Biomed. Mater. Res.* **1998,** *39* (2), 323-330.

37. Feng, W.; Brash, J.; Zhu, S. P. *J. Polym. Sci. Pol. Chem.* **2004,** *42* (12), 2931-2942.

38. Feng, W.; Brash, J. L.; Zhu, S. P. *Biomaterials* **2006,** *27* (6), 847-855.

39. Feng, W.; Zhu, S. P.; Ishihara, K.; Brash, J. L. *Langmuir* **2005,** *21* (13), 5980-5987.

40. Prucker, O.; Ruhe, J. *Macromolecules* **1998,** *31* (3), 602-613.

41. Fischer, H. *J. Polym. Sci. Pol. Chem.* **1999,** *37* (13), 1885-1901.

42. Devaux, C.; Chapel, J. P.; Beyou, E.; Chaumont, P. *Eur. Phys. J. E* **2002,** *7* (4), 345-352.

43. Husseman, M.; Malmstrom, E. E.; McNamara, M.; Mate, M.; Mecerreyes, D.; Benoit, D. G.; Hedrick, J. L.; Mansky, P.; Huang, E.; Russell, T. P.; Hawker, C. J. *Macromolecules* **1999,** *32* (5), 1424-1431.

44. Tsujii, Y.; Ejaz, M.; Sato, K.; Goto, A.; Fukuda, T. *Macromolecules* **2001,** *34* (26), 8872-8878.

45. Ejaz, M.; Tsujii, Y.; Fukuda, T. *Polymer* **2001,** *42* (16), 6811-6815.

46. Yamamoto, K.; Miwa, Y.; Tanaka, H.; Sakaguchi, M.; Shimada, S. *J. Polym. Sci. Pol. Chem.* **2002,** *40* (20), 3350-3359.

47. Kizhakkedathu, J. N.; Brooks, D. E. *Macromolecules* **2003,** *36* (3), 591-598.

Chapter 4

A Facile Method of Forming Nanoscale Patterns on Poly(ethylene glycol)-Based Surfaces by Self-Assembly of Randomly Grafted Block Copolymer Brushes

This chapter is a reproduction of the following published article in Langmuir: Gao, X.; Feng, W.; Zhu, S. P.; Sheardown, H.; Brash, J. L. *Langmuir* **2008**, *24* (15), 8303-8308.

4.1 Abstract

Poly(oligo(ethylene glycol) methacrylate) (POEGMA) block poly(methyl methacrylate) (PMMA) brushes were synthesized on the silicon wafer surfaces by the surface-initiated atom transfer radical polymerization (ATRP) method. Atomic force microscopy, ellipsometry and water contact angle methods were employed to study the surface morphology and stimulus-response behavior. It was found that simple solvent treatments could induce phase segregation of the POEGMA and PMMA segments thus introducing nanoscale patterns. The feature size could be less than 10 nm and was tunable on the nanoscale. Various patterns including spherical aggregates, wormlike aggregates, stripe patterns, perforated layers, and complete overlayers were obtained through adjusting the upper block layer thickness. These patterns could switch between the

different morphologies reversibly after the treatment with selective solvents.

4.2 Introduction

Nanotechnology has generated much interest in recent years. Various nanostructures are valuable in many fields, especially in microelectronics. In biotechnology, nanopatterns are employed to prepare protein, cell, or DNA microarrays.[1-5] They have significant commercial potential in for example the production of biomicroelectromechanical systems (bio-MEMS), biochips, microfluidic devices, biosensors, biodiagnostic devices, etc.[6-12] These patterns also enable researchers to isolate individual biomolecules in specific environments, thus providing a powerful tool to biologists for fundamental research.[13,14] A basic requirement for these nanopatterns in bioresearch is that the interface must have both specific binding capacity for the target biomolecules and a nonfouling "background". As a result, poly(ethylene glycol) (PEG) is among the most important materials to provide the nonfouling function due to its excellent resistance to nonspecific protein adsorption and cell adhesion as well as its nontoxic and nonimmunogenic properties.[6,15] Various micro- or nanosized patterned PEG surfaces have been fabricated to generate protein [16-21] or cell [15,20,22-28] arrays for the design of advanced biomedical devices.

With respect to fabrication methods, lithography is the technique most frequently

used. Delicate lithography designs have produced high quality nanopatterns for different purposes. However, when the feature size is less than 100 nm, electron-beam or certain probe tips including dip pens must be employed; these are complex procedures that incur high costs.[7,29] Simpler operations and smaller feature sizes are fundamental goals in the field of nanopatterning.

The self-assembly of block copolymers is well-known as a facile method to generate patterns in the size range of 10 - 100 nm.[29-32] Recently owing to the development of surface-initiated living polymerization methods, various block copolymer brushes have been grafted on surfaces to produce smart surfaces that can change their properties in response to external stimuli.[33-38] In 2000 Brittain et al. for the first time reported the formation of nanopatterns from the tethered polystyrene-b-poly(methyl methacrylate) brushes after the treatment of selective solvents.[39] Later Genzer et al. revealed the existence of different surface morphologies including flat, micellar, and bicontinuous morphologies when the length of each block was varied.[40,41] Furthermore, Ruhe et al. demonstrated that the brush topography variation induced by the change of external conditions could be employed to move nano objects absorbed on the surface.[42,43] In Choi et al.'s work surface-initiated ring-opening metathesis polymerization method was employed to prepare the block copolymer brushes on the surface.[44] The atomic force microscopy (AFM) images showed that different solvent treatments could give different

surface morphologies. Bruening et al. prepared amphiphilic triblock copolymer brushes and got more uniform domain size.[45] All these studies proved that the self-assembly of block copolymer brushes could be employed to prepare nanoscale patterns on polymeric surfaces.

If this method could be applied to introduce nanoscale patterns to PEG surfaces, it could be a powerful but facile method for nanopatterning in biotechnology applications. The covalent bonds of chemically grafted polymer chains with the surface can lead to patterned surfaces that are stable, thus overcoming some of the problems associated with spun-cast films due to solubility or swelling.[7] In addition, the ease of grafting various types of polymer blocks by current living polymerization methods gives the potential to incorporate numerous functionalities. Furthermore, these living polymerization methods provide polymer brushes with active chain ends. There is currently great interest in modifying the chain ends of grafts to provide biofunction or specific adsorption capacity.[46,47] The special stimulus-responsive behavior of this type of surface leads to useful materials. The self-assembly method has unique advantages including high throughput at low cost, ease in producing 3-D patterns, etc. For patterning with elements in the range <100 nm, this method could be advantageous especially in some applications, where only evenly distributed domains with a certain range of shapes and sizes are required.

In spite of all these advantages, the nanoscale features formed from tethered block copolymer brushes in these studies are not yet as uniform as those from block copolymers. The smallest feature size is still much larger than 10 nm, which can be achieved by the self-assembly of block copolymers. The improvement from the employment of triblock copolymers brushes is limited. In this work the employment of oligo(ethylene glycol) methacrylate (OEGMA) was also aimed at seeking for a new solution to improve the quality of this method. Large-size monomers such as OEGMA had not been used for the block copolymer brushes before. Here it was expected that the relatively long (in comparison to those used in other studies) side chains of Poly(oligo(ethylene glycol) methacrylate) (POEGMA) would have the confinement effect on the features on the surface. As a result better-separated domains, more uniform features, and smaller feature size were expected.

In current work we grafted poly(methyl methacrylate) (PMMA), which is known to adsorb proteins nonspecifically, to POEGMA-grafted surfaces; both of these polymers have the same methacrylate main chain but different side chains. Selective solvent treatment caused phase segregation of the POEGMA and PMMA segments thus introducing nanoscale patterns. AFM, Ellipsometry, and water contact angle methods were employed to study the surface morphology and stimulus-response behavior.

4.3 Experimental section

4.3.1 Materials

$Cu^{I}Br$ (99.999%), $Cu^{II}Br_2$ (99.999%), 2,2'-bipyridyl(Bipy) (99%), ethyl α-bromoisobutyrate (EBIB) (98%), and *N,N,N',N'',N''*- pentamethyldiethylenetriamine (PMDETA) (99%) were purchased from Aldrich and used as received. Methyl methacrylate (MMA) (99%, Aldrich) and OEGMA (98%, M_n = 300 g/mol, Aldrich) were distilled over CaH_2 under vacuum. Toluene (HPLC grade, Aldrich), methanol (HPLC grade, Aldrich), and anisole (99.0%, Aldrich) were distilled over CaH_2 twice. Deionized water from the Millipore water purification system had the minimum resistivity of 18.0 MΩ cm. Argon and nitrogen gas were of ultrahigh purity grade. Silicon wafers with the thickness of 0.56 mm were purchased from University Wafer Company (Boston, MA) and cut into 6 × 6 mm^2 pieces.

4.3.2 Self-assembly of initiator monolayer on the surface

The surface-attachable initiator, 6-(2-bromo-2-methyl) propionyloxy hexenyl trichlorosilane, was synthesized by the hydrosilylation of trichlorosilane with hex-6-en-1-yl 2-bromo-2-methylpropionate.[48] Silicon wafers were pretreated in a clean room first. They were exposed to UV/ozone for 30 min in a cleaning chamber and were subsequently immersed in 0.15 M hydrofluoric acid solution for 20 min to remove the

silicon oxide layer. After that, they were rinsed in deionized water, dried under a nitrogen stream, and exposed to UV/ozone again for 30 min to form a new contamination-free silicon oxide layer. They were then immersed in a 2.5 mM solution of 6-(2-bromo-2-methyl) propionyloxy hexenyl trichlorosilane in dry toluene for 18 h at room temperature to form a self-assembled initiator monolayer with a thickness of 1.6 ± 0.2 nm (measured by ellipsometer). The surfaces were finally cleaned ultrasonically, rinsed 3 times in toluene, and dried in an argon stream.

4.3.3 Preparation of POEGMA-b-PMMA copolymer brushes on the surface

In a typical POEGMA grafting procedure, $Cu^{I}Br$ (28.8 mg, 0.2 mmol) and Bipy (63.6 mg, 0.4 mmol) were placed in a 50-mL flask. The flask was then evacuated and backfilled 3 times with argon. Degassed OEGMA (12 g, 40 mmol) and methanol (20 mL) were then added. After degassing with argon for another 30 min, the mixture was transferred to a glovebox filled with ultrapure nitrogen. EBIB (29.4 μL, 0.2 mmol), as a free initiator, was added to the solution to start polymerization. After stirring for 30 s, the reaction mixture was transferred to small glass tubes containing initiator-grafted silicon wafers. The grafting process proceeded at room temperature for a certain period of time and was stopped by adding a methanol solution of $Cu^{II}Br_2$/Bipy. The POEGMA-grafted surfaces were then cleaned ultrasonically in methanol and rinsed thoroughly to remove physically adsorbed POEGMA. The wafers were dried in an argon stream, ready for

grafting of the second block. To graft PMMA blocks onto POEGMA-grafted surfaces, $Cu^{I}Br$ (143.5 mg, 1 mmol) and $Cu^{II}Br_2$ (44.7 mg, 0.2 mmol) were added to a 100-mL flask that had been evacuated and backfilled with argon. Degassed MMA (30 g, 300 mmol), PMDETA (250.6 μL, 1.2 mmol), and anisole (32 mL) were then added. After being degassed with stirring for another 1 h, the mixture was transferred to a glovebox, distributed into small glass tubes containing POEGMA-grafted silicon wafers. The grafting process was carried out at room temperature for a preset period of time and stopped by adding an anisole solution of $Cu^{II}Br_2$/PMDETA. The same cleaning procedure as described above was followed with toluene as the solvent.

4.3.4 Solvent treatment procedure and characterization

The surface was immersed in the indicated solvent for 4 h at 50 °C, then dried in an argon flow (ultrahigh purity grade) for ~2 min at ambient temperature. The thickness of the grafted polymer layers on the silicon wafers was measured by ellipsometer (Exacta 2000, Waterloo Digital Electronics, He - Ne laser (632.8 nm), incident angle 70°). A one-layer model was used in the estimate of diblock film thickness. The refractive index (n) and extinction coefficient (k) of Si (n = 3.865, k = 0.020) and SiO_2 (n = 1.465, k = 0) were used for the SiO_2 layer. The n = 1.500 and k = 0 values were used for the initiator and polymer layers. The water contact angle was measured using a contact angle goniometer (Model 200, Rame-Hart instrument Co.). A NanoScope IIIa Multimode

atomic force microscope (Digital Instruments, Inc.) was used to investigate surface morphology in air. The tetrahedral tip had a radius of less than 10 nm.

4.4 Results and discussion

4.4.1 Preparation of POEGMA-b-PMMA copolymer brushes on the surface

The surface grafting procedure is indicated briefly in Scheme 4-1. After the cleaning of silicon wafers in a clean room, a self-assembled initiator monolayer was formed on the surface. Surface-initiated ATRP of OEGMA was subsequently carried out in methanol at room temperature. Free initiator was added to the solution to control the polymerization and to estimate the chain length of the grafts.

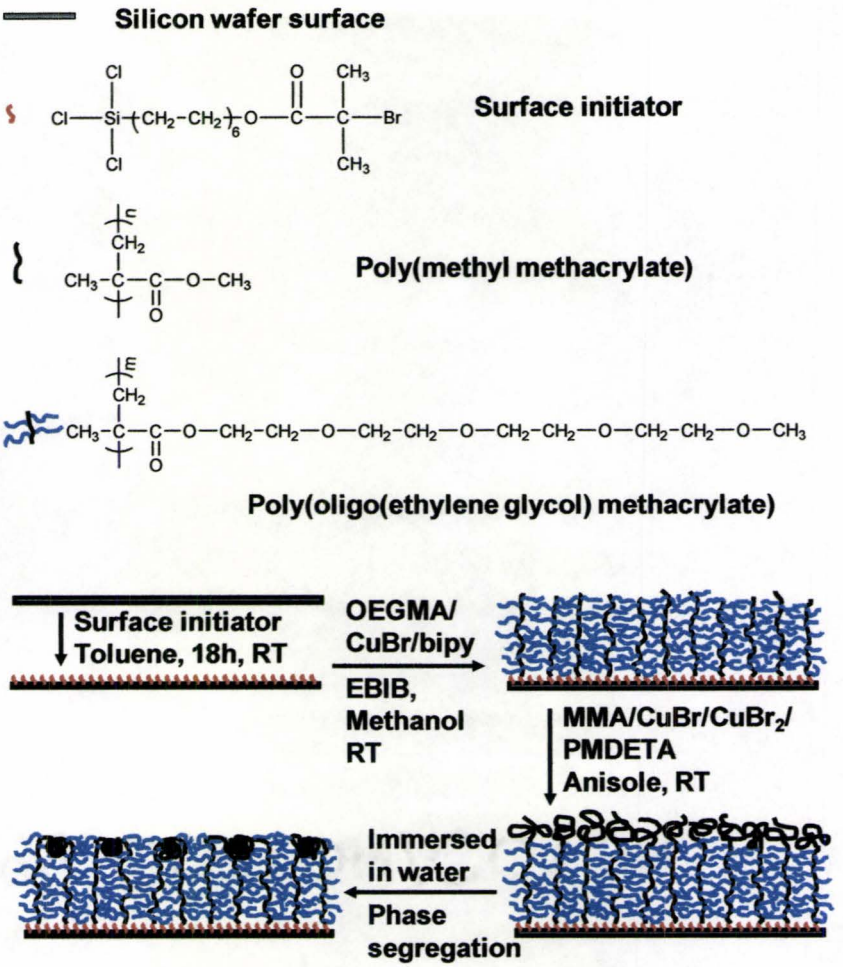

Scheme 4-1 Synthesis procedure for POEGMA-b-PMMA copolymer brushes on silicon wafer via surface-initiated ATRP.

As shown in Figure 4-1 the linear relationship between POEGMA thickness on surface and the OEGMA conversion in solution demonstrates the living nature of this polymerization system. The grafting process was stopped after 18 h at a conversion of 72% to ensure that the graft chain ends remained active. The resulting POEGMA brushes layer had a thickness of 23.4 nm and grafting density of 0.26 chains/nm^2.[48] The grafting

density was estimated with the equation of $\Gamma = d\rho / M_n$ where d is the layer thickness, ρ is the polymer bulk density, and M_n is the polymer molecular weight. An assumed bulk density of 1.0 g/cm^3 was used for POEGMA. The grafted POEGMA molecular weight was assumed to be the same as the free POEGMA in solution. The free POEGMA molecular weight was measured by gel permeation chromatography.

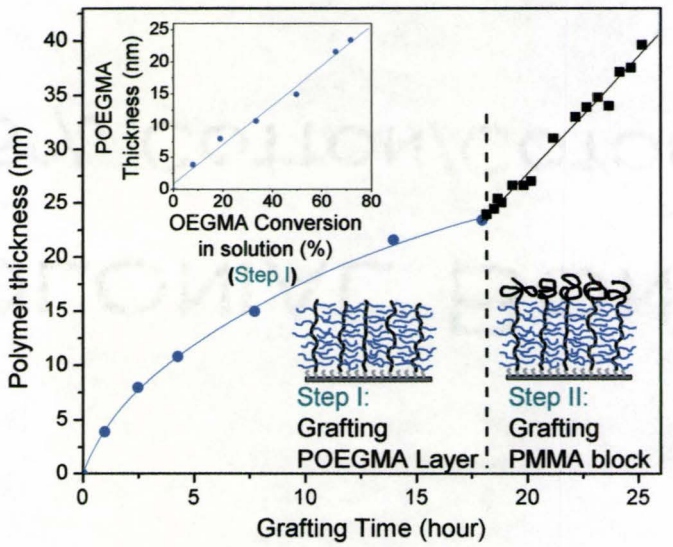

Figure 4-1 Development of polymer graft thickness on silicon wafer. Between steps I and II, the POEGMA grafted surfaces were thoroughly cleaned to remove physically adsorbed species.

Prior to the PMMA block grafting, the POEGMA grafted surfaces were cleaned ultrasonically in methanol and rinsed thoroughly to remove physically adsorbed POEGMA. Then, the surface-initiated ATRP of MMA was carried out in anisole at room

temperature. The POEGMA chain ends on the surface were reactivated to initiate PMMA grafting. Excess deactivator instead of free initiator was added to the solution to ensure good control of the grafting, especially in the early stages. As shown in Figure 4-1, the thickness of the PMMA block increased linearly with time, thus demonstrating a living grafting process.[49,50] A series of surfaces with different PMMA layer thicknesses, from 1.6 to 31.0 nm, were prepared by varying the grafting time.

4.4.2 Water contact angle measurements

Grafted block copolymer brushes have been used for making smart surfaces in the literatures.[33-38] Selective solvent treatment exposes different block segments on the surface thus modulating the surface properties. As a result, the surface can switch between hydrophilic and hydrophobic, protein-adsorbing and protein-repelling, acidic and basic, conductive and nonconductive, etc., according to the chemical composition of two polymer blocks. The surface will adopt the contact angle of the corresponding homogeneous polymer brushes. Therefore, advancing water contact angles are a simple way to examine the switch of the surfaces between the different block segments. In the solvent, the polymer chains can rearrange below their glass transition temperature. In other studies, simple solvent treatments could rearrange the conformation of block copolymer brushes with PMMA segments easily in short time and at low temperature.[39,40,42] In our work, elevated temperature, 50 °C, and relatively long time, 4 h,

were needed for the block copolymer brushes to undergo switching to the equilibrium stage (i.e., contact angle and surface morphology from AFM measurement did not change further). The reason, presumably, is that the OEGMA macromonomer has relatively long side chains, which interact/interfere with one another and slow down the phase segregation process.

Figure 4-2 shows the effect of PMMA layer thickness on water contact angle after selective solvent treatment. After treatment with CH_2Cl_2, a good solvent for PMMA, water contact angles of ~64° were obtained when the grafted PMMA layer was thicker than 1.5 nm. The value 64° is typical of the surfaces grafted with homoPMMA, indicating that the grafted PMMA layer covered the surface well when it was thicker than 1.5 nm. CH_2Cl_2 treatment caused complete coverage of the surface by PMMA. On the other hand, following treatment with water, a poor solvent for PMMA but a good solvent for POEGMA, the contact angle decreased to ~53°. In water, the PMMA chains aggregated and were "hidden" by the POEGMA layer, decreasing their contact with water. Phase segregation of PMMA and POEGMA segments was thus induced. If the PMMA segments could not be completely buried by the POEGMA, the surface would be composed of both PMMA and POEGMA, and the water contact angle would be expected to be intermediate between those for homoPMMA and homoPOEGMA brushes. The value of 53° indicated that the surfaces were composed of both POEGMA and PMMA.

The water contact angle switched between ~64° and ~53° reversibly upon treating the surface with CH_2Cl_2 => H_2O => CH_2Cl_2, etc.

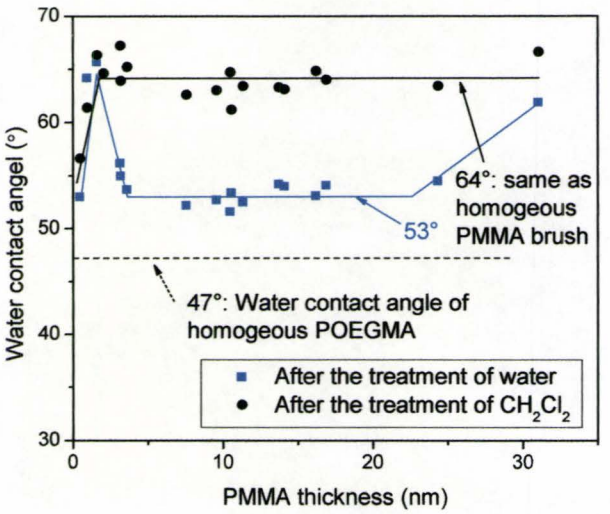

Figure 4-2 Water contact angles after selective solvent treatment. The surface was immersed in the indicated solvent for 4 h at 50 °C and then dried in an argon flow. The advancing water contact angle was measured by the sessile drop method. The measurements were repeatable, and the error was less than ±2°. The homogeneous POEGMA and PMMA brushes grafted surfaces were prepared for comparison. Their water contact angles did not change after solvent treatment.

It should be noted that, after water treatment, the surfaces which had a PMMA layer thinner than 3 nm showed higher water contact angles than those with a thicker PMMA layer. AFM images (Figure 4-3) show that these surfaces are composed of both PMMA and POEGMA. The only difference in the morphology between the thin PMMA

layer samples from the others is that their surfaces are composed of densely distributed PMMA spherical aggregates with the sizes of ~10 nm. Further effort is required to elucidate how this surface morphology affects the water contact angle.

When the PMMA layer was thicker than 30 nm, the water contact angle became close to that of homoPMMA after treating the surfaces with either H_2O or CH_2Cl_2. The surfaces might have a complete coverage of PMMA materials due to the high thickness.

4.4.3 The formation of nanoscale patterns

Figure 4-3 shows the surface morphologies as observed by AFM after water treatment. Parts a and b of Figure 4-3 show height and phase images of the same surface. The patterns formed by the phase segregation of POEGMA and PMMA are clearly observed in the phase image. The bright domains denote PMMA, while the dark areas correspond to POEGMA. The height fluctuation observed in the height image does not affect the interpretation of the phase image. In this work, the thickness of the bottom POEGMA layer was fixed at 23.4 nm; the upper PMMA layer thickness was varied from 1.6 to 31.0 nm. Different nanopatterns were obtained with increasing PMMA layer thickness.

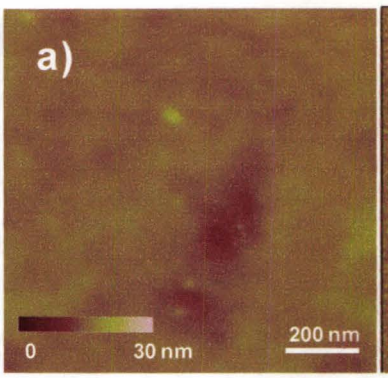

Sample No.1
Height image
PMMA block thickness:
1.6 nm

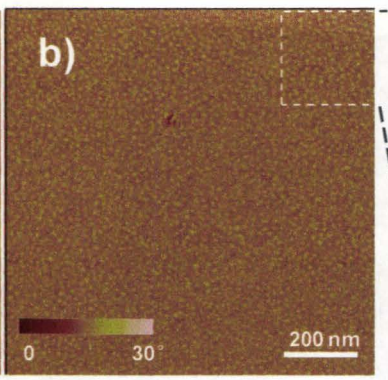

Sample No.1
Phase image
PMMA block thickness:
1.6 nm

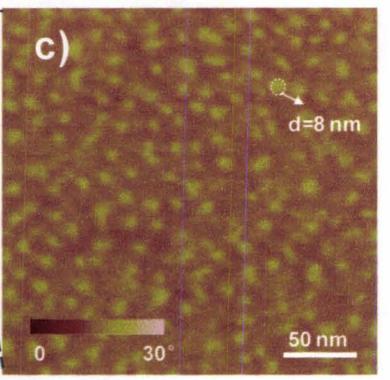

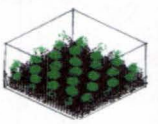

Sample No.1
Phase image
PMMA block thickness:
1.6 nm
Morphology:
Spherical aggregates

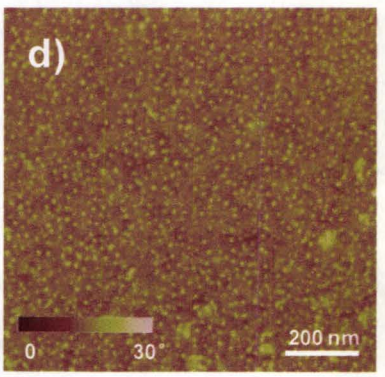

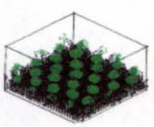

Sample No.2
Phase image
PMMA block thickness:
2.0 nm
Morphology:
Spherical aggregates

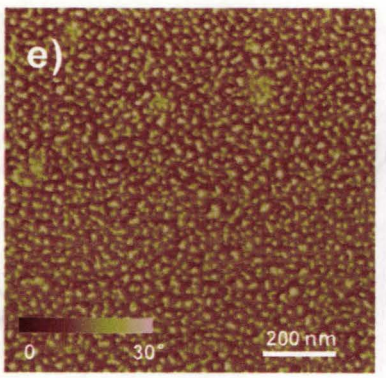

Sample No.3
Phase image
PMMA block thickness:
3.1 nm
Morphology:
Spherical aggregates

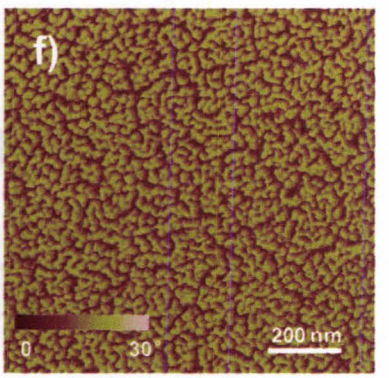

Sample No.4
Phase image
PMMA block thickness:
10.5 nm
Morphology:
Wormlike aggregates

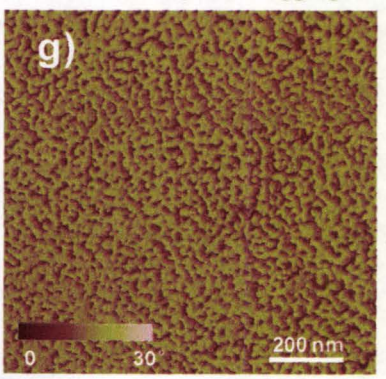

Sample No.5
Phase image
PMMA block thickness:
16.2 nm
Morphology:
Stripe pattern

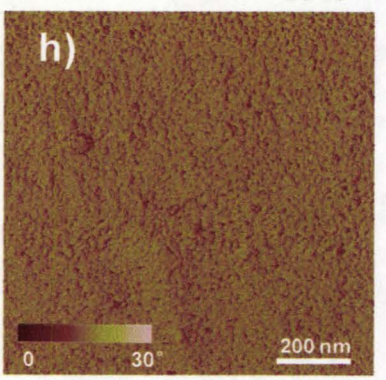

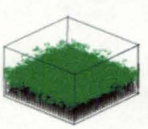

Sample No.6
Phase image
PMMA block thickness:
31.0 nm
Morphology:
Layer

Figure 4-3 AFM images of surfaces after the water treatment. All the samples have the same POEGMA layer thickness of 23.4 nm. PMMA block varies from 1.6 to 31.0 nm. The simulated surface morphologies below AFM images are from Shi's simulation. (Simulations reprinted with permission from ref 51. Copyright 2007 American Chemical Society.)

Interestingly, a simulation study performed recently by Shi et al.[51] for similar densely grafted block copolymer brushes surface shows patterns that have remarkable similarity with our experimental observations. They for the first time demonstrate, via simulation, that the self-assembly of densely grafted block copolymer brushes can give a range of patterns including spherical aggregate, wormlike, stripe, etc., on surface when the upper block thickness is varied. The results of these simulations are shown in Figure 4-3 for comparison purposes. Because the simulation is not specified to certain monomers and experimental system, the simulation images here are mainly to help readers understand different surface morphologies better.

In the present work when the PMMA layer thickness was less than 4 nm, spherical aggregates formed on the surface. Generally the feature sizes given by self-assembly of block copolymers are between 10 and 100 nm.[29,32] In Figure 4-3(b), the PMMA domain size is ~6 - 9 nm. To our knowledge, this is the smallest feature size reported to date by this method. We believe that the relatively long side chains of

POEGMA are the main determinants of this small feature size. As shown in Scheme 4-1, it is thought that all of the polymer chains are constrained to extend and stretch away from the surface at high grafting density. The PMMA domains are separated from each other by the relatively long POEGMA side chains. This minimizes the interactions between adjacent PMMA chains, so if the chain length of the PMMA is short and uniform as expected by the ATRP method, small PMMA domain sizes can be achieved. Another key role of the relatively long side chains is the prevention of the PMMA segments from being buried within the POEGMA layer completely.

Block copolymer brushes can be used as stimulus-responsive surfaces because selective solvent treatment can change the surface properties by switching between the two block types. When the upper polymer block layer is thin, it can be completely buried in the bottom block layer. In this work, the relatively long side chains of POEGMA hindered penetration of the PMMA layer into the POEGMA layer. Consequently, at equilibrium, the PMMA aggregates, of very small size, stayed at the surface following treatment with water. In addition, the use of the living polymerization method made it possible to control the PMMA layer thickness precisely resulting in nanoscale tunability of the feature size as shown in parts b, d, and e of Figure 4-3.

When the PMMA layer thickness was further increased, the spherical aggregates increased in size until they came into contact with each other. In Figure 4-3(e), it can be

seen that some spherical aggregates started to merge, forming wormlike aggregates. When the PMMA layer thickness was 10.5 nm, a wormlike aggregate pattern was formed on the surface (Figure 4-3(f)). When the PMMA layer thickness was increased further, the PMMA domains coalesced, forming a stripe pattern (Figure 4-3(g)). In the present work, no parallel stripes as described in the simulation were obtained. The formation of long-range regular patterns via self-assembly always requires external forces and extra effort (e.g., prepatterned substrates, electric field, mechanical flow field, temperature gradient, etc). When the PMMA block thickness was 31.0 nm, a complete overlayer of PMMA was observed.

4.4.4 Reversible switch between different morphologies

As mentioned previously, these patterns were formed after treatment with water. If a good solvent for PMMA was used instead, the PMMA layer might come to the surface, again giving a complete overlayer. Figure 4-4(a) demonstrates that the surface of the sample 2 changed to a complete overlayer after treatment with CH_2Cl_2, a good solvent for PMMA. This shows that treatment with CH_2Cl_2 "switched" PMMA back to the outermost surface. This observation is consistent with the results of water contact angle measurements. The surface morphology switched between complete overlayer and spherical aggregates reversibly by treating the surface with CH_2Cl_2 => H_2O => CH_2Cl_2, etc. The overlayer morphology was observed in samples with a PMMA thickness less

than 10 nm after treatment with CH_2Cl_2. For the samples with a PMMA thickness greater than 10 nm, perforated layer patterns were observed as shown in Figure 4-4(b). According to Shi's simulation,[51] perforated layers should appear in our samples with the PMMA thickness between 16 and 31 nm (between stripe pattern and overlayer) after treatment with water. In our experimental work, however, perforated layers were not observed in this range. Unexpectedly, after treatment with CH_2Cl_2, perforated layers were observed when the PMMA thickness was larger than 10 nm. In others words, both wormlike aggregates and stripe patterns changed to similar perforated layers, as shown in Figure 4-4(b), following treatment with CH_2Cl_2. From the height image, it is seen that holes remain in the PMMA layer. The bottom of the holes is the POEGMA layer as is evident from the phase image. The depth of the holes is ~3 nm. This switching between the perforated layer and the wormlike aggregate/stripe patterns was also reversible by treating the surface with CH_2Cl_2 => H_2O => CH_2Cl_2, etc. For sample 6, the surface morphology did not change after treatment with CH_2Cl_2. The surface was always covered by the PMMA layer due to its relatively high thickness.

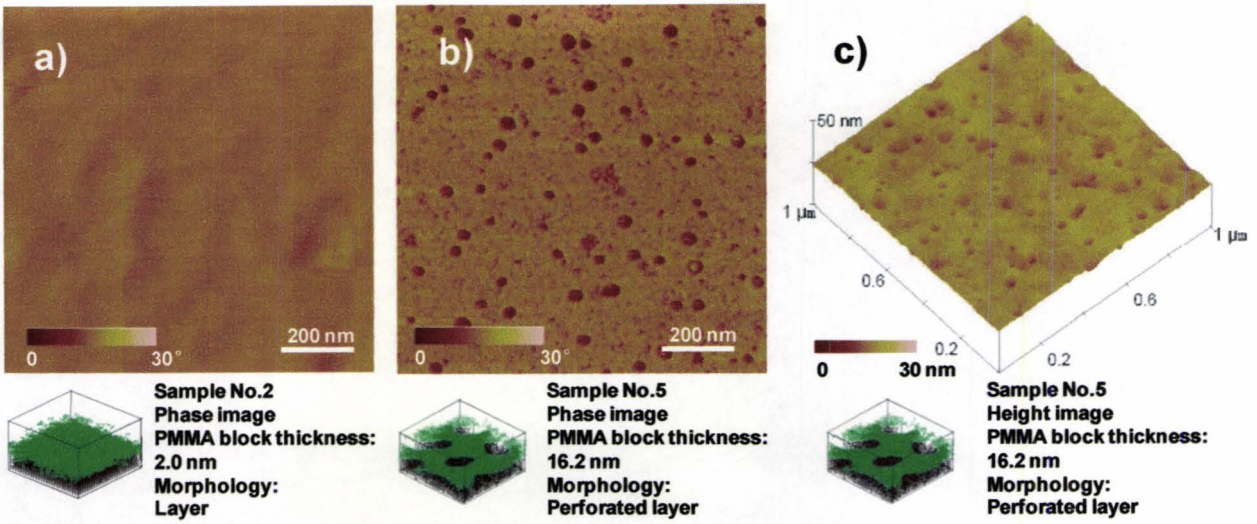

Figure 4-4 AFM images after CH_2Cl_2 treatment. The simulated surface morphologies below the AFM images are from Shi's simulation. (Simulations reprinted with permission from ref 51. Copyright 2007 American Chemical Society.)

4.5 Conclusions

In summary, we successfully introduced nanopatterns onto a PEG-based surface through the self-assembly of randomly grafted block copolymer brushes. Simple selective solvent treatments can introduce nanoscale patterns on the surface. This enables the preparation of nanoscale patterns in large areas and achieves high throughput at low cost. Different patterns including spherical aggregates, wormlike aggregates, stripe patterns, perforated layers, and complete overlayers were achieved through simply varying the upper block layer thickness. It was demonstrated for the first time the relatively long side

chains of the polymer brushes could help increase the quality of this method greatly. It helped constrain the feature size to less than 10 nm, which is the smallest size by this method so far, and tune it on the nanoscale. It also enabled to achieve a range of surface morphologies very clearly. The stimuli-responsive property of these surfaces, switching between the different morphologies reversibly after the treatment with selective solvents, was well demonstrated through AFM and water contact angle methods.

4.6 References

1. az-Mochon, J. J.; Tourniaire, G.; Bradley, M. *Chem. Soc. Rev.* **2007,** *36* (3), 449-457.
2. Fink, J.; Thery, M.; Azioune, A.; Dupont, R.; Chatelain, F.; Bornens, M.; Piel, M. *Lab Chip* **2007,** *7* (6), 672-680.
3. Kane, R. S.; Takayama, S.; Ostuni, E.; Ingber, D. E.; Whitesides, G. M. *Biomaterials* **1999,** *20* (23-24), 2363-2376.
4. Blawas, A. S.; Reichert, W. M. *Biomaterials* **1998,** *19* (7-9), 595-609.
5. Falconnet, D.; Csucs, G.; Grandin, H. M.; Textor, M. *Biomaterials* **2006,** *27* (16), 3044-3063.
6. Otsuka, H.; Nagasaki, Y.; Kataoka, K. *Curr. Opin. Colloid Interface Sci.* **2001,** *6* (1), 3-10.

7. Senaratne, W.; Andruzzi, L.; Ober, C. K. *Biomacromolecules* **2005,** *6* (5), 2427-2448.

8. Rosi, N. L.; Mirkin, C. A. *Chem. Rev.* **2005,** *105* (4), 1547-1562.

9. Blattler, T.; Huwiler, C.; Ochsner, M.; Stadler, B.; Solak, H.; Voros, J.; Grandin, H. M. *J. Nanosci. Nanotechnol.* **2006,** *6* (8), 2237-2264.

10. Whitesides, G. M.; Ostuni, E.; Takayama, S.; Jiang, X. Y.; Ingber, D. E. *Annu. Rev. Biomed. Eng.* **2001,** *3*, 335-373.

11. Khademhosseini, A.; Bettinger, C.; Karp, J. M.; Yeh, J.; Ling, Y. B.; Borenstein, J.; Fukuda, J.; Langer, R. *J. Biomater. Sci. -Polym. Ed.* **2006,** *17* (11), 1221-1240.

12. Galaev, I. Y.; Mattiasson, B. *Trends Biotechnol.* **1999,** *17* (8), 335-340.

13. Craighead, H. G.; James, C. D.; Turner, A. M. P. *Curr. Opin. Solid State Mat. Sci.* **2001,** *5* (2-3), 177-184.

14. Shim, J.; Bersano-Begey, T. F.; Zhu, X. Y.; Tkaczyk, A. H.; Linderman, J. J.; Takayama, S. *Curr. Top. Med. Chem.* **2003,** *3* (6), 687-703.

15. Ma, H. W.; Hyun, J. H.; Stiller, P.; Chilkoti, A. *Adv. Mater.* **2004,** *16* (4), 338-341.

16. Houseman, B. T.; Huh, J. H.; Kron, S. J.; Mrksich, M. *Nat. Biotechnol.* **2002,** *20* (3), 270-274.

17. Lee, K. B.; Park, S. J.; Mirkin, C. A.; Smith, J. C.; Mrksich, M. *Science* **2002,** *295* (5560), 1702-1705.

18. Bruckbauer, A.; Zhou, D. J.; Kang, D. J.; Korchev, Y. E.; Abell, C.; Klenerman, D. *J. Am. Chem. Soc.* **2004,** *126* (21), 6508-6509.

19. Falconnet, D.; Pasqui, D.; Park, S.; Eckert, R.; Schift, H.; Gobrecht, J.; Barbucci, R.; Textor, M. *Nano Lett.* **2004,** *4* (10), 1909-1914.

20. Suh, K. Y.; Seong, J.; Khademhosseini, A.; Laibinis, P. E.; Langer, R. *Biomaterials* **2004,** *25* (3), 557-563.

21. Smith, J. C.; Lee, K. B.; Wang, Q.; Finn, M. G.; Johnson, J. E.; Mrksich, M.; Mirkin, C. A. *Nano Lett.* **2003,** *3* (7), 883-886.

22. Ichino, M.; Nagasaki, Y. *J. Photopolym Sci. Technol.* **2006,** *19* (4), 451-454.

23. Revzin, A.; Tompkins, R. G.; Toner, M. *Langmuir* **2003,** *19* (23), 9855-9862.

24. Lopez, G. P.; Albers, M. W.; Schreiber, S. L.; Carroll, R.; Peralta, E.; Whitesides, G. M. *J. Am. Chem. Soc.* **1993,** *115* (13), 5877-5878.

25. Qian, X. P.; Metallo, S. J.; Choi, I. S.; Wu, H. K.; Liang, M. N.; Whitesides, G. M. *Anal. Chem.* **2002,** *74* (8), 1805-1810.

26. Csucs, G.; Michel, R.; Lussi, J. W.; Textor, M.; Danuser, G. *Biomaterials* **2003,** *24* (10), 1713-1720.

27. Khademhosseini, A.; Jon, S.; Suh, K. Y.; Tran, T. N. T.; Eng, G.; Yeh, J.; Seong, J.; Langer, R. *Adv. Mater.* **2003,** *15* (23), 1995-2000.

28. Khademhosseini, A.; Suh, K. Y.; Jon, S.; Eng, G.; Yeh, J.; Chen, G. J.; Langer, R. *Anal. Chem.* **2004,** *76* (13), 3675-3681.

29. Geissler, M.; Xia, Y. N. *Adv. Mater.* **2004,** *16* (15), 1249-1269.

30. Stoykovich, M. P.; Nealey, P. F. *Mater. Today* **2006,** *9* (9), 20-29.

31. Cheng, J. Y.; Ross, C. A.; Smith, H. I.; Thomas, E. L. *Adv. Mater.* **2006,** *18* (19), 2505-2521.

32. Krausch, G.; Magerle, R. *Adv. Mater.* **2002,** *14* (21), 1579-1583.

33. Zhao, B.; Brittain, W. J. *J. Am. Chem. Soc.* **1999,** *121* (14), 3557-3558.

34. Minko, S.; Muller, M.; Motornov, M.; Nitschke, M.; Grundke, K.; Stamm, M. *J. Am. Chem. Soc.* **2003,** *125* (13), 3896-3900.

35. Xu, C.; Wu, T.; Drain, C. M.; Batteas, J. D.; Fasolka, M. J.; Beers, K. L. *Macromolecules* **2006,** *39* (9), 3359-3364.

36. Minko, S. *Polym. Rev.* **2006,** *46* (4), 397-420.

37. Zhou, F.; Huck, W. T. S. *Phys. Chem. Chem. Phys.* **2006,** *8* (33), 3815-3823.

38. Luzinov, I.; Minko, S.; Tsukruk, V. V. *Prog. Polym. Sci.* **2004,** *29* (7), 635-698.

39. Zhao, B.; Brittain, W. J.; Zhou, W. S.; Cheng, S. Z. D. *J. Am. Chem. Soc.* **2000,** *122* (10), 2407-2408.

40. Tomlinson, M. R.; Genzer, J. *Langmuir* **2005,** *21* (25), 11552-11555.

41. Zhulina, E. B.; Singh, C.; Balazs, A. C. *Macromolecules* **1996,** *29* (19), 6338-6348.

42. Prokhorova, S. A.; Kopyshev, A.; Ramakrishnan, A.; Zhang, H.; Ruhe, J. *Nanotechnology* **2003,** *14* (10), 1098-1108.

43. Santer, S.; Ruhe, J. *Polymer* **2004,** *45* (25), 8279-8297.

44. Kong, B.; Lee, J. K.; Choi, I. S. *Langmuir* **2007,** *23* (12), 6761-6765.

45. Huang, W. X.; Kim, J. B.; Baker, G. L.; Bruening, M. L. *Nanotechnology* **2003,** *14* (10), 1075-1080.

46. Lee, B. S.; Lee, J. K.; Kim, W. J.; Jung, Y. H.; Sim, S. J.; Lee, J.; Choi, I. S. *Biomacromolecules* **2007,** *8* (2), 744-749.

47. Tugulu, S.; Arnold, A.; Sielaff, I.; Johnsson, K.; Klok, H. A. *Biomacromolecules* **2005,** *6* (3), 1602-1607.

48. Feng, W.; Chen, R. X.; Brash, J. L.; Zhu, S. P. *Macromol. Rapid Commun.* **2005,** *26* (17), 1383-1388.

49. Ramakrishnan, A.; Dhamodharan, R.; Ruhe, J. *Macromol. Rapid Commun.* **2002,** *23* (10-11), 612-616.

50. Ramakrishnan, A.; Dhamodharan, R.; Ruhe, J. *J. Polym. Sci. Pol. Chem.* **2006,** *44* (5), 1758-1769.

51. Yin, Y. H.; Sun, P. C.; Li, B. H.; Chen, T. H.; Jin, Q. H.; Ding, D. T.; Shi, A. C. *Macromolecules* **2007,** *40* (14), 5161-5170.

Chapter 5

Nanoscale Patterning Through Self-assembly of Block Copolymer Brushes with Two Hydrophilic Blocks

This chapter is based on the following article in preparation: Gao, X.; Zhu, S. P.; Sheardown, H.; Brash, J. L. Nanoscale Patterning Through Self-assembly of Block Copolymer Brushes with Two Hydrophilic Blocks, 2009.

5.1 Abstract

Poly(oligo(ethylene glycol) methacrylate) (POEGMA) –block-poly(2-(methacryloyloxy)ethyl trimethylammonium chloride) (PMETAC) brushes were synthesized on silicon wafer surfaces by a surface-initiated atom transfer radical polymerization (ATRP) method. The collapse of polyelectrolyte in salt solution was employed to induce phase segregations between these two hydrophilic blocks for the development of nanoscale patterns. The smallest feature size was around 10 nm and was tunable on the nanoscale. Various patterns including spherical aggregates, wormlike aggregates, and line patterns were obtained through adjusting the upper block layer thickness. These nanopatterns could switch between the different morphologies reversibly through the treatment of selective solvents. The adsorption behavior of fibrinogen on these patterns was studied by ellipsometry, water contact angle

measurement, AFM and radio labelling method. The results showed that these nanopatterns possessed the ability to pattern proteins. Fibrinogen was preferably adsorbed on the PMETAC aggregates with POEGMA effectively repelling the protein.

5.2 Introduction

In past decades, nanotechnology has been generating more and more interest in various fields. In biological and medical areas, nanopatterns hold the ability to pattern proteins, cells or DNAs.[1-5] These patterns have found great values in a variety of applications, for example, in the preparation of bio-microelectromechanical systems, biochips, microfluid devices, biosensors, biodiagnostic devices etc.[6-12] In biological fundamental studies, the nanostructure has helped biologists to investigate behaviors of individual biomolecules by isolating and giving them specific surroundings. [13,14]

The fabrication of nanopatterns can be divided into "top-down" and "bottom-up" methods.[15,16] The "top-down" lithographic method is well established and frequently used. It can produce high quality nanopatterns with arbitrary designs at a nanoscale precision. However, when the feature sizes less than 100 nm are required, the complex procedures associated with electron-beam or certain probe tips including dip-pens bear high costs.[7,16] The "bottom-up" method makes full use of the self-assembly of various materials to produce nanoscale patterns at low costs.[16] It has an obvious advantage when large-area

periodic nanopatterns are targeted.

The self-assembly of block copolymers has been widely employed to generate nanoscale patterns in the size range below 100 nm.[15,17,18] In the recent years, several studies were carried out to self-assemble block copolymer brushes into nanoscale patterned surfaces.[19-24] These copolymer brushes are chemically grafted on various surfaces. The chemically grafted polymer chains through covalent bonds on the surfaces can lead to stable patterned surfaces, overcoming some problems associated with spun-cast films due to solubility or swelling. The recent development of various surface-initiated living polymerization techniques offers precise design for copolymer brushes on surface. Furthermore, these living polymerization methods yield polymer brushes with active chain ends. They can be readily modified to introduce more functions to the surface (e.g. biofunction or specific adsorption capacity).

Zhao and Brittain *et al.*[25] for the first time demonstrated the feasibility of introducing nanoscale patterns by self-assembly of the tethered polystyrene-b-poly(methyl methacrylate) brushes after some treatment of selective solvents. Later Genzer and Ruhe *et al.*[26-29] showed that, by varying chain lengths of the blocks, different surface morphologies including flat, micellar and bicontinuous morphologies could be achieved. In Choi *et al.*'s work, the solvent treatments were found to affect surface morphologies as well.[30] Bruening and Baker *et al.*[31] prepared amphiphilic triblock

copolymer brushes on the surface and achieved more uniform domain sizes. In our previous work,[32] we introduced various nanopatterns to a poly(ethylene glycol) (PEG)-based surface through self-assembly of the grafted poly(oligo(ethylene glycol) methacrylate) (POEGMA) -block- poly(methyl methacrylate) (PMMA) brushes. Simple water treatments induced phase segregations of the POEGMA and PMMA segments and thus generated the nanoscale patterns. The smallest feature size was less than 10 nm. Various patterns including spherical aggregates, wormlike aggregates, line patterns, perforated layers and complete overlayers were obtained by varying the upper block layer thickness. These patterns possessed some unique stimuli-responsive properties and were switchable between the different morphologies with simple solvent treatments. All these studies showed that the self-assembly of block copolymer brushes represents a promising approach for the preparation of nanoscale patterns on surfaces.

The objective of this work is to prepare nanoscale patterns by self-assembly of block copolymer brushes to pattern biomolecules for potential biological and medical applications. One basic requirement for these nanopatterns is that their interfaces must have both binding capacity for the targeted biomolecules and at the same time a non-fouling background which can resist the non-specific adsorption of proteins or cells. POEGMA is chosen in this work to provide a non-fouling background. PEG-based polymers are the most important type of materials that provide non-biofouling functions

because of their excellent resistance to non-specific protein adsorption and cell adhesion,[33-37] as well as their non-toxic and non-immunogenic properties.[6,34] Various patterned PEG-based surfaces have been prepared to pattern proteins[38-43] or cells [34,36,42,44-49] for different applications. A hydrophobic polymer has always been used as the top block, to assure phase segregation. In our previous work, PMMA was used as the hydrophobic top block for the phase separation.[32] Hydrophobic polymers have ability to adsorb proteins non-selectively. The patterns prepared from this design have potentials to pattern biomolecules. However, this surface design has its limitation in bioapplications. Although a hydrophobic surface can adsorb proteins, it has been found that some adsorbed proteins greatly changed their conformations on the surface, and as a result, lost their bioactivities. Furthermore, the non-selectivity of hydrophobic surfaces makes it challenging in further modification of chain ends for selectively capture of targeted biomolecules.

The use of hydrophilic polymer as the top block could provide an ideal solution to this problem. However, the difficulty lies in that the phase segregation between two hydrophilic blocks cannot be induced by simple water treatment. The approach in the current work is to use a polyelectrolyte as the top block. In salt solutions, the polyelectrolyte collapses and forms patterns on the surface. Furthermore, the static electrolyte charges may bring more advantages, e.g. external electric field may be applied

to control the formation of patterns. The objective of this work is therefore to prepare the nanoscale patterns from block copolymer brushes having two hydrophilic segments by salt solution treatment and to explore the ability of the polymer patterned surface in developing protein patterns on the surface.

5.3 Experimental section

5.3.1 Materials

$Cu^{I}Br$ (99.999%), $Cu^{I}Cl$ (99.99%), $Cu^{II}Cl_2$ (99.995%), 2,2'-bipyridyl (Bipy) (99%), ethyl α-bromoisobutyrate (EBIB) (98%), and methanol (HPLC grade, Aldrich) were purchased from Aldrich and used as received. Oligo(ethylene glycol) methacrylate (OEGMA) (98%, M_n = 300 g/mol, Aldrich) was distilled over CaH_2 under vacuum. [2-(Methacryloyloxy)ethyl]trimethylammonium chloride (METAC) solution (75 wt. % in H_2O, M_n = 207.70 g/mol, Aldrich) was passed through an inhibitor remover column (Aldrich) to remove the inhibitor, monomethyl ether hydroquinone. Toluene (HPLC grade, Aldrich) was distilled over CaH_2 twice. Deionized water from the Millipore water purification system had the minimum resistivity of 18.0 MΩ·cm. Argon and nitrogen gas were of ultra-purity grade. Silicon wafers with 0.56 mm thickness were purchased from University Wafer Company (Boston, MA) and cut into 12×6 mm^2 pieces.

5.3.2 Self-assembly of initiator monolayer on surface

Silicon wafers were treated first in a clean room environment before the grafting process. They were exposed to UV/ozone for 30 min, and then immersed in 0.15 M hydrofluoric acid solution for 20 min to remove the silicon oxide layer. After that, they were rinsed thoroughly by deionized water, dried under a nitrogen stream, and exposed to UV/ozone again for 30 min to form a new contamination-free silicon oxide layer. The surface-attachable ATRP initiator, 6-(2-bromo-2-methyl) propionyloxy hexenyl trichlorosilane (BMPHTC) was synthesized beforehand.[50] The pre-treated silicon wafers were subsequently immersed in a 2.5 mM solution of BMPHTC in dry toluene for 18 h at room temperature to form a self-assembled initiator monolayer with a thickness of 1.6 ± 0.2 nm. The surfaces were finally cleaned in toluene ultrasonically, rinsed 3 times, and then dried in an argon stream.

5.3.3 Preparation of POEGMA-b-PMETAC copolymer brushes on surface

To graft POEGMA brushes onto silicon wafers, $Cu^{I}Br$ (28.8 mg, 0.2 mmol) and Bipy (63.6 mg, 0.4 mmol) were first added to a 50-mL flask.[32] The flask was then evacuated and backfilled with argon 3 times to remove oxygen. Degassed OEGMA (12 g, 40 mmol) and methanol (20 ml) were then transferred into the flask. The solution was degassed with argon for another 30 min before it was transferred to a glove box filled

with ultra-pure nitrogen. The free initiator EBIB (29.4 μL, 0.2 mmol) was added to the solution to initiate polymerization. After stirring for another 30 sec, the reaction mixture was allocated to small glass tubes containing initiator-grafted silicon wafers. The grafting reaction was stopped by adding a methanol solution of $Cu^{II}Br_2$/Bipy after a certain period of time. The POEGMA-grafted surfaces were then cleaned ultrasonically in methanol, rinsed thoroughly to remove physically adsorbed POEGMA, and finally dried in an argon stream, ready for grafting the second block. To graft PMETAC block onto POEGMA-grafted surfaces, $Cu^{I}Cl$ (89.1 mg, 0.9 mmol), $Cu^{II}Cl_2$ (24.2 mg, 0.18 mmol) and Bipy (337.3 mmg, 2.16 mmol) were first placed into a 50-mL flask. It was evacuated and backfilled with argon for 3 times. Degassed METAC solution (10 g, 36 mmol METAC), methanol (10ml) and water (2.5ml) were then added to the flask. The mixture was degassed for another hour, then transferred to a glove box, distributed into small glass tubes with POEGMA-grafted silicon wafers. The grafting process was carried out at room temperature for a preset period of time and stopped by adding a methanol/water (volume ratio of 2:1) solution of $Cu^{II}Cl_2$/Bipy. The same cleaning procedure as described above was followed.

5.3.4 Characterization

The thickness of the grafts on the silicon wafers was measured by ellipsometer (Exacta 2000, Waterloo Digital Electronics, He-Ne laser (632.8 nm), incident angle 70°).

The water contact angle was measured with a contact angle goniometer (Model 200, Rame-Hart instrument Co.). A NanoScope IIIa Multimode atomic force microscope (Digital Instruments, Inc.) was employed to observe surface morphology in air.

5.3.5 Protein adsorption experiments

Protein adsorption experiments were carried out in isotonic tris buffered saline (TBS) with radioiodinated fibrinogen. The molecular weight and dimension of fibrinogen are 340,000g/mol and 450×90×90 $Å^3$, respectively. Its adsorption behavior on POEGMA surfaces was evaluated in our previous work.[51] To count the amount of protein adsorption on the surface, fibrinogen was radiolabeled with Na125I via the iodine monochloride (ICl) method.[52] Ion exchange chromatography was employed to remove unbound radioactive iodide. The solutions for protein adsorption contained only 10% radiolabeled proteins. The surfaces were immersed in the protein solution for 2 h allowing protein adsorption to reach equilibrium. The surfaces were then put into fresh TBS solution for 5 min (3 cycles) to remove loosely adsorbed proteins, dried and measured by a Wizard 3″ 1480 Automatic Gamma Counter (Perkin-Elmer Life Sciences) to count the amount of proteins adsorbed on the surface. For surface morphology observation by AFM method, the same procedure was used except that regular fibrinogen without radio labeling was used.

5.4 Results and discussion

5.4.1 Preparation of POEGMA-b-PMETAC copolymer brushes

The surface grafting procedure is described briefly in Scheme 5-1. After the pre-treatment of silicon wafers in a clean room, an initiator monolayer was grafted onto the surface. The surface-initiated ATRP of OEGMA was subsequently carried out at room temperature. The free initiator was added to the solution to generate deactivator and thus to assure the living character of ATRP. As shown in Figure 5-1, the thickness of POEGMA brushes grow linearly with the OEGMA conversion in the solution, demonstrating the living character of this system. The grafting process was stopped after 18 h with at 72% conversion to prevent the chain ends from termination. The surfaces were cleaned ultrasonically in methanol and rinsed thoroughly to remove physically adsorbed POEGMA chains. The resulting POEGMA brushes had a thickness of 23.4 nm and an estimated grafting density of 0.26 chains/nm^2.[50]

PMETAC block was grafted to the brushes through ATRP chain extension of POEGMA. The chain ends of the POEGMA brushes were reactivated by the catalyst in the solution to initiate the PMETAC grafting. Excess deactivator, instead of free initiator, was added to maintain the living character of ATRP, especially in the early stages. As shown in Figure 5-1, the thickness of the PMETAC block increased linearly with time,

indicating a living grafting process.[53,54] Surfaces having PMETAC block thicknesses varying from 2.4 to 10.6 nm were prepared by controlling the grafting time.

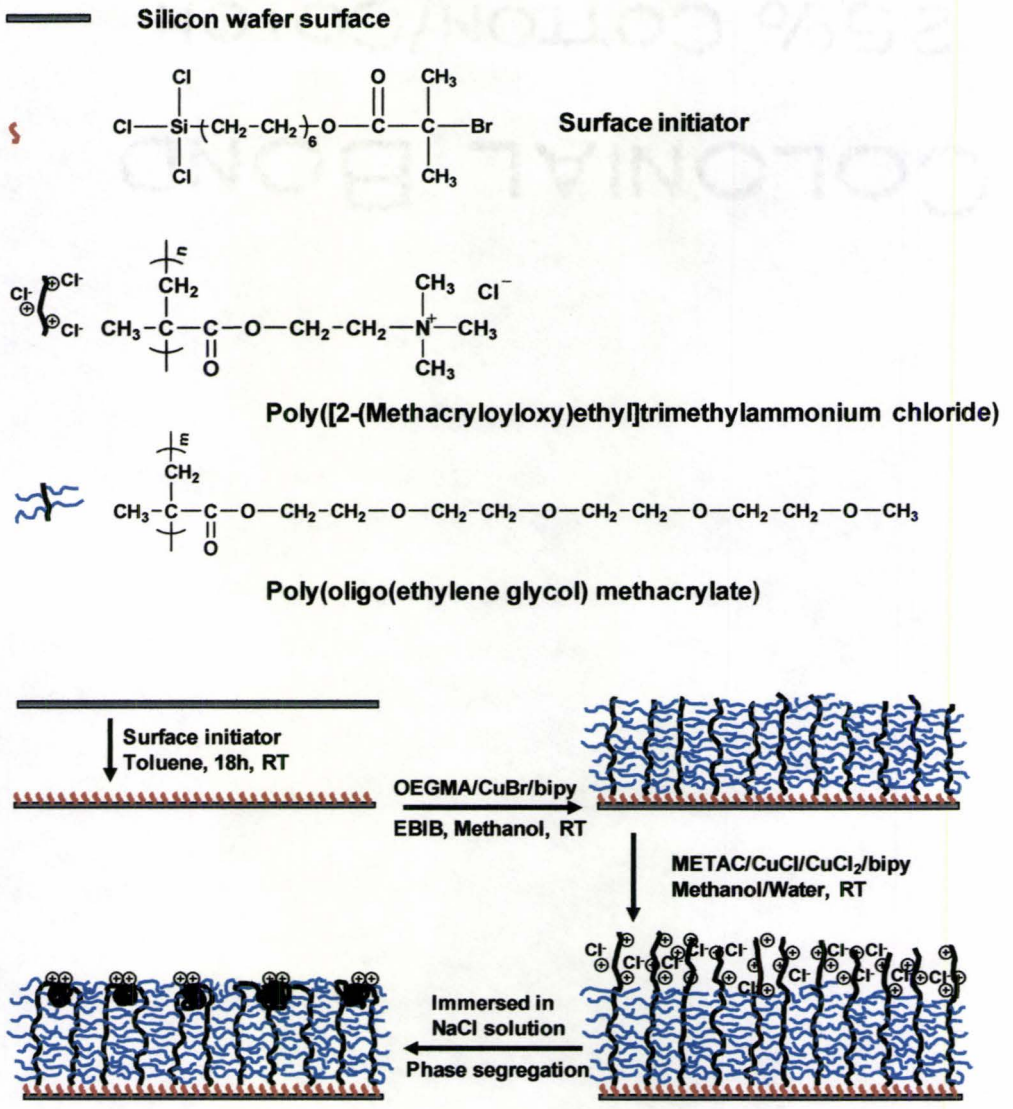

Scheme 5-1 Synthesis procedure for POEGMA-b-PMETAC copolymer brushes on silicon wafer via surface-initiated ATRP.

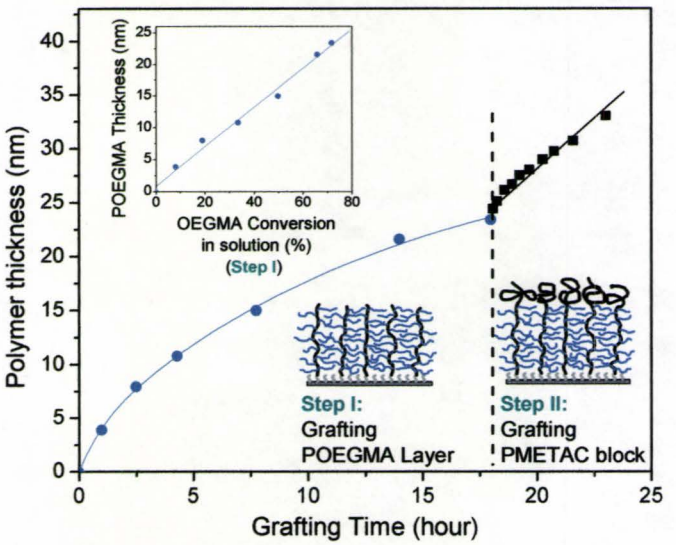

Figure 5-1 Development of polymer graft thickness on silicon wafer.[32] The thickness data are repeatable with the error less than 5%.

5.4.2 Formation of nanoscale patterns

The surfaces were immersed in the 0.5 mol/L NaCl solution for 4 h at room temperature, and were then dried in an argon flow (ultra-purity grade) for ~2 min. The dry state surface morphologies were observed by AFM, as shown in Figure 5-2. Figure 5-2(a) and (b) give the height and phase images of the same surface. The height image gives the height variation on the surface. The obtained patterned surface was still flat, as shown in Figure 5-2(a). The phase image detects the chemical variation on the surface. Figure 5-2(b) shows the patterns developed from the phase segregation between POEGMA and PMETAC. In the NaCl solution, PMETAC, a strong polyelectrolyte,

collapsed on the POEGMA surface and thus formed the nanoscale aggregates. The bright domains denote PMETAC, while the dark areas correspond to POEGMA. The chemical variations on the surface were the target in this work; therefore only phase images were examined in details.

In the current study, the bottom POEGMA layer thickness was fixed to ~23.4 nm and the upper PMETAC layer thickness was varied from ~2 nm to ~12.0 nm. Different nanoscale patterns were achieved through varying PMETAC layer thickness. The simulations from Shi *et al* [55] for the similar densely grafted block copolymer brushes were given below the corresponding AFM images. The simulation work showed that the self-assembly of densely grafted block copolymer brushes could give a range of patterns including spherical aggregate, wormlike and line pattern *etc.* on the surface when the upper block thickness was varied. Our experimental observation verified the theoretical simulation with the remarkably similar patterns.

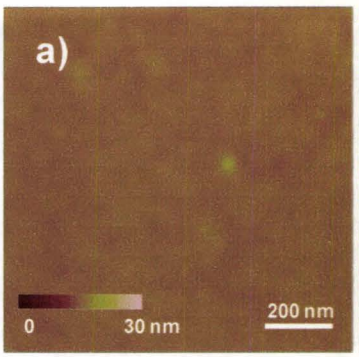

Sample No.1
Height image
PMETAC block thickness:
2.4 nm

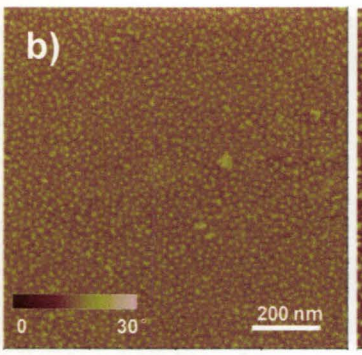

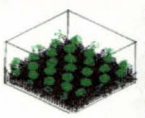

Sample No.1
Phase image
PMETAC block
thickness: 2.4 nm
Morphology:
Spherical aggregates

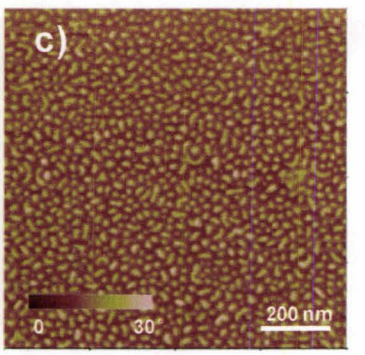

Sample No.2
Phase image
PMETAC block
Thickness: 5.8 nm
Morphology:
Spherical aggregates

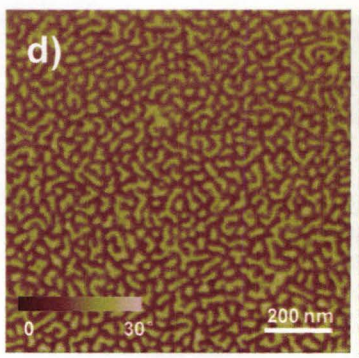

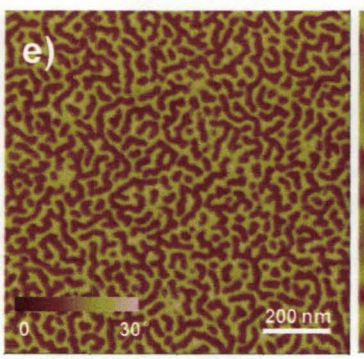

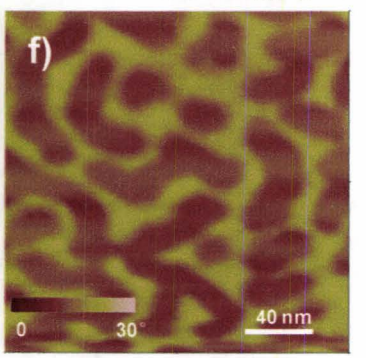

Sample No.3
Phase image
PMETAC block
Thickness: 7.3 nm
Morphology:
wormlike aggregates

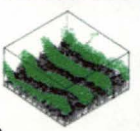

Sample No.4
Phase image
PMETAC block
Thickness: 10.6 nm
Morphology:
Line patterns

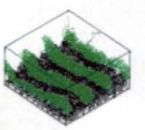

Sample No.4
Phase image
PMETAC block
Thickness: 10.6 nm
Morphology:
Line patterns

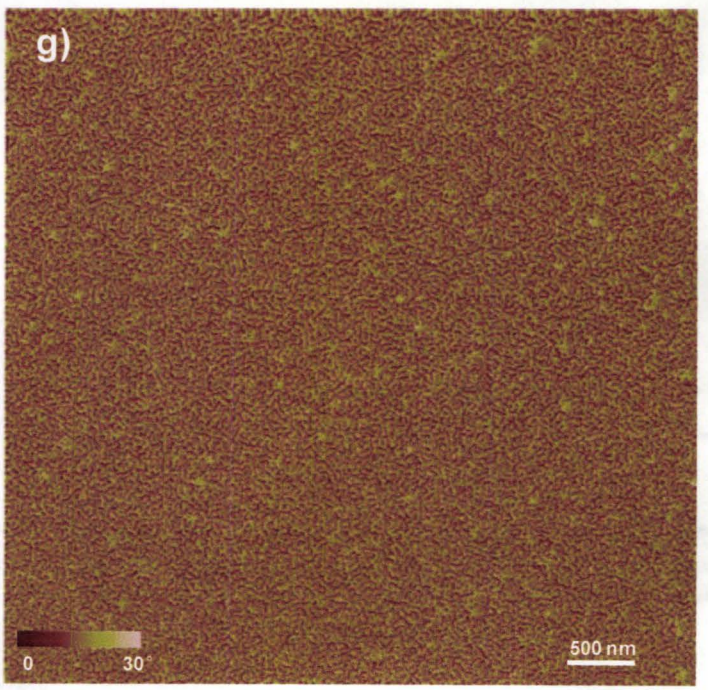

Sample No.4
Phase image
PMETAC block
Thickness: 10.6 nm
Morphology:
Line patterns

Figure 5-2 AFM image of surface in air. All the samples have the same POEGMA layer thickness of 23.4 nm. PMMA block varies from 2.4 nm to 10.6 nm. The simulated surface morphologies beside AFM images are from Shi's simulation (reprinted with permission from ref 55. Copyright 2007 American Chemical Society.)

Sample 1 and Sample 2 had the PMETAC layer thickness less than 6 nm, forming spherical aggregates as shown in Figure 5-2(b) and (c). The smallest PMETAC domain size was less than 10 nm. In our previous work, the smallest domain size achieved by the self-assembly of POEGMA-block-PMMA brushes was 6~9 nm. These feature sizes are among the smallest ones achieved by the self-assembly of block copolymers, which normally gives feature sizes between 10 and 100 nm.[16,18] We believe that the long side chains of POEGMA effectively isolated the PMETAC aggregates and resulted in the small feature sizes.

When the PMETAC layer thickness was further increased, the spherical aggregates increased in size until they came into contact with each other forming the wormlike aggregates. As shown in Figure 5-2(d), the wormlike aggregates formed when the PMETAC layer thickness was 7.3 nm. When the PMETAC layer thickness was increased to 10.6 nm, the PMETAC domains coalesced, forming a line pattern (Figure 5-2 (e)). In our studies, no parallel lines were achieved as described in Shi's simulation. External aids (e.g. pre-patterned substrates, electric field, mechanical flow field,

temperature gradient etc) may help form the long-range regular patterns via the self-assembly method.

Figure 5-2(f) gives a scan area of 200 nm × 200 nm to closely examine the line pattern. It is evident that the feature size is quite uniform, although the self-assembly method can only give random patterns. These random patterns with the uniform feature size can be employed as modules to prepare nanoscale products where only a random nanoscale structure is required, e.g. nanoscale membranes, nanoparticles and nanofibers, high-efficient catalysis, etc.

The advantage of the self-assembly method lies in its ability to prepare large area patterns at low costs. Figure 5-2(g) gives a scan of 5 μm×5 μm area. As it can be seen, no defects are observed. The feature size is very uniform in the large area.

5.4.3 Stimuli-responsive behavior

The nanoscale patterns formed after the surfaces were treated with NaCl solution. When the surfaces were treated with pure water, the PMETAC blocks stretched out from the surface, giving a complete PMETAC overlayer. Figure 5-3(a) and (b) show the surface morphologies of Sample 3 and Sample 4 after the water treatment. The bright dots in Figure 5-3(a) were caused by AFM tip contaminations. This switch of the surface morphologies was reversible through the treatment with different solvents. The overlayer

morphology was observed in the samples having PMETAC thickness greater than 7 nm after treated with water. The overlayers in Sample 1 and Sample 2 were incomplete, because the PMETAC layers were too thin.

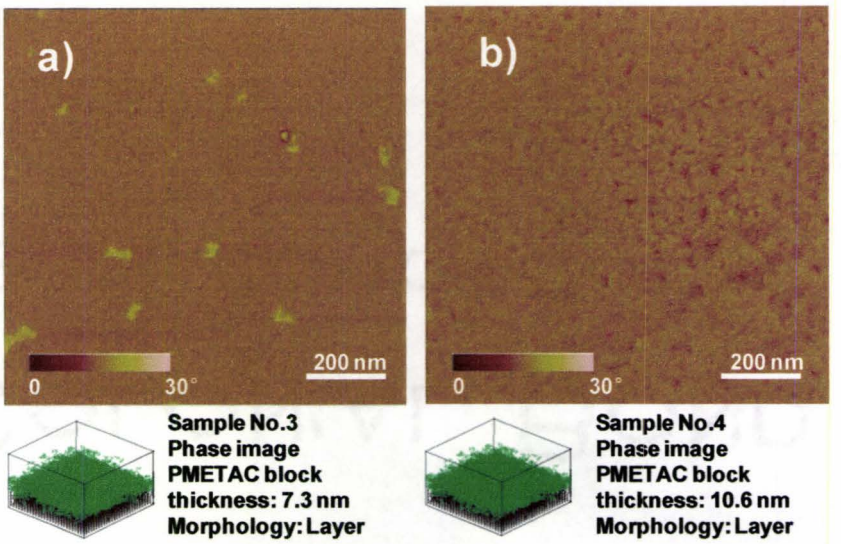

Figure 5-3 AFM images after water treatment. The simulated surface morphologies below the AFM images are from Shi's simulation (reprinted with permission from ref 55. Copyright 2007 American Chemical Society.)

5.4.4 Protein adsorption on nanoscale patterns

Ellipsometry, water contact angle measurement, AFM, and radio labelling method were used to study the fibrinogen adsorption behaviours on these surfaces. Figure 5-4 shows an AFM image of fibrinogen adsorbed on the POEGMA surface. Fibrinogen aggregated easily when its concentration was high.

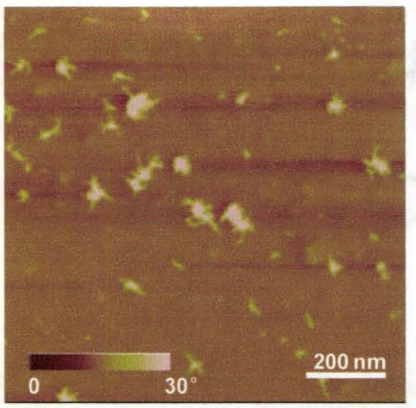

Figure 5-4 AFM phase image of fibrinogen on a POEGMA surface.

The surfaces grafted with POEGMA brushes have been widely studied for their biocompatibility in resisting protein adsorption. It was found in our previous work that the surfaces grafted with POEGMA brushes adsorbed only 26 ng/cm^2 fibrinogen. Compared to the unmodified silicon wafer of 773 ng/cm^2, it was about 95% reduction. Figure 5-5 shows the water contact angle measurements. The water contact angle of the POEGMA surface did not change significantly before and after fibrinogen adsorption. However, the water contact angle of silicon wafer surface was increased from 40° to 70° after the fibrinogen adsorption. The monolayer adsorption of fibrinogen on a flat surface is estimated to be between 140 to 700 ng/cm^2. The adsorption amount of 773 ng/cm^2 on silicon wafer indicates a complete coverage. The ellipsometry could not detect any increase in thickness of the POEGMA surface after fibrinogen adsorption. However, an increase of 13 nm in thickness was detected on silicon wafer after the fibrinogen adsorption, as shown in Figure 5-6. All the measurements confirmed the excellent

performance of POEGMA brushes in resisting fibrinogen adsorption.

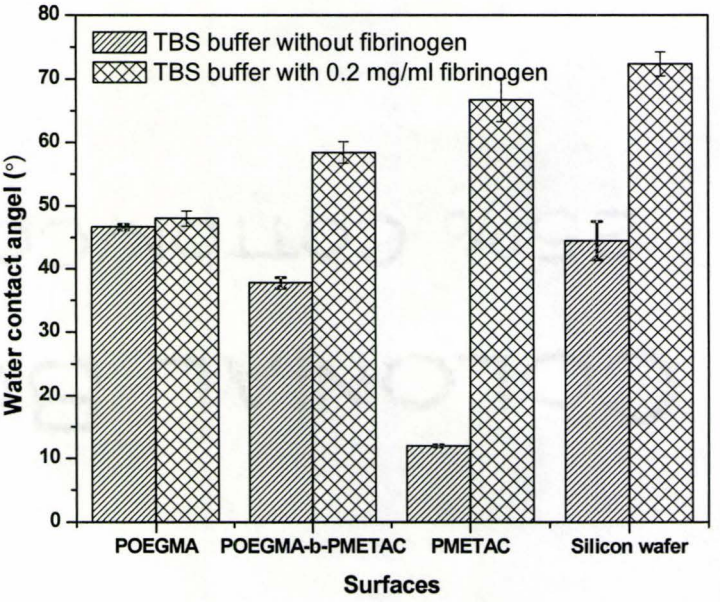

Figure 5-5 Water contact angle of the surfaces before and after fibrinogen adsorption. The advancing water contact angle was measured by the sessile drop method.

PMETAC could also adsorb proteins through electronic interactions. Figure 5-6 shows an increase of 8 nm thickness, suggesting adsorption of fibrinogen on the surface grafted with PMETAC brushes. The water contact angle changed from 10° to 70°, close to the typical value of a complete coverage of fibrinogen. The radio labelling experiment gave 240 ng/cm^2 fibrinogen adsorbed on the PMETAC surface, also in the monolayer range. Figure 5-7 shows an AFM image the homogeneous surface, indicating a complete

covered PMETAC surface. All the results confirmed a monolayer of fibrinogen on the PMETAC surface.

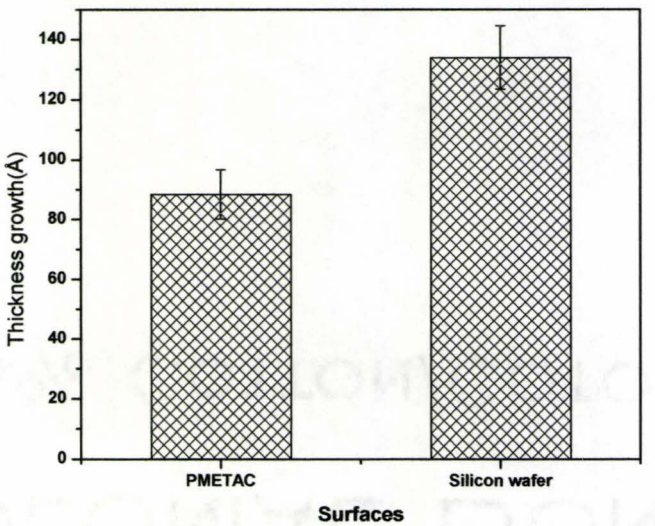

Figure 5-6 The increase in thickness on the surfaces after fibrinogen adsorption.

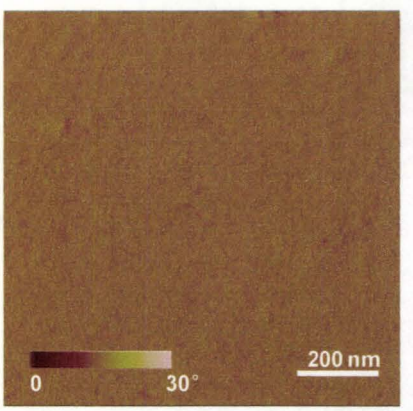

Figure 5-7 AFM phase image of fibrinogen on the PMETAC surface.

Based on the above fibrinogen adsorption behavior on POEGMA and PMETAC brushes, it was hypothesized that the nanopatterns prepared in this work from

POEGMA-b-PMETAC have the ability to pattern proteins. As illustrated in Scheme 5-2, the PMETAC aggregates attract fibrinogen, while the POEGMA background repels the protein. A protein pattern similar to the original polymer pattern would form.

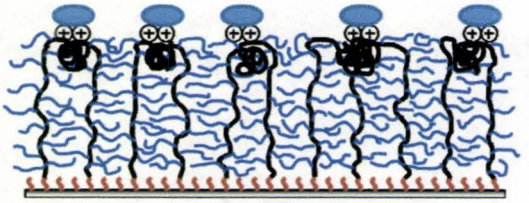

Scheme 5-2 The fibrinogen adsorption scheme on POEGMA-b-PMETAC nanopatterns.

The protein concentration in solution is an important factor that determines the amount of protein adsorption on the surface. Three levels of concentration were used in this work to study. The contrasts between fibrinogen and POEGMA background as shown in Figure 5-4 are close to those between PMETAC and POEGMA in Figure 5-2. However, a careful examination of three images in Figure 5-8 revealed that fibrinogen was preferably adsorbed on PMETAC with an increase in the protein concentration. The contrast between PMETAC domains and POEGMA background increased obviously while the fibrinogen concentration increased from 0.02 mg/ml (Figure 5-8(a)) to 0.2 mg/ml (Figure 5-8(b)). It is well known that fibrinogen tends to aggregate easily. It is evident in Figure 5-8(b) that some fibrinogen aggregated and even covered a part of the POEGMA background. The aggregated fibrinogen has the exactly same color as the PMETAC domains, suggesting a complete coverage of the PMETAC domains by

fibrinogen of 0.2 mg/ml. When the fibrinogen concentration was further increased to 1 mg/ml, more fibrinogen aggregated and covered the POEGMA background. It becomes clear that there exists an optimal fibrinogen concentration (about 0.2 mg/ml) for a complete coverage of the PMETAC domains but leaving POEMGA background clean.

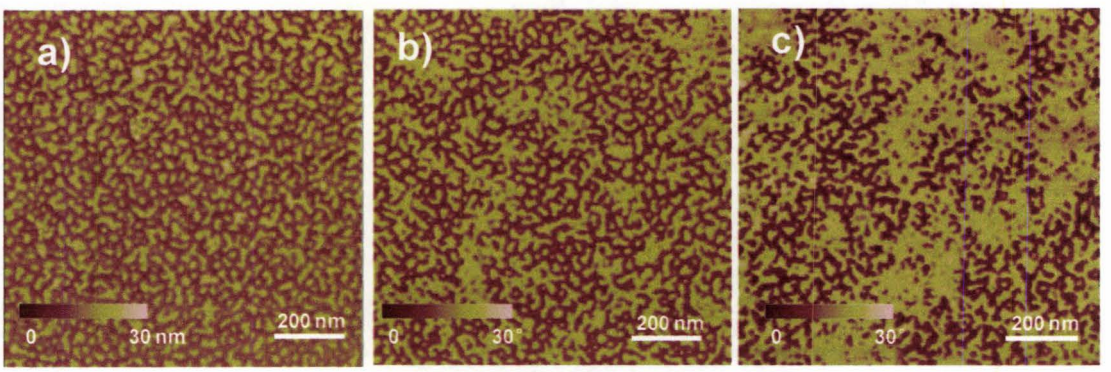

Figure 5-8 AFM phase image of fibrinogen on POEGMA-b-PMETAC nanopatterns after protein adsorption with different fibrinogen concentrations: (a) 0.02 mg/ml, (b) 0.2 mg/ml and (c) 1 mg/ml.

The water contact angle after the protein adsorption at 0.2 mg/ml was 60°, between POEGMA (45°) and surfaces covered completely by fibrinogen (70°). The surface was clearly partially covered.

The quantitative study was also carried out in the radio labelling experiment. Increasing the thickness of PMETAC block changed the patterns from spherical to wormlike aggregates, followed by line patterns. The adsorbed fibrinogen was also

expected to increase with the increase of PMETAC composition. Figure 5-9 shows that the amount of absorbed fibrinogen increased from a value close to POEGMA to that of PMETAC.

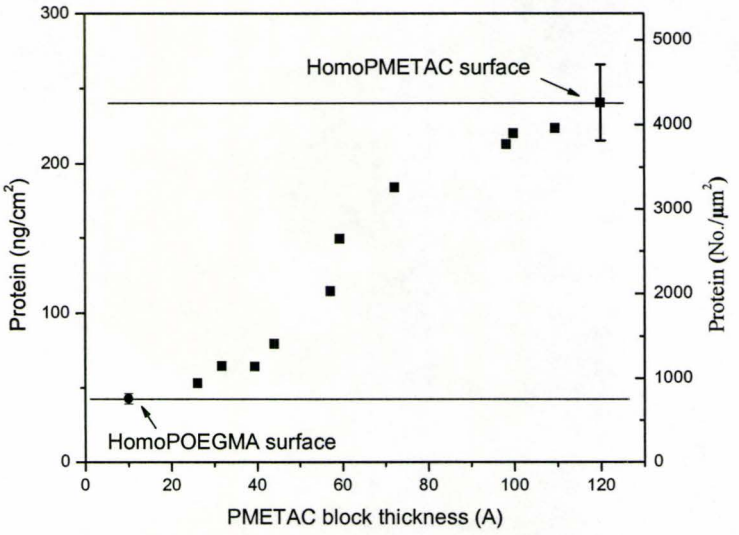

Figure 5-9 The fibrinogen adsorption on POEGMA-b-PMETAC nanopatterns with different PMETAC block thickness.

5.5 Conclusion

Various nanopatterns have been introduced through the self-assembly of grafted block copolymer brushes having two hydrophilic components. The design of two hydrophilic components was to avoid hydrophobic areas where proteins could change their conformations and lose their activity. The polyelectrolyte collapsed in salt solutions

and induced phase segregation between the two hydrophilic blocks. The nanopatterns including spherical aggregates, wormlike aggregates and line patterns were obtained by simple adjustment of the thickness of upper block layer. The long side chains of POEGMA brushes helped constrain the feature size to about 10 nm and fine tune the size on a nanoscale. These patterns were reversibly switchable through treatments with selective solvents.

The behavior of fibrinogen adsorption on these patterns was studied by ellipsometry, water contact angle, AFM and radio labelling experiment. The results showed that PMETAC aggregates attracted fibrinogen while the POEGMA background repelled the protein. The polymer nanopatterns prepared in this work possessed the ability to pattern proteins. Protein patterns identical to the original polymer patterns were introduced with a proper level of the protein concentration.

5.6 References

1. az-Mochon, J. J.; Tourniaire, G.; Bradley, M. *Chem. Soc. Rev.* **2007,** *36* (3), 449-457.

2. Fink, J.; Thery, M.; Azioune, A.; Dupont, R.; Chatelain, F.; Bornens, M.; Piel, M. *Lab Chip* **2007,** *7* (6), 672-680.

3. Kane, R. S.; Takayama, S.; Ostuni, E.; Ingber, D. E.; Whitesides, G. M. *Biomaterials* **1999,** *20* (23-24), 2363-2376.

4. Blawas, A. S.; Reichert, W. M. *Biomaterials* **1998,** *19* (7-9), 595-609.

5. Falconnet, D.; Csucs, G.; Grandin, H. M.; Textor, M. *Biomaterials* **2006,** *27* (16), 3044-3063.

6. Otsuka, H.; Nagasaki, Y.; Kataoka, K. *Curr. Opin. Colloid Interface Sci.* **2001,** *6* (1), 3-10.

7. Senaratne, W.; Andruzzi, L.; Ober, C. K. *Biomacromolecules* **2005,** *6* (5), 2427-2448.

8. Rosi, N. L.; Mirkin, C. A. *Chem. Rev.* **2005,** *105* (4), 1547-1562.

9. Blattler, T.; Huwiler, C.; Ochsner, M.; Stadler, B.; Solak, H.; Voros, J.; Grandin, H. M. *J. Nanosci. Nanotechnol.* **2006,** *6* (8), 2237-2264.

10. Whitesides, G. M.; Ostuni, E.; Takayama, S.; Jiang, X. Y.; Ingber, D. E. *Annu. Rev. Biomed. Eng.* **2001,** *3*, 335-373.

11. Khademhosseini, A.; Bettinger, C.; Karp, J. M.; Yeh, J.; Ling, Y. B.; Borenstein, J.; Fukuda, J.; Langer, R. *J. Biomater. Sci. -Polym. Ed.* **2006,** *17* (11), 1221-1240.

12. Galaev, I. Y.; Mattiasson, B. *Trends Biotechnol.* **1999,** *17* (8), 335-340.

13. Craighead, H. G.; James, C. D.; Turner, A. M. P. *Curr. Opin. Solid State Mat. Sci.* **2001,** *5* (2-3), 177-184.

14. Shim, J.; Bersano-Begey, T. F.; Zhu, X. Y.; Tkaczyk, A. H.; Linderman, J. J.; Takayama, S. *Curr. Top. Med. Chem.* **2003,** *3* (6), 687-703.

15. Cheng, J. Y.; Ross, C. A.; Smith, H. I.; Thomas, E. L. *Adv. Mater.* **2006,** *18* (19), 2505-2521.

16. Geissler, M.; Xia, Y. N. *Adv. Mater.* **2004,** *16* (15), 1249-1269.

17. Stoykovich, M. P.; Nealey, P. F. *Mater. Today* **2006,** *9* (9), 20-29.

18. Krausch, G.; Magerle, R. *Adv. Mater.* **2002,** *14* (21), 1579-1583.

19. Zhao, B.; Brittain, W. J. *J. Am. Chem. Soc.* **1999,** *121* (14), 3557-3558.

20. Minko, S.; Muller, M.; Motornov, M.; Nitschke, M.; Grundke, K.; Stamm, M. *J. Am. Chem. Soc.* **2003,** *125* (13), 3896-3900.

21. Xu, C.; Wu, T.; Drain, C. M.; Batteas, J. D.; Fasolka, M. J.; Beers, K. L. *Macromolecules* **2006,** *39* (9), 3359-3364.

22. Minko, S. *Polym. Rev.* **2006,** *46* (4), 397-420.

23. Zhou, F.; Huck, W. T. S. *Phys. Chem. Chem. Phys.* **2006,** *8* (33), 3815-3823.

24. Luzinov, I.; Minko, S.; Tsukruk, V. V. *Prog. Polym. Sci.* **2004,** *29* (7), 635-698.

25. Zhao, B.; Brittain, W. J.; Zhou, W. S.; Cheng, S. Z. D. *J. Am. Chem. Soc.* **2000,** *122* (10), 2407-2408.

26. Tomlinson, M. R.; Genzer, J. *Langmuir* **2005,** *21* (25), 11552-11555.

27. Zhulina, E. B.; Singh, C.; Balazs, A. C. *Macromolecules* **1996,** *29* (19), 6338-6348.

28. Prokhorova, S. A.; Kopyshev, A.; Ramakrishnan, A.; Zhang, H.; Ruhe, J. *Nanotechnology* **2003,** *14* (10), 1098-1108.

29. Santer, S.; Ruhe, J. *Polymer* **2004,** *45* (25), 8279-8297.

30. Kong, B.; Lee, J. K.; Choi, I. S. *Langmuir* **2007,** *23* (12), 6761-6765.

31. Huang, W. X.; Kim, J. B.; Baker, G. L.; Bruening, M. L. *Nanotechnology* **2003,** *14* (10), 1075-1080.

32. Gao, X.; Feng, W.; Zhu, S. P.; Sheardown, H.; Brash, J. L. *Langmuir* **2008,** *24* (15), 8303-8308.

33. Gao, X.; Kucerka, N.; Nieh, M. P.; Katsaras, J.; Zhu, S. P.; Brash, J. L.; Sheardown, H. *Langmuir* **2009,** *25* (17), 10271-10278.

34. Ma, H. W.; Hyun, J. H.; Stiller, P.; Chilkoti, A. *Adv. Mater.* **2004,** *16* (4), 338-341.

35. Lutz, J. F.; Andrieu, J.; Uzgun, S.; Rudolph, C.; Agarwal, S. *Macromolecules* **2007,** *40* (24), 8540-8543.

36. Revzin, A.; Tompkins, R. G.; Toner, M. *Langmuir* **2003,** *19* (23), 9855-9862.

37. Lee, B. S.; Lee, J. K.; Kim, W. J.; Jung, Y. H.; Sim, S. J.; Lee, J.; Choi, I. S. *Biomacromolecules* **2007,** *8* (2), 744-749.

38. Houseman, B. T.; Huh, J. H.; Kron, S. J.; Mrksich, M. *Nat. Biotechnol.* **2002,** *20* (3), 270-274.

39. Lee, K. B.; Park, S. J.; Mirkin, C. A.; Smith, J. C.; Mrksich, M. *Science* **2002,** *295* (5560), 1702-1705.

40. Bruckbauer, A.; Zhou, D. J.; Kang, D. J.; Korchev, Y. E.; Abell, C.; Klenerman, D. *J. Am. Chem. Soc.* **2004,** *126* (21), 6508-6509.

41. Falconnet, D.; Pasqui, D.; Park, S.; Eckert, R.; Schift, H.; Gobrecht, J.; Barbucci, R.; Textor, M. *Nano Lett.* **2004,** *4* (10), 1909-1914.

42. Suh, K. Y.; Seong, J.; Khademhosseini, A.; Laibinis, P. E.; Langer, R. *Biomaterials* **2004,** *25* (3), 557-563.

43. Smith, J. C.; Lee, K. B.; Wang, Q.; Finn, M. G.; Johnson, J. E.; Mrksich, M.; Mirkin, C. A. *Nano Lett.* **2003,** *3* (7), 883-886.

44. Ichino, M.; Nagasaki, Y. *J. Photopolym Sci. Technol.* **2006,** *19* (4), 451-454.

45. Lopez, G. P.; Albers, M. W.; Schreiber, S. L.; Carroll, R.; Peralta, E.; Whitesides, G. M. *J. Am. Chem. Soc.* **1993,** *115* (13), 5877-5878.

46. Qian, X. P.; Metallo, S. J.; Choi, I. S.; Wu, H. K.; Liang, M. N.; Whitesides, G. M. *Anal. Chem.* **2002,** *74* (8), 1805-1810.

47. Csucs, G.; Michel, R.; Lussi, J. W.; Textor, M.; Danuser, G. *Biomaterials* **2003,** *24* (10), 1713-1720.

48. Khademhosseini, A.; Jon, S.; Suh, K. Y.; Tran, T. N. T.; Eng, G.; Yeh, J.; Seong, J.; Langer, R. *Adv. Mater.* **2003,** *15* (23), 1995-2000.

49. Khademhosseini, A.; Suh, K. Y.; Jon, S.; Eng, G.; Yeh, J.; Chen, G. J.; Langer, R. *Anal. Chem.* **2004,** *76* (13), 3675-3681.

50. Feng, W.; Chen, R. X.; Brash, J. L.; Zhu, S. P. *Macromol. Rapid Commun.* **2005,** *26* (17), 1383-1388.

51. Feng, W.; Zhu, S. P.; Ishihara, K.; Brash, J. L. *Langmuir* **2005,** *21* (13), 5980-5987.

52. Archambault, J. G.; Brash, J. L. *Colloid Surf. B-Biointerfaces* **2004,** *33* (2), 111-120.

53. Ramakrishnan, A.; Dhamodharan, R.; Ruhe, J. *Macromol. Rapid Commun.* **2002,** *23* (10-11), 612-616.

54. Ramakrishnan, A.; Dhamodharan, R.; Ruhe, J. *J. Polym. Sci. Pol. Chem.* **2006,** *44* (5), 1758-1769.

55. Yin, Y. H.; Sun, P. C.; Li, B. H.; Chen, T. H.; Jin, Q. H.; Ding, D. T.; Shi, A. C. *Macromolecules* **2007,** *40* (14), 5161-5170.

Chapter 6

Chain Conformation of a New Class of PEG-Based Thermoresponsive Polymer Brushes Grafted on Silicon as Determined by Neutron Reflectometry

This chapter is a reproduction of the following published article in Langmuir: Gao, X.; Kučerka, N.; Nieh, M.P.; Katsaras, J.; Zhu, S.; Brash, J. L.; Sheardown, H. *Langmuir* **2009**, *25* (17), 10271-10278.

6.1 Abstract

The thermoresponsive PEG-based copolymer poly[2-(2-methoxyethoxy)ethyl methacrylate-co-oligo(ethylene glycol) methacrylate] (P(MEO_2MA-co-OEGMA)) was grafted onto a silicon wafer, and its chain conformation in aqueous solution was studied by neutron reflectometry. The effects of temperature and salt concentration on the polymer's conformation were evaluated. With increasing temperature, it was found that the polymer brushes underwent a transition from an extended state to a compressed state, and eventually a collapsed state above the lower critical solution temperature. The presence of salt significantly affected the well-extended brushes but had little effect on compressed and collapsed brushes. This PEG-based thermoresponsive surface exhibited good protein adsorption resistance. Interestingly, extended and collapsed brushes showed

the same level of protein repulsion, something that was not expected.

6.2 Introduction

In past decades, surface modification techniques have played important roles in biology and medicine fields for various purposes (e.g., antifouling of surfaces by proteins). Recently, there have been many novel areas developed that require so-called "smart biological surfaces", which can respond to external stimuli such as solvent type, pH, temperature, electric and magnetic fields, and so forth.[1-6] These smart surfaces can alter their properties (e.g., hydrophilicity, biological activity, protein adsorption/repulsion, cell adhesion, migration, and so forth) in response to small changes in the external environment. In fact, there are potentially significant applications in the areas of bioseparation, diagnostics, drug delivery, gene therapy, and implants. Furthermore, these surfaces are able to recognize biological events by emitting measurable electronic or opto-electronic signals. As such, they can be used as biosensors for bioanalysis, clinical diagnosis, and environmental monitoring.

Among smart surfaces, thermoresponsive surfaces, which can respond to temperature variations, are some of the most important (since temperature, as a stimulus, can be easily regulated). Moderate changes in temperature close to physiological temperature have practically little effect on the biosystem. As a result, many

thermoresponsive surfaces have been developed. Until recently, thermoresponsive materials have mainly been limited to poly(N-isopropylacrylamide) (PNIPAM) and its copolymers.[7-9] PNIPAM has a lower critical solution temperature (LCST) of 32 °C, between room temperature and physiological temperature. Below its LCST the surface polymer brushes in solution are in the well-extended conformation. However, when the temperature is above 32°C, the polymer chains undergo a sharp phase transition, forming a collapsed layer. A sharp change in surface properties is thus trigged by a moderate temperature stimulus. As a result of this property, thermoresponsive surfaces based on PNIPAM have been developed for various applications.

Recently, a new class of biocompatible thermoresponsive material, namely, poly(2-(2-methoxyethoxy)ethyl methacrylate -*co*- oligo(ethylene glycol) methacrylate) (P(MEO_2MA-co-OEGMA)), has attracted much attention.[10-15] Similar to the amide group in PNIPAM, the oligo(ethylene glycol) in this copolymer has various hydrogen-bonding interactions with water when temperature varies, giving its thermoresponsive ability. This random copolymer has been shown to have a LCST in water. The phase transition is reversible and is almost independent of external conditions. Furthermore, the copolymer's LCST can be readily altered (from 26 to 92 °C), simply by varying the copolymer's composition. The great interest in these new thermo-responsive materials lies in the fact that they are entirely constructed with

poly(ethylene glycol) methacrylate. Poly(ethylene glycol) (PEG)-based polymers are the most popular materials in bio-related applications because of their excellent resistance to non-specific protein adsorption and cell adhesion, as well as their non-toxic and non-immunogenic properties.

This new class of thermoresponsive polymer surfaces may lead to products that will hopefully be incorporated into various biomedical devices. So far, there have only been a few reports in the literature regarding this new thermoresponsive surface. In 2007, Huck et al.[16] grafted this copolymer onto a surface using the surface-initiated atom transfer radical polymerization (ATRP) method. The thermoresponsive collapse transition of polymer brushes on the surface was demonstrated by water contact angle measurements and liquid atomic force microscopy (AFM). In 2008, Lutz et al.[17] used the same type of thermoresponsive surfaces to control cell adhesion over the temperature range between 25 – 37 $^{\circ}$C. Glinel et al.[18] replaced OEGMA with a hydroxyl-terminated oligo(ethylene glycol) methacrylate (HOEGMA) monomer. A natural antibacterial peptide, magainin I, was then immobilized through grafting of hydroxyl group, giving an antibacterial surface. The amount of hydroxyl reactive groups could be readily adjusted by changing the monomer mixture composition.

Knowledge regarding the conformation of polymer brushes on a surface is crucial when designing smart surfaces. However, obtaining such information can be

challenging, and as such, not much is known with regard to these new materials on the surface. Huck et al.[16] used the aqueous AFM method to study variations of polymer brush thickness in water as a function of temperature. As expected, brush thickness decreased when the temperature was raised above the copolymer's LCST. This work demonstrated a novel approach in the design of PEG-based thermoresponsive surfaces for biological and medical applications. However, it should be noted that in aqueous solutions AFM measurements are approximate. As polymer brushes in a good solvent are well-extended with dissolution into the solvent, the penetration of an AFM tip into polymer brushes can further complicate matters. The measured thicknesses strongly depend on the applied force (i.e., the stronger the applied force, the deeper the AFM tip penetrates into the brushes). Moreover, besides brush thickness there is other useful information (e.g., global brush conformation, water fraction surrounding the chains) needed in order to effectively design thermoresponsive devices.

Neutron and X-ray reflectometry have emerged as powerful, noninvasive surface/interface probes used to characterize the structures of materials on solid and liquid surfaces.[19-22] Here, we employed neutron reflectometry (NR) to study the conformation of polymer brushes on surfaces *in situ* in water. Importantly, thermal neutrons, because of their low energies (~ 10 meV), do not have any deleterious effect on sometimes fragile polymeric samples. Neutron reflectometry is also a bulk probe giving

rise to the average polymer brush conformation over the entire sample. The water fraction inside the polymer brushes can also be estimated. Small changes in conformation in different environments can be monitored by the NR method.

Another issue that needs to be addressed with regard to these new thermoresponsive surfaces is their biocompatibility. A major advantage of this new class of PEG-based materials lies in their protein repulsion ability. However, there are still two concerns: First, about 90% of POEGMA have only two ethylene oxide (EO) repeat units per side chain. Although homoPOEGMA has well been accepted as a biocompatible material, popular candidates often have 4.5 to 9 repeat EO units.[23-25] These new thermoresponsive copolymers with 90% POEGMA having only two EO repeat units have more hydrophobic methacrylate backbone that may play an important role in determining the performance of the polymer. To the best of our knowledge, there are no reports on protein repulsion with regard to surfaces modified by this new type of PEG-based brush. Secondly, polymer brushes might lose their protein repelling ability in a collapsed state above LCST. Thermoresponsive surfaces have been used to control cell adhesion.[17,26] For example, Rimmer *et al.*[26] employed PNIPAM surfaces as culture for cells above LCST and found that the cells adhered on the collapsed PNIPAM chains. When the temperate was decreased below LCST, the extended PNIPAM chains expelled the cells. If these PEG-based thermo-responsive surfaces adsorb large amount

of proteins when in the collapsed state, their potential applications could be limited. It is also fundamentally important to investigate and understand the relationship between polymer extension and their protein repelling ability.

The objective of this work is twofold. The first objective is to elucidate the detailed conformations of this new class of polymer brushes on substrates immersed in an aqueous environment, below and above the polymer's LCST, and to study the effects of some the influencing factors on their conformation. The second is to evaluate their resistance to protein adsorption. In particular, we want to compare their protein repelling performances below and above LCST.

6.3 Experimental section

6.3.1 Materials

$Cu^{I}Cl$ (99%), $Cu^{II}Cl_2$ (97%) and 2,2'-bipyridyl (Bipy) (99%) were purchased from Aldrich and used as received. 2-(2-Methoxyethoxy)ethyl methacrylate (MEO_2MA) (95%, M_n = 188.22 g/mol, Aldrich) and oligo(ethylene glycol) methacrylate (OEGMA) (98%, M_n = 475 g/mol, Aldrich) were distilled over CaH_2 under vacuum. Toluene (HPLC grade, Aldrich) was stirred over CaH_2 overnight and then distilled twice. Methanol (HPLC grade, Aldrich) was distilled over CaH_2 prior to use. Deionized water from the Millipore water purification system had the minimum resistivity of 18.0 MΩ·cm.

Argon and nitrogen gases were of ultrahigh-purity grade. Silicon wafers (6 mm thick, 101.6 mm diameter) for neutron reflectometry experiments were purchased from Wafer World Inc. (West Palm Beach, FL). Silicon wafers for radiolabeled protein adsorption experiments had a thickness of 0.56 mm and were cut into 12 × 6 mm^2 pieces. Lysozyme was purchased from Sigma chemical Co. (St. Louis, MO) and used as received. The molecular weight and dimensions of lysozyme are 14300 g/mol and 45 × 30 × 30 $Å^3$, respectively. All other materials were commercially available and used as received.

6.3.2 Self-assembly of initiator monolayer on silicon wafers

The surface-attachable ATRP initiator, 6-(2-bromo-2-methyl) propionyloxy hexenyl trichlorosilane, was synthesized by the hydrosilylation of trichlorosilane with hex-6-en-1-yl 2-bromo-2-methylpropionate. Silicon wafers were pretreated as described previously.[27] They were then immersed in a 2.5 mM solution of 6-(2-bromo-2-methyl) propionyloxy hexenyl trichlorosilane in dry toluene for 18 h, at room temperature to form a self-assembled initiator monolayer with a thickness of 1.9 ± 0.2 nm. The silicon wafers were then removed from solution, ultrasonically cleaned in dry toluene, rinsed sequentially with toluene and methanol, and then dried in an argon stream.

6.3.3 Grow P(MEO_2MA-co-OEGMA) copolymer brushes from surface

In a typical procedure of grafting P(MEO_2MA-co-OEGMA) copolymer brushes, $Cu^{I}Cl$ (297 mg, 3.3 mmol), $Cu^{II}Cl_2$ (44.37 mg, 0.33 mmol) and Bipy (1632 mg, 10.41 mmol) were added into a 250 mL flask. The flask was then evacuated and backfilled with argon (procedure repeated 3 times). Degassed MEO_2MA (35.76 g, 190 mmol), OEGMA (4.75 g, 10 mmol), deionized water (66.7 mL) and methanol (33.3 mL) were then transferred into the flask. After degassing with argon for another hour, the mixture was transferred into a glovebox filled with ultrapure nitrogen, distributed into glass containers with the initiator-modified silicon wafers inside. The grafting process was carried out at room temperature for 200 min and stopped by adding a methanol solution of $Cu^{II}Cl_2$/Bipy, as shown in Scheme 6-1. The polymer-grafted silicon wafers were then ultrasonically cleaned in methanol, rinsed thoroughly, and dried in an argon stream. The comonomer ratio of MEO_2MA/OEGMA in the methanol/water solution was varied to achieve samples with different LCSTs. In this work, two ratios, MEO_2MA/OEGMA = 95:5 (sample 1) and MEO_2MA/OEGMA = 85:15 (sample 2), were chosen.

6.3.4 Characterization

The thickness of grafted polymer layers on silicon wafers was measured by ellipsometry (Exacta 2000, Waterloo Digital Electronics) using a He - Ne laser (632.8

nm). The incident angle was set to 70°. The refractive index (n) and extinction coefficient (k) of Si (n = 3.865, k = 0.020) and SiO_2 (n = 1.465, k = 0) were used to determine the SiO_2 layer thickness. Values of n = 1.500 and k = 0 were used for the initiator and polymer layers. All the measurements were conducted in air at room temperature. A contact angle goniometer (model 200, Rame-Hart instrument Co.) was used to measure the water contact angle of the various surfaces. The advancing water contact angle was measured by the sessile drop method.

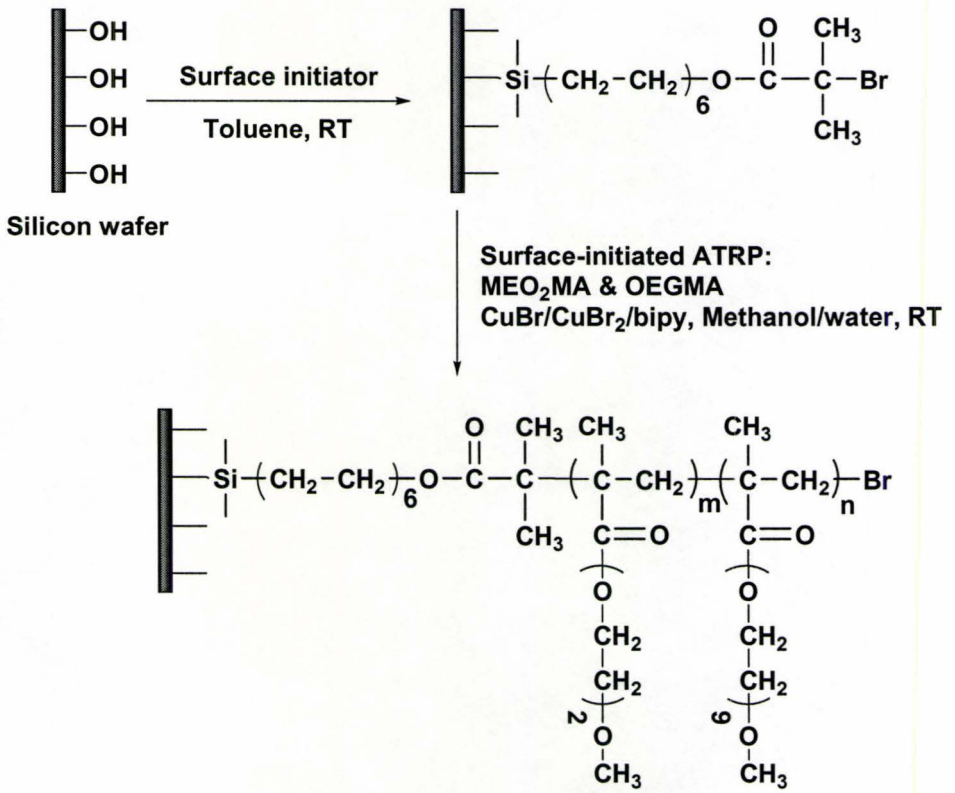

Scheme 6-1 Synthesis procedure for P(MEO_2MA-co-OEGMA) copolymer brushes on silicon wafer surface via surface-initiated ATRP.

6.3.5 Neutron reflectometry experiments

NR experiments were carried out at the D3 reflectometer located at the National Research Universal (NRU) reactor (Chalk River, ON). 2.37 Å wavelength (λ) neutrons were chosen using a pyrolytic graphite monochromator. During the NR measurements, the neutron incident angle (θ) and reflected angle (2θ) were varied systematically, giving rise to the specular neutron momentum transfer Q_z: $Q_z = (4\pi \sin\theta)/\lambda$. The reflected intensity was recorded while the neutron momentum transfer Q_z varied from 0.006 to 0.1 $Å^{-1}$. The data were normalized with respect to the incident beam intensity in order to account for any variation due to changes in slit width. The background was determined by offsetting the detector by $+0.5^{o}$ (i.e., $2\theta + 0.5^{o}$).

The samples were measured both in air and in aqueous solution. For the dry condition, the silicon wafer was placed on the sample table exposed to air. In this case, the path of the incident neutron beam was air → sample → SiO_2 → Si. In the case of samples in water (D_2O or D_2O buffer solutions), the silicon wafer was placed in a specially designed sample cell, described elsewhere.[28] The incident neutron beam path was Si → SiO_2 → sample → aqueous solution. The different path arrangements for dry and wet conditions were to ensure the total reflection condition at low angles.

PARRATT 32 (BENSC, Berlin) software was employed to analyze the data. In

the case of dry samples, a three-layer (SiO_2, initiator monolayer, polymer layer) model was used. For samples in water, a stretched parabolic decay was added to the polymer layer, as a result of the polymer chains extending into the aqueous environment. The stretched parabolic function used was as follows:[29] $\Phi_{poly}(z) = \Phi_{0,poly}\left[1-(z/h)^2\right]^{\alpha}$, where z is the distance from the interface, $\Phi_{poly}(z)$ is the polymer volume fraction at a distance z, and $\Phi_{0,poly}$ is the polymer volume faction at a distance 0. The parameters h and α modify the parabolic decay shape.

The best fit scattering length density (SLD, a function describing the density and atomic composition) profile normal to the surface was obtained by minimizing the chi squares (χ^2). SLD profiles were then converted to volume fraction profiles based on the SLDs of the initiator layer, polymer layer, and D_2O. The SLD of the components was estimated from[30] $SLD = dN_A\sum b_i/M$, where d is the mass density of the component, N_A is Avogadro's number, M is the molecular weight of the component, and $\sum b_i$ is the sum of the neutron scattering lengths of the various atoms making up the sample.

6.3.6 Protein adsorption experiments

Protein adsorption experiments were carried out in isotonic tris buffered saline (TBS) with radioiodinated proteins. In this work, lysozyme was chosen as the model protein. It is a small spherical protein with the dimension of 45 × 30 × 30 $Å^3$, suitable

for model studies. Its adsorption behavior on polymer surfaces has been studied in our previous work.[31] The iodine monochloride (ICl) method was employed to radiolabel lysozyme with Na125I (MP Biomedicals, Inc., Irvine, CA).[32] Unbound radioactive iodide was removed by ion exchange chromatography. The solutions for protein adsorption contained 10% radiolabeled lysozyme. The surfaces were first kept in TBS solution for 12 h in order to completely hydrate the polymer brushes. Surfaces were then immersed in the protein solution for 2 h allowing protein adsorption to reach equilibrium. The samples were then put into fresh TBS solution for 5 min (3 cycles) to remove any loosely adsorbed protein. The samples were then dried and measured by a Wizard 3″ 1480 Automatic Gamma Counter (Perkin-Elmer Life Sciences) to determine the amount of proteins adsorbed onto each surface.

6.4 Results and discussion

6.4.1 Ellipsometry and contact angle results

Ellipsometry measurements showed that the P(MEO_2MA-*co*-OEGMA) copolymer layers on sample 1 (S1, 5% OEGMA) and sample 2 (S2, 15% OEGMA) were 1228 Å and 1161 Å, respectively. Besides similar thicknesses, both samples had a surface water contact angle of ~40°, indicative of hydrophilic surfaces.

In this work, $Cu^{II}Cl_2$, instead of free initiator, was added to the polymerization

solution for good control of ATRP and high graft polymer molecular weight. There were no free polymer chains formed in the solution. As a result, chain length and grafting density of the grafted polymer on the surface could not be estimated. In order to have an approximation, we adopted the grafting density data from our previous work. In the work, homoPOEGMA brushes were grafted from silicon wafer with the same surface-initiated ATRP method.[33] The only difference was the ~4.5 side chain EO units. The grafting density was 0.26 chains/nm^2 and the polydispersity was around 1.3, measured from the free polymer in solution. It was assumed that the grafting densities of the copolymer brushes in this work were close to that of homoPOEGMA. The chain length could then be estimated from the equation of $\Gamma = d\rho / M_n$ where Γ is the grafting density, d is the layer thickness, ρ is the polymer bulk density, and M_n is the molecular weight. The monomer molecular weights of S1 and S2 are 202.6 and 231.2 g/mol, respectively. A bulk polymer density of 1.0 g/cm^3 was assumed. The estimated chain lengths of the S1 and S2 polymers were 1400 and 1150 OEGMA monomeric units, respectively. It should be noted that these chain lengths could be overestimated because the copolymer side chain length of ~2.5 EO units is smaller than 4.5 of homoPOEGMA. The shorter side chains might yield a grafting density higher than 0.26 chains/nm^2; therefore, the real chain length could be shorter than the estimated value.

6.4.2 NR measurements of dry samples

Samples were first measured in air in order to obtain the dry thickness of the grafts and the parameters needed to subsequently model the hydrated samples. Figure 6-1 shows the NR profiles for S1 and S2 in air. The three-layer model representing SiO_2, the initiator layer, and the polymer brushes was used to fit the data. The theoretical SLDs of Si, SiO_2 and air were chosen and kept constant throughout the modeling procedure. Other parameters, including the thickness and SLDs of the initiator and polymer layers were allowed to vary until χ^2 was minimized. The best fits (lines) to the data are shown in Figure 6-1, with the various model parameters summarized in Table 6-1. The thicknesses of the S1 and S2 surface polymer layers are 1185 and 1131 Å, respectively. These values are in good agreement with those obtained by ellipsometry.

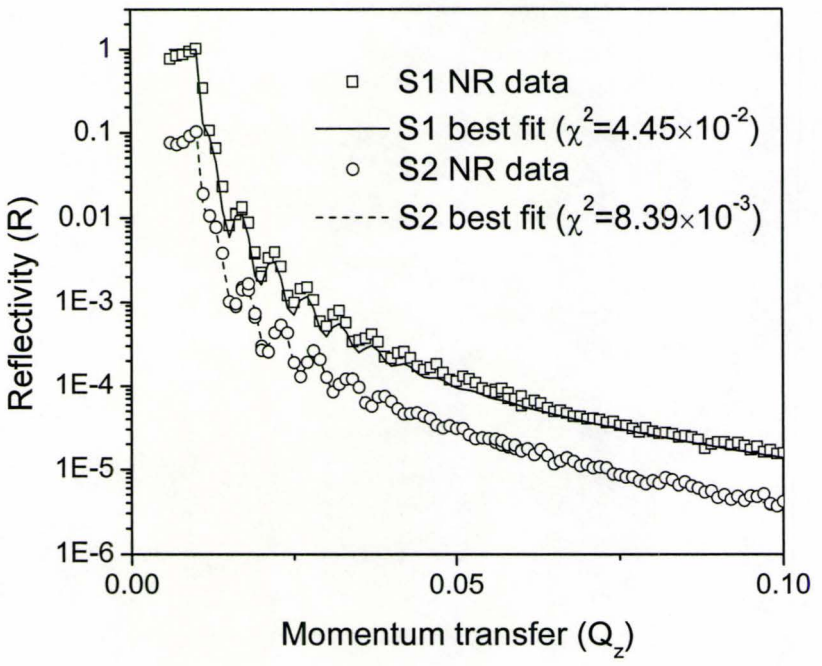

Figure 6-1 Neutron reflectivity profiles for dry samples and the best fits to the data. The curves were offset by arbitrary factors in order to better distinguish the data.

Table 6-1 Model parameters for surface grafts in the dry state.

species		SLD (10^{-6} Å^{-2})	thickness (Å)	
			measured from NR	measured from ellipsometry
Air		0.00[a]	N/A	N/A
D_2O		6.34[a]	N/A	N/A
Si wafer		2.07[a]	N/A	N/A
SiO_2 layer	S1	3.48[a]	16[b]	14[b]
	S2	3.48[a]	16[b]	14[b]
initiator layer	S1	0.22[a]	24[b]	19[b]
	S2	0.22[a]	22[b]	19[b]
polymer layer	S1	0.81[b]	1185[b]	1228[b]
	S2	0.73[b]	1131[b]	1161[b]

[a] Theoretical value. [b] Measured value.

6.4.3 Thermo-responsive behavior of samples in water

Polymer brush conformations of S1 in D_2O were measured at different temperatures. The NR profiles and their best fits are shown in Figure 6-2(a). The data were fitted using the three-layer model (i.e., SiO_2, initiator, and polymer layer) along with a stretched parabolic decay (mentioned previously). The initiator/polymer layer SLDs and SiO_2 layer thickness were adopted from the dry-state measurements and were fixed during fitting. The validity of the stretched parabolic decay for POEGMA brushes hydrated in water has been previously demonstrated.[34] Using this model, the NR data were well fit, as shown in Figure 6-2(a). In the case of some NR data, the Kiessig fringes were absent as a result of a diffuse polymer/water interface.

The SLD profiles of polymer brushes on the surface were determined from the best fits to the data. They were then easily converted to polymer volume fraction profiles by assuming that the volumes were additive. The SLD for the binary polymer/solvent system can be written as follows: $\rho_{mix}(z) = \Phi_{poly}(z) \times \rho_{poly} + \left[1 - \Phi_{poly}(z)\right] \times \rho_{solvent}$, where $\rho_{mix}(z)$ is the SLD of the polymer/solvent mixture at a distance z from the interface, $\Phi_{poly}(z)$ is the polymer fraction at a distance z, and ρ_{poly} and $\rho_{solvent}$ are the SLDs of the polymer and the solvent, respectively.

The polymer volume fraction profiles of S1 at four different temperatures are

shown in Figure 6-2(b). At 288 K, the polymer brushes were well extended into water. The swelling ratio, defined as the thickness of the polymer layer in water divided by the thickness of the polymer layer in dry state, was studied. In this work, the thickness of the polymer layer in water was approximated at the distance where the polymer fraction decreased to about 10%. At 288 K, the swelling ratio of polymer brushes in D_2O was approximately 1.8. As EO groups can form hydrogen bond with water, a hydration layer was built up surrounding the polymer chains. As a result, the polymer chains extended completely into water. The fraction of water inside the polymer layer was determined to be greater than 50%, implying that water is a good solvent for P(MEO_2MA-*co*-OEGMA) copolymer brushes at low temperatures.

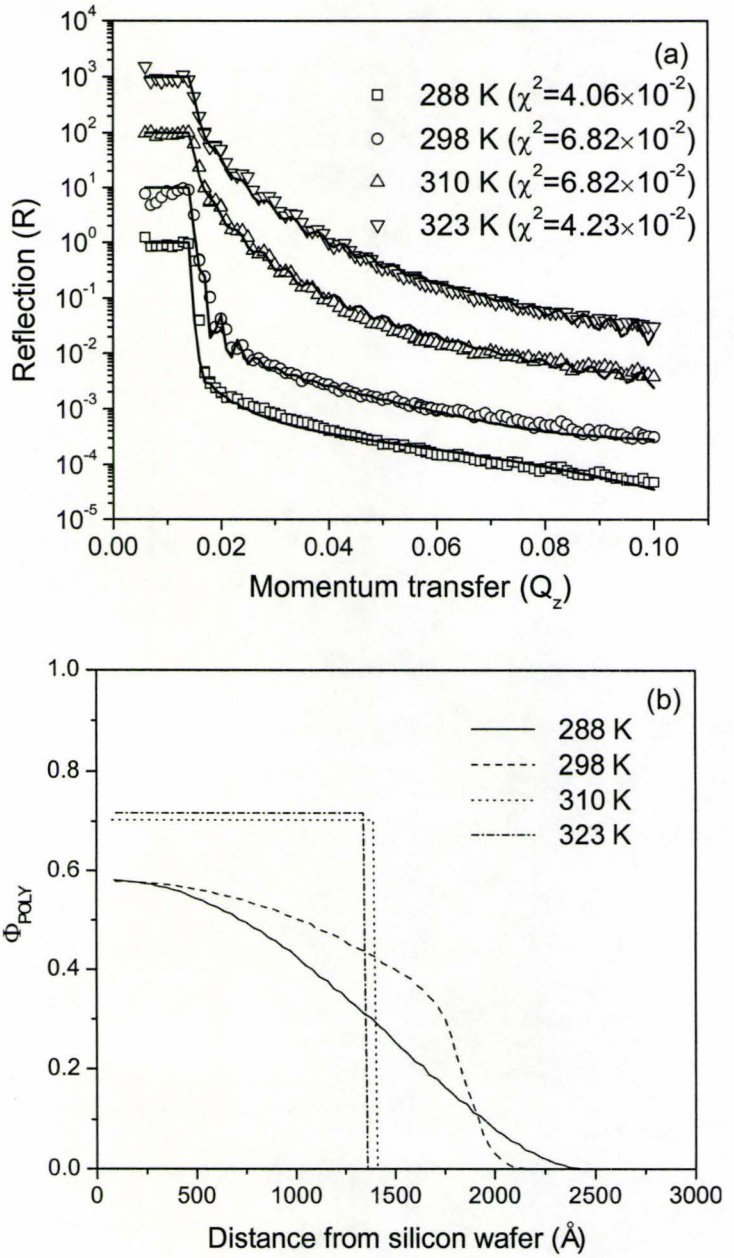

Figure 6-2 (a) Neutron reflectivity profiles of S1 in D_2O and the best fits to the data. The curves were offset by arbitrary factors in order to better distinguish the data. (b) Volume fraction profiles of polymer brushes.

When the temperature was increased to 298 K, there was a slight decrease in the

polymer brushes thickness, indicative of a decrease in the affinity between EO groups and water molecules. Although this resulted in a decreased water fraction inside the polymer layer, the average volume fraction of water was still greater than 50%, indicating that P(MEO_2MA-*co*-OEGMA) copolymer brushes are still hydrophilic at this temperature.

When the temperature was increased to 310 K (above the polymer's LCST), the polymer brushes collapsed, excluding much of the water from the polymer layer. This resulted in the appearance of a distinct interface between the polymer layer and water. The swelling ratio decreased to around 1.2, while the volume fraction of water inside the polymer layer decreased to approximately 30%. When the temperature was increased to 323 K, the polymer layer experienced a further collapse, expelling even more water. It should be noted that these polymer brushes could also have a parabolic decay even in the collapsed state. However, the current simulation results gave a sharp polymer-water interface, although the stretched parabolic decay has already been added to the model. Because of the uncertainness of the interface roughness for these surfaces at the moment, only the swelling ratio in the collapsed state was discussed in this work.

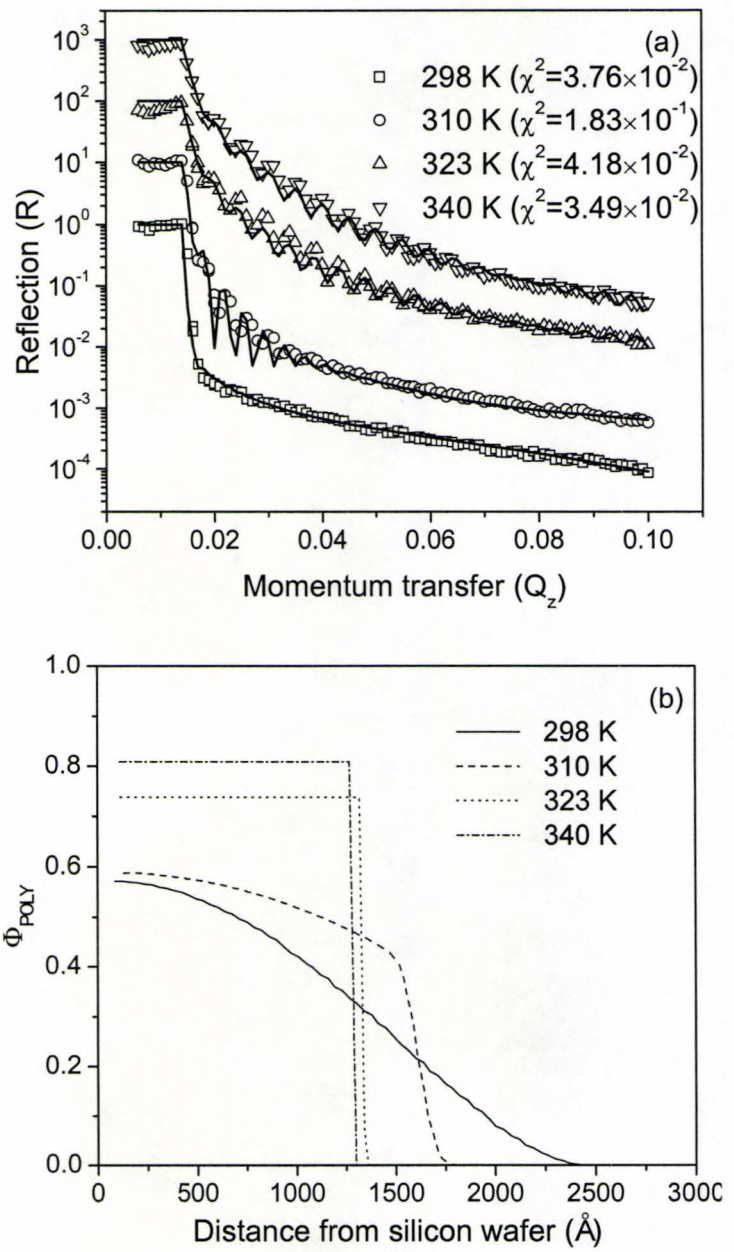

Figure 6-3 (a) Neutron reflectivity profiles of S2 in D_2O and the best fits to the data. The curves were offset by arbitrary factors in order to better distinguish the data. (b) Volume fraction profiles of polymer brushes.

Figure 6-3(a) shows NR reflectivity data for S2 and the best fits to the data (solid lines) at four different temperatures. The polymer volume fraction profiles are shown in Figure 6-3(b). For S2, the composition of OEGMA with 9 EO repeat units was increased from 5% (S1) to 15%. As a result, its LCST in water was determined to be around 321 K, higher than that of S1 (305 K). As shown in Figure 6-3(b), at 298 K the polymer brushes extended into D_2O, indicating a well-developed hydration layer around the polymer chains. The swelling ratio was approximately 1.8, similar to that of S1 at 288 K.

When the temperature was increased to 310K, the polymer brushes were obviously compressed and the swelling ratio decreased to around 1.4. An interface formed between the water and polymer layer, which indicated that the hydration layer surrounding the polymer chains was partially destroyed at a temperature close to the polymer's LCST. Despite the fact that at this temperature the polymer chains were not as extended as those at low temperature, the volume fraction of water inside the polymer layer was still greater than 50%, much higher than the amount of water in collapsed polymers. At this temperature, the polymer chains were still not in the collapsed state yet.

When the temperature was raised to 323 K, higher than the polymer's LCST, the polymer brushes collapsed. The swelling ratio was determined to be less than 1.2, while

the water volume fraction inside the polymer layer was around 30%. When the temperature was 340 K, the polymer layer swelling ratio was only around 1.1, while the water fraction further decreased to about 20%.

6.4.4 The effect of salts

For the application in biomedical devices, the effect of salts must be taken into consideration. Salts are well-known to change polymer solubility in water by disrupting the hydration structure surrounding the polymer's chains. This so-called "salting out" effect may change LCST of the thermoresponsive polymers.[35,36] As a result, the presence of salts affects performance of the thermoresponsive behavior. On the other hand, in some cases, this effect was employed to design "salt-responsive" polymers.[37]

Polymer brush conformations in TBS buffer were measured and compared to those in pure D_2O. The results showed that salt differentially affected polymer brushes, depending on their conformational state. In order to clarify the salt effect, polymer brush conformations are subdivided into three states (i.e., extended, compressed, and collapsed states), as shown in Scheme 6-2.

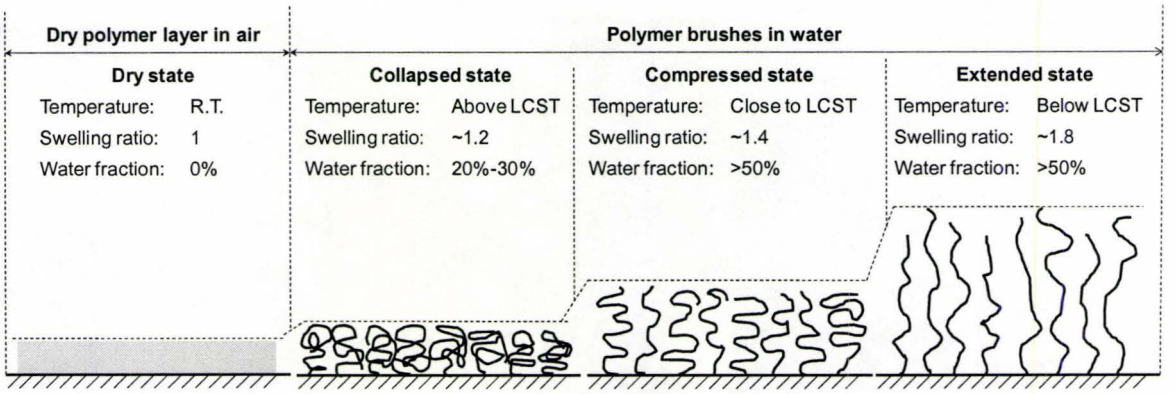

Scheme 6-2 Polymer brush conformation in aqueous solutions.

When the hydration layer around the polymer chains is well developed, the chains extend deeply into the bulk water, exhibiting a swelling ratio of approximately 1.8 and a water volume fraction of greater than 50%. The polymer brushes in this state are defined as being extended (S1 at 288 K and 298 K, S2 at 298 K). When the temperature is close to the polymer's LCST, hydrogen bonds between the EO groups and water molecules are significantly affected, with the hydration layer undergoing partial degradation. In this case, the polymer chains are not well-extended in water. Although water volume inside the polymer layer is still greater than 50%, the swelling ratio decreases to around 1.4. An interface between the polymer layer and water is formed, and the polymer brushes are described as being in the compressed state (S2 at 310 K). When the temperature is above the polymer's LCST, polymer brushes collapse and the swelling ratio decreases to approximately 1.2. The water faction of the collapsed polymer is about 30%.

The thermoresponsive P(MEO_2MA-*co*-OEGMA) in solution undergoes a sharp phase transition as PNIPAM does.[12] Huck et al.[16] also observed a sharp collapse transition in their experiment. The collapse occurred within a 10 °C temperature range. In the present work, three states were observed. However, only the transition from the compressed state to the collapsed state is considered to be a phase transition and it is very sharp considering that the temperature range was smaller than 10 °C. The transition of from the extended state to the compressed state was gradual caused by the change in swelling ratio. Both of the states had water fraction larger than 50%. There was no phase transition happened in this range.

When the polymer brushes are in the extended state, there is a well developed hydration layer around the polymer chains. The presence of salt had the greatest impact on the extended polymer chains because of its significant disruption of the hydration layer. As shown in Figure 6-4, in TBS buffer the polymer chains on S1 at 298 K were more compressed than in pure water. Distinct changes in the swelling ratio were also observed. Chain conformation changed from the extended state, in pure water, to the compressed state in TBS buffer because of the partial disruption of the hydration layer by the salt.

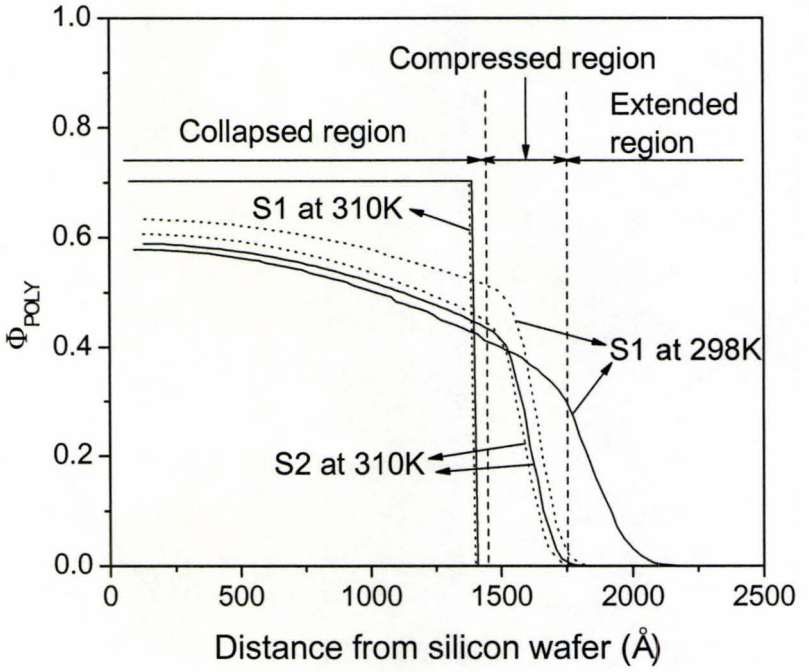

Figure 6-4 Volume fraction profiles of polymer brushes.

Solid line: in pure D_2O. Dotted line: in TBS buffer.

For the polymer brushes in the compressed region, for example S2 at 310 K, the effect of salt was less pronounced. As shown in Figure 6-4, the polymer chains in TBS buffer compressed only slightly. The reason was that the hydration structure around the polymer brushes in the compressed state was already partially destroyed because of the elevated temperature. As a result, when salt was added, the "salting-out" effect did not have significant impact on the polymer conformation, as it had on well-extended polymer chains. For collapsed polymers (e.g., S1 at 310 K), the presence of salt had no effect on the polymer conformation, as the affinity between polymer segments was greater than that between EO groups and water.

6.4.5 The effect of copolymer composition

In Figure 6-5, the conformations of polymer brushes on S1 and S2 are compared at three different temperatures in order to elucidate the effect of copolymer composition on their thermoresponsive behavior. At room temperature (298 K), both two composition designs gave extended polymer brushes on the surface. However, the higher OEGMA composition brushes (i.e., S2 with 15% OEGMA) had a better affinity for water, which enabled the copolymer chains to extend more deeply into the water.

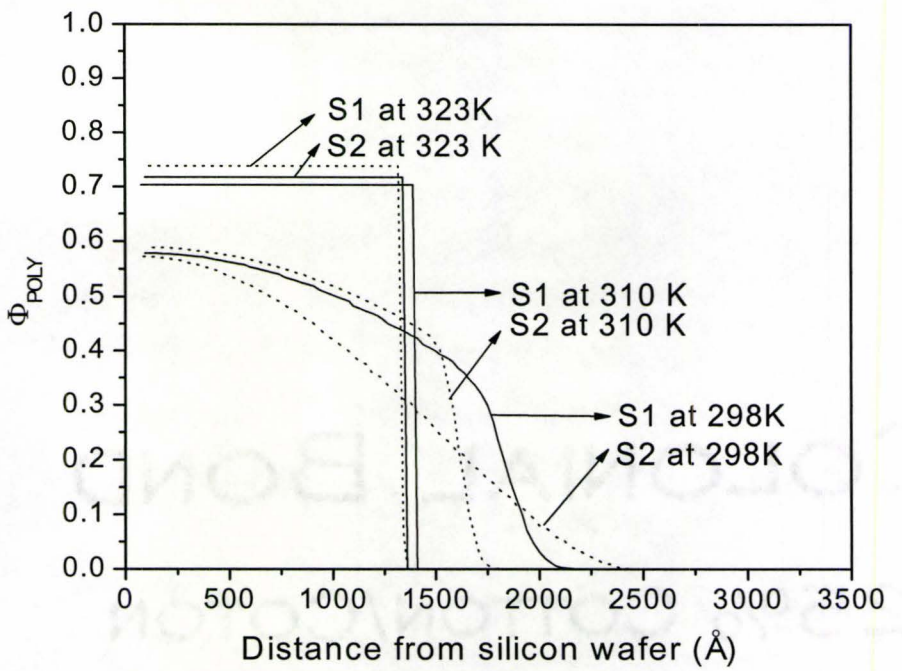

Figure 6-5 Volume fraction profiles of S1 and S2 polymer brushes.

At around 310 K, the polymer brushes with 5% OEGMA on S1 were already in the collapsed state, while those with 15% OEGMA on S2 were still extended. However,

because the temperature was close to the S2 sample's LCST, the affinity between EO groups and water became less favorable, the polymer brushes were in the compressed state. At 323 K, both S1 and S2 brushes were in the collapsed state, with no significant difference in the polymer brush conformation. Moreover, they exhibited the same swelling ratio (~1.2) and water volume fraction within the polymer layer.

6.4.6 The effect of protein

Besides salt, various proteins inside the human body may also affect the conformation of polymer brushes. Here, we studied the possible impact of lysozyme on polymer brush conformation. Lysozyme is abundant in some secretions, e.g., tears, saliva, mucus, and so forth. The lysozyme used in this work is from chicken egg white. The conformations of S1 and S2 in TBS buffer at two different protein concentrations (i.e., 0.5 mg/mL and 1 mg/mL, respectively), were investigated. The measurements were performed at two different temperatures, one below the polymer's LCST, and the other above. As shown in Figure 6-6, at the same temperature, the NR curves with different protein concentrations overlapped. This showed that the addition of lysozyme had no effect on polymer brushes conformation, regardless of their conformational state.

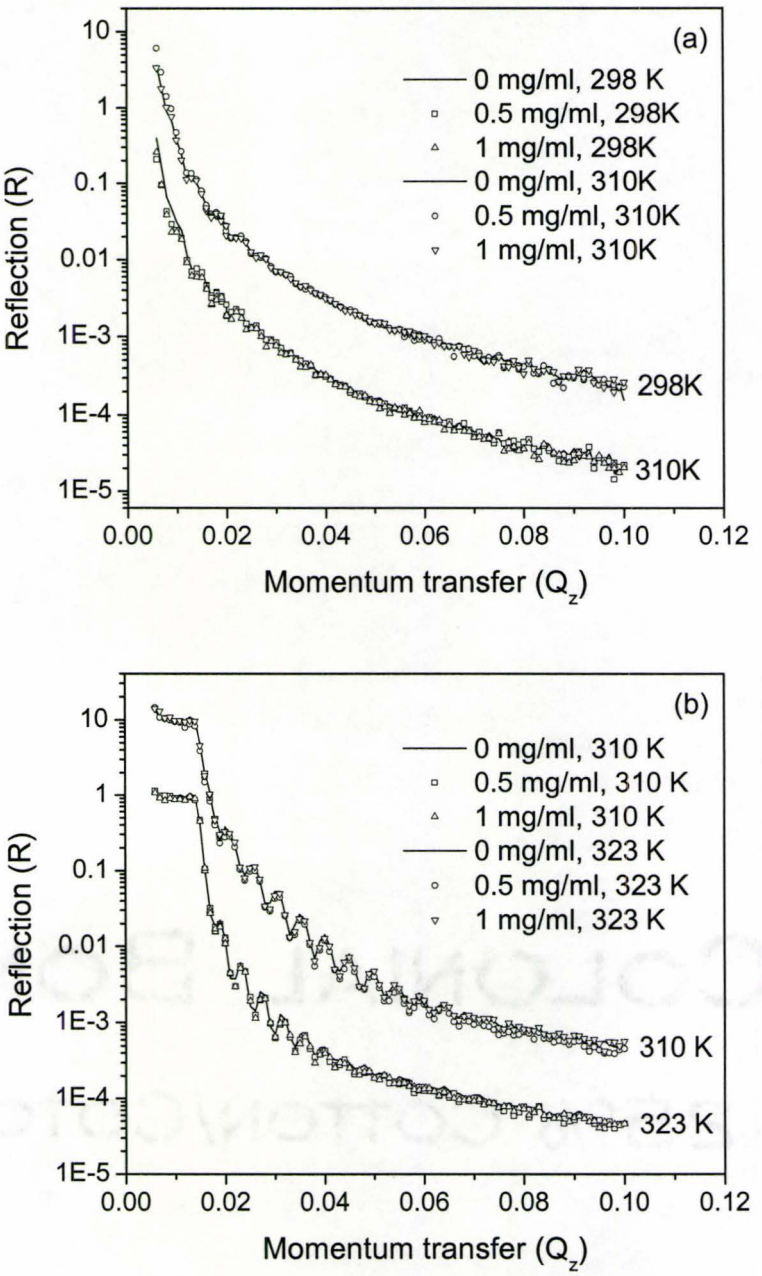

Figure 6-6 Neutron reflectivity profiles of (a) S1 and (b) S2 in TBS buffers with lysozyme. The curves were offset by arbitrary factors in order to better distinguish the data.

6.4.7 Protein adsorption resistance

As shown in Figure 6-7, the bare silicon wafer adsorbed around 800 ng/cm^2 of lysozyme at room temperature. In comparison, the amount of lysozyme adsorbed on S1 and S2 surfaces at room temperature was around 40 ng/cm^2, which meant a 95% reduction in protein adsorption. Surfaces grafted with homoPOEGMA (with 4.5 repeat EO units) brushes were also studied as comparison. As can be seen, the protein adsorption resistance performance of S1 and S2 modified with the current copolymer brushes was close to the surface grafted with homoPOEGMA containing 4.5 repeat EO units.

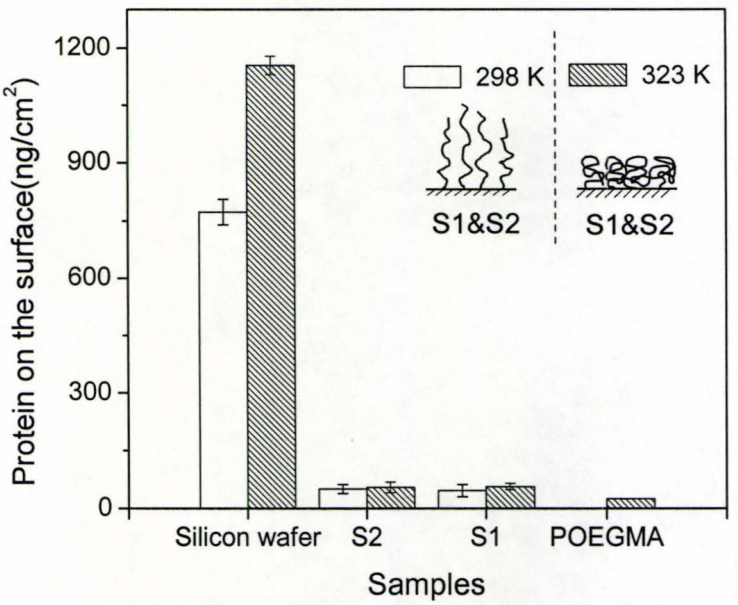

Figure 6-7 Lysozyme adsorption on the surfaces at different temperatures.

In most cases, an increase in temperature results in increased protein adsorption. For the present studies, when temperature was increased to 323 K the adsorbed protein amount on bare silicon increased to around 1150 ng/cm^2. At 323 K, the polymer brushes on S1 and S2 were both in the collapsed state; however, the amounts of adsorbed protein were still very low, close to those at room temperature. This finding of no significant difference between the extended and collapsed states in protein repelling performance is somewhat interesting. It is well-known that protein adsorption is affected by various interactions between components in the system (e.g., protein, water, surface, and other solutes). The change to the overall Gibbs energy determines the final equilibrium state: $\Delta G = \Delta H - T\Delta S$, where H, S, *and* T are enthalpy, entropy, and temperature, respectively. In the case of protein adsorption, the change to the Gibbs energy must be negative. In different systems, protein adsorption can be either entropically or enthalpically driven.

The enthalpy is believed to be the main factor for the surfaces grafted with PEO to resist protein adsorption. The change in enthalpy is associated with several factors during the protein adsorption process: e.g., van der Waals, electrostatic force, hydration forces, and hydrophobic interactions. The highly repulsive hydration force from the surfaces with tethered PEO is the main force in repelling proteins. Here, the polymer layers remain hydrophilic in both the extended and collapsed states, thus effectively

reducing protein adsorption. As mentioned, at temperatures below the LCST, the polymer chains extended deeply into water with a well-developed hydration layer surrounding the polymer chains. However, at temperatures above the polymer's LCST, the affinity between polymer segments is larger than that between EO groups and water, causing the polymer brushes to collapse. Nevertheless, the water fraction inside the collapsed polymer layer is still greater than 20% [Figure 6-2(b) and Figure 6-3(b)], i.e., the polymers remain hydrophilic. As a result, at the polymer-water interface a hydration layer is probably still present, effectively resisting the adsorption of protein.

6.5 Conclusions

In conclusion, PEG-based thermoresponsive surfaces were prepared by grafting P(MEO_2MA-*co*-OEGMA) copolymer brushes on silicon wafers via the surface-initiated ATRP method. The detailed conformation information of the polymer brushes in aqueous solutions as a function of temperature was obtained using the NR method. Polymer conformation changed from the well-extended state to the compressed state, and subsequently to the collapsed state with increased temperature. The addition of salt was found to affect the brushes differentially, depending on the development of the hydration layer around the polymer chains. For well-extended polymer brushes in water, salt strongly influenced the polymers conformation, most likely by significantly disrupting the hydration layer surrounding the brushes. On the other hand, in the case of

compressed and collapsed polymer brushes, the addition of salt had little effect. The presence of protein (lysozyme) in solution did not impact polymer conformation. The current thermoresponsive surfaces were found to have good protein adsorption resistance. Both extended and collapsed copolymer brushes gave good protein repelling performance.

6.6 References

1. Galaev, I. Y.; Mattiasson, B. *Trends Biotechnol.* **1999,** *17* (8), 335-340.
2. Mendes, P. M. *Chem. Soc. Rev.* **2008,** *37* (11), 2512-2529.
3. Sanjuan, S.; Tran, Y. *Macromolecules* **2008,** *41* (22), 8721-8728.
4. Sanjuan, S.; Tran, Y. *J. Polym. Sci. Pol. Chem.* **2008,** *46* (13), 4305-4319.
5. Biesalski, M.; Johannsmann, D.; Ruhe, J. *J. Chem. Phys.* **2004,** *120* (18), 8807-8814.
6. Biesalski, M.; Ruhe, J. *Macromolecules* **2002,** *35* (2), 499-507.
7. Zhou, F.; Huck, W. T. S. *Phys. Chem. Chem. Phys.* **2006,** *8* (33), 3815-3823.
8. Luzinov, I.; Minko, S.; Tsukruk, V. V. *Prog. Polym. Sci.* **2004,** *29* (7), 635-698.
9. Liu, Y.; Mu, L.; Liu, B. H.; Kong, J. L. *Chem. -Eur. J.* **2005,** *11* (9), 2622-2631.
10. Han, S.; Hagiwara, M.; Ishizone, T. *Macromolecules* **2003,** *36* (22), 8312-8319.
11. Lutz, J. F.; Akdemir, O.; Hoth, A. *J. Am. Chem. Soc.* **2006,** *128* (40), 13046-13047.

12. Lutz, J. F.; Hoth, A. *Macromolecules* **2006,** *39* (2), 893-896.

13. Lutz, J. F.; Andrieu, J.; Uzgun, S.; Rudolph, C.; Agarwal, S. *Macromolecules* **2007,** *40* (24), 8540-8543.

14. Yamamoto, S.; Pietrasik, J.; Matyjaszewski, K. *Macromolecules* **2007,** *40* (26), 9348-9353.

15. Lutz, J. F. *J. Polym. Sci. Pol. Chem.* **2008,** *46* (11), 3459-3470.

16. Jonas, A. M.; Glinel, K.; Oren, R.; Nysten, B.; Huck, W. T. S. *Macromolecules* **2007,** *40* (13), 4403-4405.

17. Wischerhoff, E.; Uhlig, K.; Lankenau, A.; Borner, H. G.; Laschewsky, A.; Duschl, C.; Lutz, J. F. *Angew. Chem. -Int. Edit.* **2008,** *47* (30), 5666-5668.

18. Glinel, K.; Jonas, A. M.; Jouenne, T.; Leprince, J.; Galas, L.; Huck, W. T. S. *Bioconjugate Chem.* **2009,** *20* (1), 71-77.

19. Kucerka, N.; Nieh, M. P.; Pencer, J.; Harroun, T.; Katsaras, J. *Curr. Opin. Colloid Interface Sci.* **2007,** *12* (1), 17-22.

20. Yim, H.; Kent, M. S.; Huber, D. L.; Satija, S.; Majewski, J.; Smith, G. S. *Macromolecules* **2003,** *36* (14), 5244-5251.

21. Yim, H.; Kent, M. S.; Mendez, S.; Lopez, G. P.; Satija, S.; Seo, Y. *Macromolecules* **2006,** *39* (9), 3420-3426.

22. Zhang, J. M.; Nylander, T.; Campbell, R. A.; Rennie, A. R.; Zauscher, S.; Linse, P. *Soft Matter* **2008,** *4* (3), 500-509.

23. Dormidontova, E. E. *Macromolecules* **2002,** *35* (3), 987-1001.

24. Lee, B. S.; Lee, J. K.; Kim, W. J.; Jung, Y. H.; Sim, S. J.; Lee, J.; Choi, I. S. *Biomacromolecules* **2007,** *8* (2), 744-749.

25. Ma, H. W.; Li, D. J.; Sheng, X.; Zhao, B.; Chilkoti, A. *Langmuir* **2006,** *22* (8), 3751-3756.

26. Collett, J.; Crawford, A.; Hatton, P. V.; Geoghegan, M.; Rimmer, S. *J. R. Soc. Interface* **2007,** *4* (12), 117-126.

27. Gao, X.; Feng, W.; Zhu, S. P.; Sheardown, H.; Brash, J. L. *Langmuir* **2008,** *24* (15), 8303-8308.

28. Harroun, T. A.; Fritzsche, H.; Watson, M. J.; Yager, K. G.; Tanchak, O. M.; Barrett, C. J.; Katsaras, J. *Rev. Sci. Instrum.* **2005,** *76* (6), 065101-1-065101-5.

29. Kent, M. S.; Majewski, J.; Smith, G. S.; Lee, L. T.; Satija, S. *J. Chem. Phys.* **1998,** *108* (13), 5635-5645.

30. Sirard, S. M.; Gupta, R. R.; Russell, T. P.; Watkins, J. J.; Green, P. F.; Johnston, K. P. *Macromolecules* **2003,** *36* (9), 3365-3373.

31. Feng, W.; Zhu, S. P.; Ishihara, K.; Brash, J. L. *Langmuir* **2005,** *21* (13), 5980-5987.

32. Archambault, J. G.; Brash, J. L. *Colloid Surf. B-Biointerfaces* **2004,** *33* (2), 111-120.

33. Feng, W.; Chen, R. X.; Brash, J. L.; Zhu, S. P. *Macromol. Rapid Commun.* **2005,** *26* (17), 1383-1388.

34. Feng, W.; Nieh, M. P.; Zhu, S.; Harroun, T. A.; Katsaras, J.; Brash, J. L. *Biointerphases* **2007,** *2* (1), 34-43.

35. Van Durme, K.; Rahier, H.; Van Mele, B. *Macromolecules* **2005,** *38* (24), 10155-10163.

36. Zhang, Y. J.; Furyk, S.; Bergbreiter, D. E.; Cremer, P. S. *J. Am. Chem. Soc.* **2005,** *127* (41), 14505-14510.

37. Magnusson, J. P.; Khan, A.; Pasparakis, G.; Saeed, A. O.; Wang, W. X.; Alexander, C. *J. Am. Chem. Soc.* **2008,** *130* (33), 10852-10853.

Chapter 7
Contributions and Recommendations

7.1 Knowledge contributions of the thesis work

Surface modification with polymeric materials has been applied widely in various fields. Recently, however, the development of surface-initiated living polymerization methods has brought a breakthrough. A variety of well-controlled novel polymer structures and functionalities have been introduced onto the surface by the living polymerization technique. A large number of surfaces with new functionalities come into being. It has been seen that the surface-initiated living polymerization technique is being applied to more and more fields. In this work, the surface-initiated ATRP was first given a comprehensive quantitative study that elucidated its mechanism and provided the guidance to the applications of this technique. It was then employed in the preparation of stimuli-responsive surfaces.

In Chapter 3, a detailed physical picture of surface-initiated ATRP was described and, base on it, a comprehensive kinetic model was developed using the method of moment. Combined with the experimental data, a quantitative analysis about the surface-initiated ATRP mechanism was carried out. To our best knowledge, this work gave the most comprehensive modeling study about the surface-initiated ATRP so far.

All the information of the grafted polymer chains including active chain concentration, radical concentration, chain length, polydispersity during the surface-initiated ATRP were given. Influencing factors were investigated. Furthermore, a new radical termination mechanism, termed as migration-termination, was proposed for surface-initiated living polymerization. The proposed mechanism offered a good explanation for the experimental observations. Because the crowding of polymer chains on the surface could induce a 2-D gel-effect, a more living polymerization, resulting in longer chain length and lower polydispersity on the surface, is believed to be possible. All this information helps understand the mechanism of the surface-initiated ATRP and provide guidance to the application of this technique.

In Chapter 4, the surface-initiated ATRP was employed to graft POEGMA-b-PMMA brushes on the silicon wafer surfaces. Simple solvent treatments were found to give nanoscale patterns via the phase segregation of the POEGMA and PMMA segments. It was the first time for the self-assembly of block copolymer brushes method to be employed to introduce nanopatterns to the PEG-based surfaces for potential applications in the biological and medical fields. Various patterns including spherical aggregates, wormlike aggregates, stripe patterns, perforated layers and complete overlayers were obtained through adjusting the upper block layer thickness. Furthermore, the nanopatterns prepared in this way possessed the unique stimuli-responsive property,

switching between the different morphologies reversibly after the treatment with selective solvents. In addition, this work for the first time demonstrated that the long side chains of the polymer brushes could help increase the quality of this method greatly. It helped constrain the feature size to less than 10 nm, which is the smallest size by this method so far, and tune it on the nanoscale. It also enabled to achieve a range of surface morphologies more clearly.

In Chapter 5, POEGMA-b-PMETAC brushes were synthesized by surface-initiated ATRP method to introduce nanopatterns. The employment of two hydrophilic segments was to avoid hydrophobic areas because they could change the conformation of proteins and make them lose their activity. The collapse of polyelectrolyte in salt solution was employed to introduce phase segregation between the two hydrophilic segments. A variety of nanopatterns and their stimuli-responsive ability were observed. The adsorption behaviors of fibrinogen on these patterns were thoroughly studied by ellipsometry, water contact angel measurement, AFM and radio labelling method.

In Chapter 6, the surface-initiated ATRP was employed to graft a new biocompatible thermo-responsive copolymer, P(MEO_2MA-co-OEGMA), onto a silicon wafer. This new class of thermo-responsive polymer surfaces, entirely constructed with poly(ethylene glycol) methacrylate, may lead to products that can hopefully be

incorporated into various biomedical devices. The thermo-responsive behavior of these copolymer brushes was demonstrated in this work. Their chain conformations in aqueous solution at both extended and collapsed states were for the first time shown by NR method. The effects of temperature and salt concentration on the chain conformation were evaluated. The protein repulsion ability of these surfaces was also studied for the first time. The results showed that this PEG-based thermo-responsive surface exhibited good protein adsorption resistance. It was surprising to observe the same level of protein repulsion from the extended and collapsed brushes.

7.2 Recommendations for future work

The studies in this thesis are expected to prompt applications of the surface-initiated ATRP technique. The further developments are recommended as following:

7.2.1 Long-range regular patterns

The advantage of the self-assembly method to prepare nanoscale patterns lies in its simplicity to prepare large area patterns at low costs. It is especially advantageous in applications where only evenly distributed domains with a certain range of shapes and sizes are required. However, its main disadvantage is that the patterns are not regular in long-range. In other words, the patterns forming from the self-assembly of the block

copolymer brushes are random and unpredictable, although they have uniform feature sizes. In order to achieve long-range regular patterns via the self-assembly method, external forces, e.g. pre-patterned substrates, electric field, mechanical flow field, temperature gradient etc., are always required. In the current work, an electric field was ever tried for the patterning from the phase segregation of POEGMA-b-PMETAC brushes. However, the patterns were not aligned as expected. In future work, more efforts are required to develop techniques which can be coupled with the current self-assembly method to prepare controlled long-range regular patterns. That will extend the applications of the current self-assembly method significantly.

7.2.2 Direct AFM observation on nanopatterns in different solvents

Currently, the observations of surface morphologies of block copolymer brushes are performed by AFM in air. The conformations of block copolymer brushes in the air differ from those in solvent. However, many applications of these stimuli-responsive surfaces are in certain solvents. Their conformations in solvent are mainly derived from the observation in air. As a result, the direct observation of the conformations under corresponding conditions is essential. The difference between polymer morphologies in air and solvent can then be compared directly.

Furthermore, the in-situ observation of this phase reconstruction is important to

understand the phase transition. The phase conformation, reconstruction rate and influencing factors under certain conditions can only be understood when the surface can be observed under certain conditions. So far only one in-situ observation of responsive polymers on surface has been reported.[1] The image resolution from a liquid-AFM is very low. Little information has been obtained. If the liquid-AFM method with high resolution can be developed to give direct observation of the in-situ phase transition, it would provide great help for better understanding these stimuli-responsive surfaces.

7.2.3 Introduce more functionalities to the nanopatterns

One advantage of employing the s-ATRP method to prepare polymer brushes is that the obtained polymer brushes have active chain ends. Simple chemical modification can introduce different functionalities. The modification of polymer brushes prepared by the surface-initiated ATRP method to introduce more functionalities or specific adsorption capacity for protein has attracted great interest recently.[2,3] These techniques can also be used for the current nanopatterns prepared by the surface-initiated ATRP method to give specific adsorption ability for unique proteins or other functions. The application of these nanopatterns can be extended greatly.

7.2.4 Systemic study on P(MEO_2MA-co-OEGMA) brushes

P(MEO_2MA-co-OEGMA) brushes are a new type of thermo-responsive polymers.

Besides our work by the NR method, only a single study from Huck *et al.*[4] in 2007 was reported on the investigation of their chain conformations. In their work, an aqueous-AFM method was employed to measure the swelling ratio. The thermo-responsive collapse transition of the polymer brushes on the surface was demonstrated by the work from both groups. The chain conformation was also revealed by NR in our work. However, more systematic work is needed before the wide application of this new type of thermo-responsive surfaces. It is interesting to know how the other influencing factors, e.g. copolymer composition, comonomer type, molecular weight, end group functionality, salt type, salt concentration, etc., affect the performance of the current thermo-responsive polymer brushes. Especially considering the surface-initiated living polymerization has been employed to prepare these polymer brushes, many factors including chain length, grafting density and copolymer composition etc. can be adjusted easily. Such systemic work helps for wide applications of this new type of the thermo-responsive surfaces in various fields.

7.3 References

1. Lin, Y. H.; Teng, J.; Zubarev, E. R.; Shulha, H.; Tsukruk, V. V. *Nano Lett.* **2005,** *5* (3), 491-495.
2. Lee, B. S.; Lee, J. K.; Kim, W. J.; Jung, Y. H.; Sim, S. J.; Lee, J.; Choi, I. S. *Biomacromolecules* **2007,** *8* (2), 744-749.

3. Tugulu, S.; Arnold, A.; Sielaff, I.; Johnsson, K.; Klok, H. A. *Biomacromolecules* **2005,** *6* (3), 1602-1607.

4. Jonas, A. M.; Glinel, K.; Oren, R.; Nysten, B.; Huck, W. T. S. *Macromolecules* **2007,** *40* (13), 4403-4405.